Master's thesis

NTNU
Norwegian University of Science and Technology
Faculty of Social and Educational Sciences
Department of Geography

Charlotte Hagen Næss

Shell deposition and storminess

A study of the geochemical properties of the shell layers found in the fringing saltmarsh of Saltatjørna in Hå

Master's thesis in geograhy with teacher education
Supervisor: Chantel Nixon
Co-supervisor: Max Holthuis
May 2023

NTNU
Norwegian University of
Science and Technology

Charlotte Hagen Næss

Shell deposition and storminess

A study of the geochemical properties of the shell layers found in the fringing saltmarsh of Saltatjørna in Hå

Master's thesis in geograhy with teacher education
Supervisor: Chantel Nixon
Co-supervisor: Max Holthuis
May 2023

Norwegian University of Science and Technology
Faculty of Social and Educational Sciences
Department of Geography

NTNU
Norwegian University of
Science and Technology

Abstract

As one of the consequences of human-caused climate change, average sea levels are rising at an increasing rate. As part of QUANTSEA, a larger project that aims to reconstruct more recent sea level changes in Norway, the focus of this thesis is to look into records of storms and storm surges. For the project, two cores were sampled from a microtidal saltmarsh in south-western Norway. The several shell layers observed in the cores were suspected to be connected to storm layers deposited from bigger storms. The goal of the thesis is to research whether there are any consistent geochemical signatures associated with these distinct fragmented shell layers, and how they differentiate from the rest of the core stratigraphy, which is presumed to represents average conditions in Saltatjørna. In order to answer this, the cores were scanned with X-ray fluorescence (XRF), and the data was then transformed and analyzed. Some samples also underwent a loss-on-ignition (LOI) analysis.

The results show a trend in the analytical concepts, were the levels of the elemental proxies Ca and Sr generally increased over the shell layers, while the other proxies used, Fe, Zr, Cl and Br, all decreased. The LOI also showed much less organic content over the shell layers. Together with other observations, such as CT scans, historical photographs, and measurements of the sill elevation and wrack line, the thesis concludes that there is a correlation. The Sr and Ca levels indicate marine influence, whereas the decreasing Fe is a proxy for decreasing terrigenous materials. Combined with knowledge of the tidal range around the study area, it is concluded that this marine influence is not the result of regular tides, but rather rarer, larger storm surges.

Sammendrag

Som en av konsekvensene fra menneskeskapte klimaendringer, stiger det gjennomsnittlige havnivået i en økende skala. Som en del av QUANTSEA, et større prosjekt med mål om å rekonstruere nylige havnivåendringer i Norge, ser denne oppgaven nærmere på historien av storm og stormflo. I forbindelse med dette prosjektet ble det tatt to sedimentkjerner fra en mikrotidal saltmyr i sør-vestlige Norge. Det ble funnet flere lag med fragmenterte skjell som ble mistenkt for å være knyttet til stormlag deponert fra større stormer. Formålet med denne masteroppgaven er å undersøke om det eksisterer noen konsistente geokjemiske signaturer knyttet til disse fragmenterte skjell-lagene, og hvordan de skiller seg fra resten av stratigrafien i kjernen, som antas å representere de gjennomsnittlige forholdene i Saltatjørna. For å svare på dette ble kjernene skannet med røntgenfluorescens (XRF) og dataen ble deretter behandlet og analysert. I tillegg ble det gjennomført loss-on-ignition (LOI) analyse på deler av kjerneprøven.

Resultatene viser en trend i de analytiske konseptene, der nivåene i de elementære representantene Ca og Sr generelt øker over skjell-lagene. Samtidig synker de andre elementære representantene som ble brukt, Fe, Zr, Cl og Br. LOI analysene viste også mye mindre organisk innhold over skjell-lagene. Sammen med andre observasjoner, CT skanning, historiske fotografier, og målinger av «sill» og «wrack line»[1] konkluderer oppgaven med at det er en korrelasjon. Nivåene av Sr og Ca indikerer marin påvirkning, mens den synkende verdien av Fe er en indikasjon for synkende input av terrigene materialer. Kombinert med kunnskap om tidevann-nivået rundt studieområdet, konkluderes det med at denne marine påvirkningen ikke er et resultat av regelmessig tidevann, men helle sjeldnere, større stormfloer.

[1] «Sill» er en (gjerne parallell) plateinntrengning mellom eldre lag av ofte sedimentær bergart; «wrack line» kan i noen tilfeller oversetter til tangsone eller tangvoll og viser til stedet langs kysten hvor organisk materiale avsettes ved høyvann.

Acknowledgements

As my time at NTNU comes to a close, I find myself reflecting over the past five years, filled with more challenges, both physical and mental, than I ever thought I'd face in such a short time. However I've come out stronger on the other side, and the end of the era is marked by with the completion of this thesis. It has given me an opportunity to deepen my interest of natural geography, and given me a stronger insight into the climate.

As such, it must be mentioned that this could not have happened without the help of quite a few people. First and foremost, my supervisor Chantel Nixon, and co-supervisor Max Holthuis. Chantel, I will be forever grateful for you putting up with me, answering all my questions, and patiently guiding me through the mess that is writing a thesis for the first time. And Max, for also answering all my questions, and teaching me the most important facts about the rabbit-hole that is XRF. A thanks also needs to be given to the rest of the QUANTSEA team that collected the cores at Saltatjørna, and the EARTHLAB at UiB for conducting the XRF analysis and CT scans; there would be no data without your contribution!

I also want to thank all the people I met along the way, that has given me love, support, inspiration, or opportunities, all of which made me get to where I am today. Naturally I also wish to give thanks and appreciation to my friends and classmates, who was of undeniable emotional support during this steep learning curve and intense period of writing, either by giving help and advice along the way, or by providing good distractions in form of excellent gossip and countless trips to the store. You all helped make this possible, and I will miss our time together.

Table of Contents

Figure List

Table list

1 Introduction

1.1 Background and Actualization

Human-caused global climate change has led to damage and loss of several ecosystems (IPCC, 2023). The Intergovernmental Panel on Climate Change (IPCC), a body of the United Nations focusing on climate change, published their 6th Assessment Report in 2023, which states that damage to ecosystems from climate change and other human impacts are far greater than previously indicated (IPCC, 2023). Emissions of greenhouse gases have increased global temperatures, which cause widespread changes to processes and conditions in the atmosphere, hydrosphere, cryosphere and biosphere (IPCC, 2023). An ongoing mass extinction event has started, glaciers and ice sheets are melting, and sea level is rising (IPCC, 2023). Food and water security is at risk and human health has been compromised. The IPCC (2023) report also states that if the temperatures continues to rise, many of these ongoing changes will continue to happen, and eventually cause irreversible damage (IPCC, 2023).

Global sea level is already rising, and in the past century, has been rising at an average rate of approximately 1.7 mm per year, but has been accelerating approximately since the 1960s, mostly due to melting of glaciers and ocean warming causing thermal expansion (Simpson et al., 2015). Global Mean Sea Level (GMSL) is a measure of average sea level change over time across the world's oceans, while local changes in sea-level are known as relative sea-level change (RSL); RSL is also affected by things like local land-level changes. The predicted rise for global average sea-level within the next century is between 0.26-0.82 m. In Norway, projections for relative sea-level rise are expected to be lower due to glacioisostatic uplift, at -0.1 to 0.55 m (Simpson et al., 2015). In addition to sea-level rise caused by thermal expansion and melting glaciers, coastal landscapes are exposed to storm surges and coastal flooding, which can temporarily add between 1-3 m of extra water. Storm surges can be connected to extreme weather, and as there is a prediction that this will occur more often, it follows that storm surges will also be more frequent (Simpson et al., 2015). If the outline of Norway was measured in a straight line, approximately 50% would be maritime. Combined with the rapid environmental changes happening all over the globe and predictions for higher sea-levels and more extreme weather, sea-level research is highly relevant for Norway.

1.2 Thesis aim and research question

This thesis aims to investigate a sedimentary record of several storms in one coastal basin in southwestern Norway. Logging historical sea levels and storm surges can be helpful in predicting future events and documenting how coastal environments are impacted. The thesis focuses on a record of likely storms and storm surges from a microtidal saltmarsh in Saltatjørna, a small intertidal basin in Rogaland County, Norway. Two cores were collected from Saltatjørna as a part of a larger project called QUANTSEA (Quantifying Past and Future Sea-Level in Norway); the work package under which this thesis operates aims to reconstruct recent (i.e. the past 2000 years or less) RSL change in southern and northern Norway. Several distinct, broken-shell layers were observed in the cores from Saltatjørna and hypothesized to be storm layers. The research question that this thesis hopes to answer is therefore:

Are there consistent geochemical signatures associated with the distinct shell layers, and how do they differentiate from the rest of the core stratigraphy, which is presumed to represents average conditions in Saltatjørna?

To address the research question, two core samples of different depths from the same borehole where examined: the first core extends from the surface to 1 m depth, while the second core extends from 1 m below the surface to 172 cm depth. Both cores were scanned with X-ray fluorescence (XRF) to determine geochemical composition of the sediments at different depths. Core samples from the upper 1 m core also underwent a loss-on-ignition analysis to determine the amount of organic material.

1.3 Structure

This thesis consists of 6 chapters, beginning with the Introduction, which provides some background information, the research question, and describes the relevance of the project. Chapter 2 presents all the background information necessary to be able to understand the research. Terms introduced include sea level, tides, storm surges, salt marshes and sediment deposition, in addition to a description of the study area. Chapter 3 introduces the analytical concepts of the methods used, as well as a description of the fieldwork and lab work done in the process of the thesis. The results of the fieldwork and lab work are presented in Chapter 4, which are discussed and analyzed in Chapter 5. The thesis is concluded in Chapter 6.

2 Theory and Background

2.1 Sea level

Sea level refers to the position of the sea surface above or below a vertical datum, for example, the reference ellipsoid (which is a mathematically defined surface that approximates the geoid, which in turn, is the shape the ocean surface would take under the influence of only gravity and the Earth's rotation) (Simpson et al., 2015). While GMSL is useful for keeping track of climate change and the effects of melting ice sheets on sea level, it is not very relevant for people who live and work in coastal areas, since relative sea-level change (RSL) can vary so much from GMSL (Simpson et al., 2015). At a smaller scale, RSL, which describes the relative position of the sea surface where it meets the land, and which changes on timescales ranging from seconds (e.g. tsunamis) to hours (e.g. tides) to millennia (e.g. glacial-interglacial cycles), is a more practical and relevant measure (Benn & Evans, 2010; Chappell, 2004).

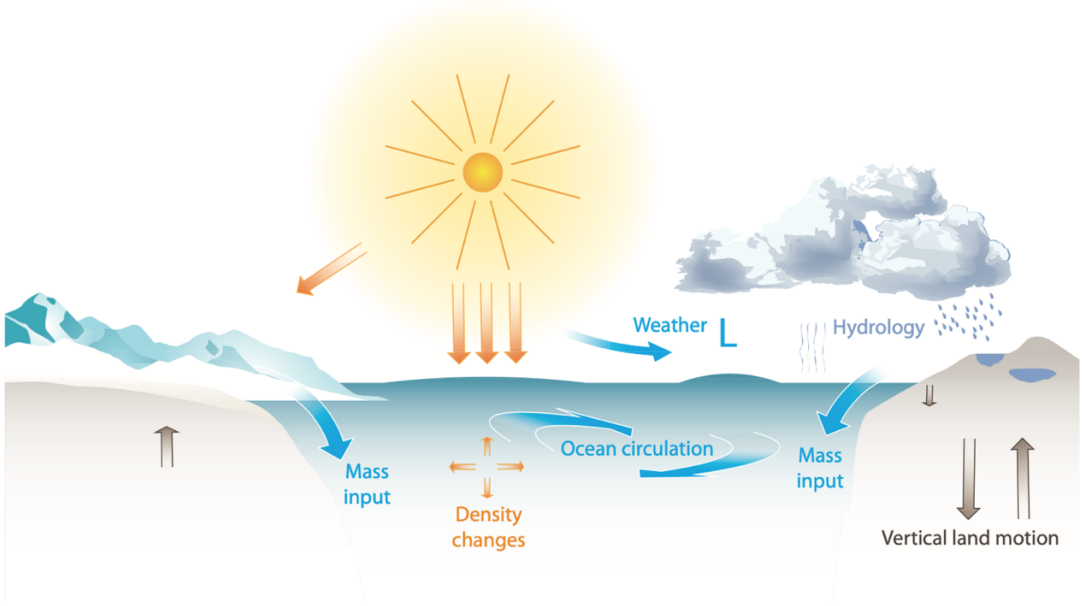

Figure 1: Factors that affect changes in sea level (Simpson er at., 2015)

GMSL has changed throughout the geologic past, due to both the quantity of ocean water, as well as the shape of ocean basins (Benn & Evans, 2010; Chappell, 2004). The total amount of water has remained fairly constant throughout time, however there have been significant changes in the amount that is held up in reservoirs such as glaciers, lakes, groundwater and continental ice sheets. Variations in the volume of water in the world's oceans due to changes in such reservoirs are known as eustatic sea-level changes (Benn & Evans, 2010; Chappell, 2004). Both eustatic and glacioisostatic changes drive RSL change today, where the term,

glacioisostatic, refers to the vertical motion of the Earth's crust related to loading and unloading of ice sheets today and in the past (figure 1) (Benn & Evans, 2010; Chappell, 2004). Big changes in the amount of water stores on land or added to the sea, causes changes in the gravity field and thus a redistribution of mass (Simpson et al., 2015). This redistribution of mass can also be caused by winds. In Norway, the vertical land motion is highly significant when looking at RSL, as it is still experiencing glacioisostatic uplift since the deglaciation of the Fennoscandian sheet ca. 15000 years ago, and occurring at approximately 1-5mm per year (Simpson et al., 2015).

Other factors that drive GMSL at a regional level are changes in ocean density, salinity and temperature, as well as ocean circulation (figure 1) (Simpson et al., 2015). Increased heat causes thermal expansion, as warmer water expands in volume due to the spatial arrangements of molecules, and more salty water caused it to contract. These factors are referred to as changes in steric height (Simpson et al., 2015). There are also smaller, more regional and local sea level changes, at decadal, annual and even shorter intervals, caused by meteorology and tides, which vary from place to place. For instance will al low atmospheric pressure cause the RSL to rise, and high pressure will depress the RSL (figure 1). A low-pressure storm will also cause changes in RSL (Simpson et al., 2015). The effects of tides and storms are described further in section 2.1.2 and 2.1.3.

2.1.1 Past, present and future RSL change

It is estimated that the difference in RSL between the height of the last ice age and the last full ice-sheet melt (including the Greenland and Antarctic ice sheets), would be approximately 170 meters (Simpson et al., 2015). Historical sea levels from different geologic ages (millions of years ago) are referred to as paleoclimatic sea levels. The climatic changes at these ages happened naturally, without human interference. To reconstruct what sea levels might have been at these times, scientists find historical shorelines, samples from lakes or bogs, or fossils, and calculate the date of the positions of these indicators. This dating is then corrected for vertical land movement from glacioisostatic changes, together with known local horizontal changes, to create a fairly certain sea level reconstruction (Simpson et al., 2015). This can be seen in figure 2, which shows the estimates highest marine limit during the last interglacial, compared to today sea level.

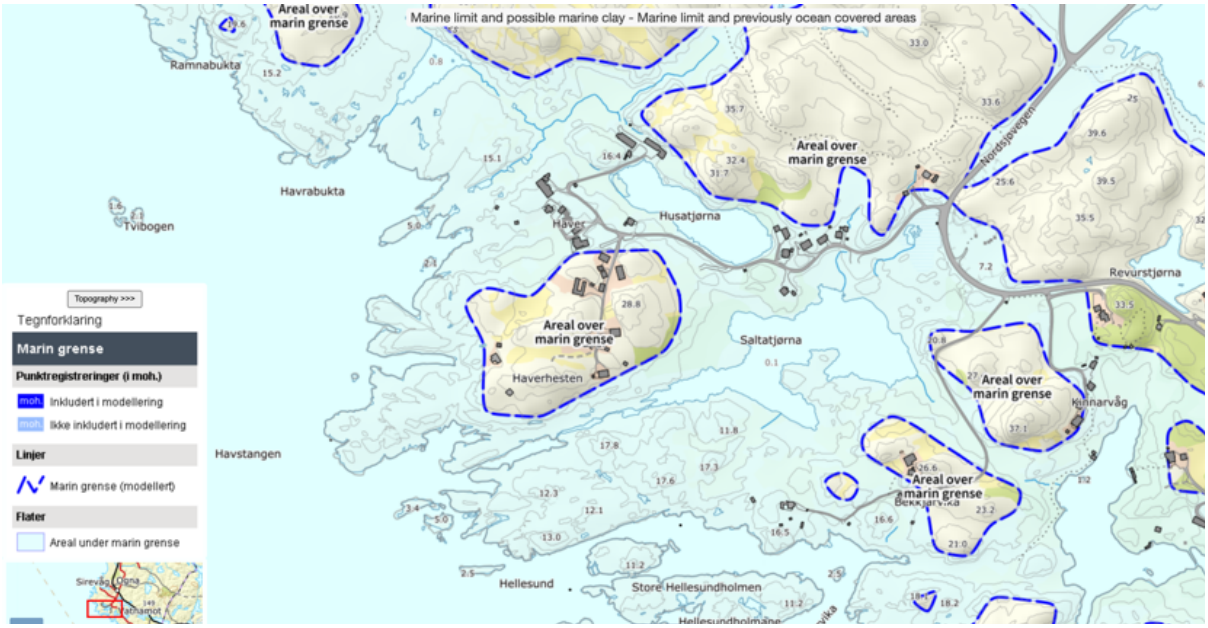

Figure 2: A reconstruction of marine limit during the last interglacial, in the study area, showing it was completely submerged at some point. The dark blue line indicates the marine limit, and the area colored light blue is the area that was below the marine limit…(Norges Geologiske Undersøkelse, 2023b)

During the Pliocene (which occurred around 3-5 million years ago), the planet had had long warmer periods with an average temperate about 3° C warmer than the Quaternary, and with levels of CO_2 close to today's range (400-420 ppmv) and (Simpson et al., 2015). There was much less polar ice during this Epoch, and eustatic sea level has been estimated to have been approximately 10 - 25 m higher than present (Lowe & Walker, 2015; Simpson et al., 2015).

During the last interglacial period, around 130,000 to 120,000 years ago, average temperatures have been estimated to be 1-2° C above pre-industrial levels (i.e. before ca. 1760 AD) (Simpson et al., 2015). At this time CO_2 levels were much lower than they are today (280-300 ppmv), and the warming was caused by the Earth's orbit caused the Northern Hemisphere to be closer to the sun during summer (Simpson et al., 2015). It is estimated that at this time, GMSL was a minimum of 6 m higher than today, partially due to warmer oceans, as well as smaller ice sheets, meaning less water frozen on land (Simpson et al., 2015).

Approximately 21,000 years ago, at the last glacial maximum, GMSL was around 125 meters lower than present day, as much water was trapped in ice sheets (Chappell, 2004). The continental ice sheets have since mostly melted, contributing to the current GMSL, which has been more or less constant in the last 2000 years, with small fluctuations of +/- 20 cm (Chappell, 2004). During the last interglacial, GMSL rose at a rate of 20-60 cm per century (Simpson et al., 2015). Current rates of GMSL rise are around 30 cm per century. It is estimated

that during the collapse of large continental ice sheets around 20 000 – 10 000 years ago, the rise in GMSL was as much as 4 m per century (Simpson et al., 2015).

More recent RSL changes have been recorded by instruments such as tide gauges and satellites (from the 18th century and later for tide gauges and from the 1970s for satellite altimetry). Data from instrumental records have shown that change in GMSL over the last century has been occurring at rates of 1.7 mm per year (+/- 2 mm) (Rhein et al. 2013, in Simpson et al., 2015). These data also suggest an acceleration in GMSL rise in the past 100 years compared to the previous 200 years (Simpson et al., 2015).

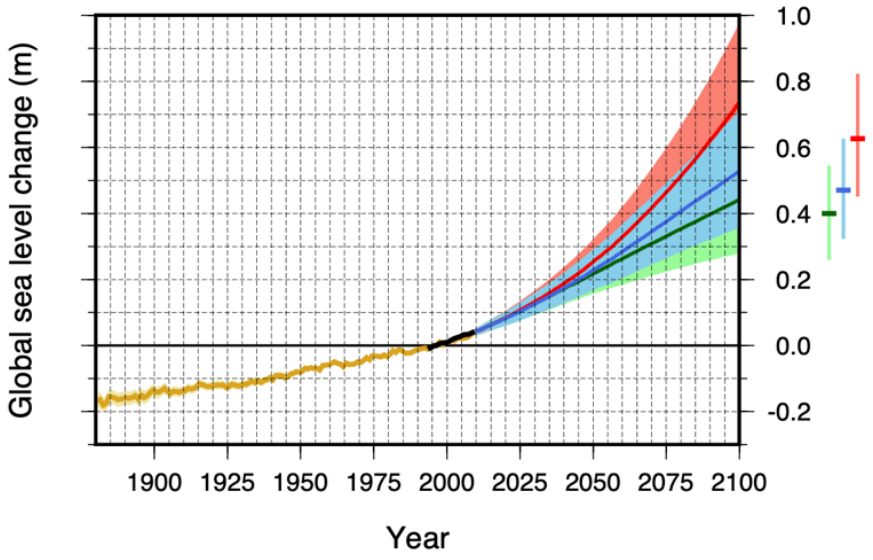

Figure 3: Projected global RSL for years 2091-2100, showing different degrees of severity regarding CO_2 concentrations. Red model being a high emission scenario, blue a medium emission scenario and green a low emission scenario (Simpson et al., 2015).

Future GMSL rise between 2081-2100 is likely to be between 0.26 m to 0.82 m, depending on concentrations of greenhouse gases, aerosols and other climate drivers (IPCC, year). These projections are shown in figure 3. In this scenario, the thermal expansion and glacier melt are projected to accelerate GMSL rise, as is meltwater from the Greenland Ice Sheet and that from other glaciers and ice caps. In Norway, the sea levels rise is predicted to be between -0.1m and 0.55m, a lower number than the global due to the isostatic uplift (Simpson et al., 2015).

2.1.2 Tides

Tides are a natural, cyclical falling and rising of the ocean (Holden, 2012). Tides are not noticeable in the deep ocean, however, along coastlines, tides can range from less than 1 m to over 16 m (Holden, 2012). The main forces that drives this process is the gravitational attraction

between the Earth and the Moon, as well as the connection between the Earth and the Sun, with the Moon having almost double the effect compared to the Sun (Holden, 2012). The tides cause a rise and fall in the water level twice per day in most coastal areas (Holden, 2012).

Tidal motion can be broken into tidal systems, knowns as amphidromes, where the tide travels around a central amphidrome point as a single wave (Arthur & Marone, n.d.). The amount of the rise and fall varies greatly around the Earth, depending on the distance from this point, from ≈0 to 38 m, where it will be practically zero closets to the center (NOAA, 2023). One such point is located near Egersund, southwestern Norway (Figure 5) (Jakobsen, 2018).

The tides also vary during the year, as the interaction between the Earth and moon and the Earth and sun varies. The highest height of the tides occur during spring tides, which is when the Earth, sun and moon are all aligned. This can happen during both full moon and new moon. When the moon and the sun are at an right angle to the Earth, their forces compete and tides are the lowest, knows as neap tides (Holden, 2012). A full tidal cycle, from spring tide to spring tide, takes 14 days, as the moon uses 28 days to complete its cycle around the Earth (Holden, 2012; Jakobsen, 2018; NOAA, 2023).

2.1.3 Storm surges

In the higher latitudes, such as northern Europe, the coasts are exposed to extratropical cyclones, that often are remnants of hurricanes that form in the southwest of the Atlantic basin (Gornitz, 2019). Extratropical cyclones usually have a lower windspeed than hurricanes, but tend to cover a greater area. The North Sea is prone to coastal flooding as a result of extratropical storms that pass over the shallow shelf waters (Gornitz, 2019). The Norwegian coast is not unknown to the effects of incoming storms that originate from the southwest, and push amounts of water towards the shores, known as storm surges (Simpson et al., 2015).

When a cyclonic weather system hits, storm surges appear as a response to changes in the atmospheric pressure and strong winds (Gornitz, 2019; Parnell, 2004). Reduced air pressure related to a storm causes water levels to rise, over the normal tides. Storm surges can last between one hour and four days, but most last between 6-18 hours (Gornitz, 2019; Parnell, 2004). There are mainly two actions that lead to storm surges. The first one is wind set-up, which is a rapid change in wind speed or direction, also called wind shear. Wind set-up causes extreme stress on the movements of the ocean and the water is held up against the windward coasts. The other action is the pressure set-up caused by the inverse barometer effect. This

occurs when a drop in atmospheric pressure causes the mean water surface level to increase (Gornitz, 2019; Parnell, 2004). In extreme storm surges, the wind set-up has the most significant effect. The size of the surge depends on a number of factors, such as wind speed, the track and position of the storm, the slope of the continental shelf, and the configuration of the shoreline (Gornitz, 2019; Parnell, 2004).

The biggest surges comes from hurricanes, and globally there have been reported up to 8 m increase in water levels from this (Parnell, 2004). In higher latitudes, the surges are more common in the 1-3 m range (Parnell, 2004). If a storm surge appears together with a high astronomical tide, the effect of the storm surge is naturally intensified. If a storm surge impacts an open coast, it usually increases the wave set-up as well. Longer periods of wave motions in the surf increases water levels on the beach. This will also cause a significant coastal erosion (Parnell, 2004). In southern Norway, the storm surges are much greater than the astronomical tides, and thus the storm surges can cause great impact regardless of the tidal period. In the northern and western Norway, the astronomical tidal difference is much greater, and a storm surge during low tide generally doesn't surpass the astronomical tide (Simpson et al., 2015).

Floods, as well as other natural events such as earthquakes or landslides, have return periods, which are defined as a risk evaluation of the frequency at which a flood of that size is likely to occur again. If the frequency is 1 in 100, then that event has a return period of 100 years (Jones, 1997). The return levels for storm surges in Norway is demonstrated in figure 4.

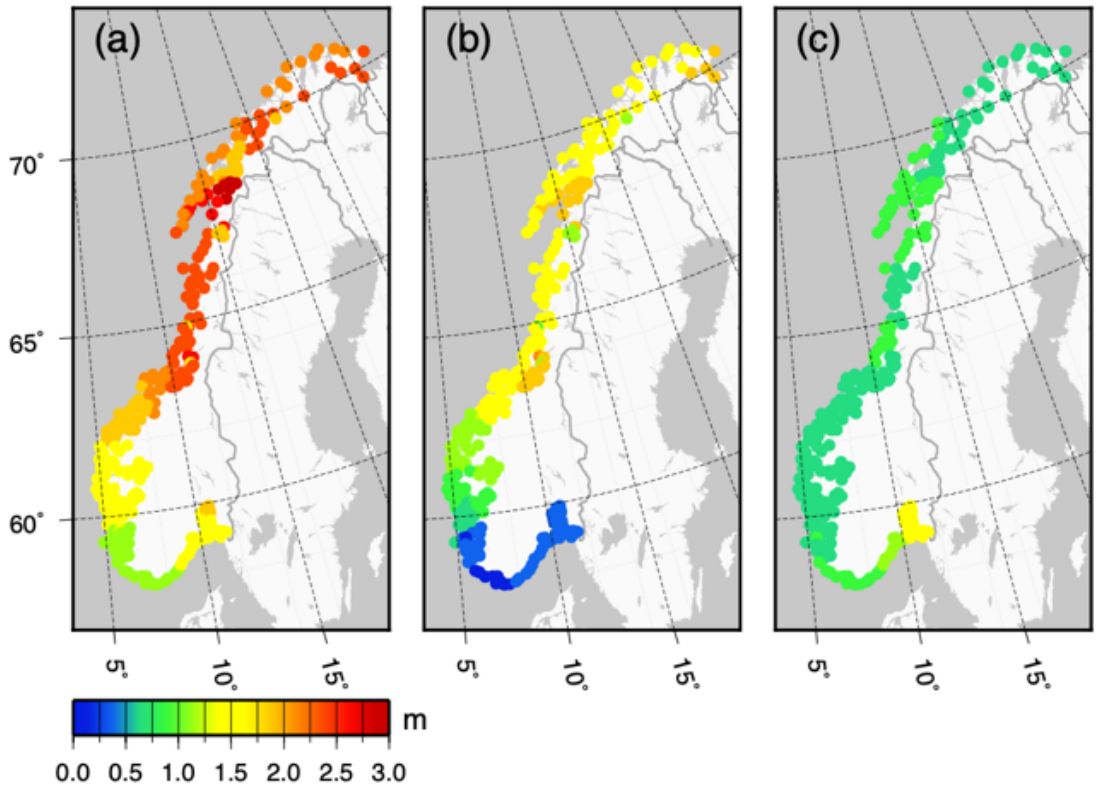

Figure 4: Return levels in Norway; a) 200 year return level in meters above sea level; b) highest astronomical tide in meters above sea level; c) the 200 year return height in meters about highest astronomical tides in order to compare the significance of the extreme levels (Simpson et al., 2015).

2.2 Estuaries and Salt Marshes

The point where rivers meet the sea in semi-enclosed water bodies are called estuaries. Today they occur mostly as a result of the post-glacial rise in sea-level that has flooded the mouth of the river (Healy, 2019a). Here, a mix of freshwater and seawater exists, commonly known as brackish water, and both marine and fluvial processes occur. The two main geomorphological elements that are part of estuaries are tidal channels and tidal mudflats. Tidal channels or inlets are opening in shoreline barriers that connect the ocean to the estuary and thus become a major source for sediment transportation. This means that estuaries mostly consist of sand-sized sediments (Healy, 2019a). Tidal mudflats occur further in from the strong flow of currents, and here the sediments are carried inward mostly during high tide, and deposited as the tide turns. How often this happens depends on both the height of the tide as well as the elevation of the mudflat (Holden, 2012). As sediment is deposited, the mudflat builds upwards, causing it to be flooded more rarely. If the frequency of the flooding is low, salt-tolerant, or halophytic shrubs and plant species, in particular grasses, will flourish and take over the mudflat, creating a system called salt marshes (Healy, 2019a, 2019b; Holden, 2012).

Salt marshes mostly form in the upper intertidal zone, where there is less wave energy, creating an ideal environment for the deposition of fine-grained silts and clays (French, 2004). Salt marshes also have a good supply of organic debris, such as roots, stems, leaves or branches, which adds to the sedimentation. The combination of sediments causes a sloping, vegetated platform, with a vertical accretion rate in the range of millimeters per year, depending on the location and on how quickly relative sea level is rising (Holden, 2012). Wide, shallow channels are a common sign of a saltmarsh in early development, whereas steep-edged channels are a sign of longer continued accretion of older marshes (Healy, 2019b). The long-term morphodynamics of saltmarshes is dependent on elevation, tidal flooding and sedimentation. As the sediment accumulate, the elevation of the marsh increases, and thus the older marshes are less frequently flooded. As the marshes gradually gets less tidal range, the importance of non-tidal flooding, such as storm surges, to depose of sediments increase (Healy, 2019b). Another important factor for the creation of salt marshes is sea level. As sea level has globally risen during most of the Holocene episodes of saltmarsh expansion have occurred (French, 2004). However, this is not the case for areas that were formerly glaciated (French, 2004; Holden, 2012).

Saltmarshes have been shown to have a high biological productivity (Healy, 2019b). A saltmarsh consists of a complex interaction between ecological, climactic, edaphic and hydrogenic factors, and is formed through physical, biological and geochemical processes) (French, 2004) As such, the biological productivity is also governed by complex interaction of vegetation, substrate and fauna, combined with tide water, sediments and marine nutrient (French, 2004; Healy, 2019b). This combination of varying factors makes saltmarshes a very complex and interesting subject, with a wide range of terrestrial and marine habitats and organisms (French, 2004; Healy, 2019b). The combination of fresh- and saltwater often creates gradual, though not continuous, zones of vegetation. Closest to the sea, there are often mostly halophytes like sea grasses and glasswort, e.g. Zostera and Salicornia, as well as vegetation that withstand brackish waters, such as Spartina. The more stable zones of marshes are more terrestrially influenced, and thus colonized by less salt-tolerant plants. In such areas, there are more rushes, grasses and herbs (e.g. Juncus, Puccinellia, Sporobolus, Aster, Plantago) (Healy, 2019b). The vegetation in saltmarshes shows to be productive in dissipating wave energy, which can prove cost efficient in creating sea defenses, are effective for trapping sediment, and can provide habitat for sea birds and nurseries for fish (French, 2004).

2.3 Storm and tsunami deposition in sheltered coastal areas

The main sources of terrestrial sediments in salt marshes and estuaries that which are carried from rivers and glaciers toward the sea, products of coastal erosion, sediments from offshore that are carried landward, as well as accumulation of biogenic debris (Smithson et al., 2002). Of these, the products of coastal erosion is very low, whereas the biogenic material contribute significantly on a local level. In temperate high latitudes, there are heavy influences from glacial sediments from Pleistocene (Smithson et al., 2002). Wave motion has a maximum limit of 20 meters past the submarine contour to where it can move sand, but there are still evidence of plenty of offshore source in the sea level changes between the Last Glacial Period and the current interglacial, a difference of about 120-130 m, between 15 000 years before present and 5000 years before present (Smithson et al., 2002). The end of this change provides a limit to future deposition from the offshore source. The area where waves are broken forms a barrier towards the sea where coarse sediments cannot transfer except during storm events. Storm events and strong tides also contribute to increased mass erosion (Smithson et al., 2002).

The biggest difference between sedimentary records of storms vs tsunamis are that tsunami deposits are less than 25 cm thick and can extend up to several hundred meters inland (Morton et al., 2007). Sandy deposits from bigger storms or hurricanes, however, tend to be more than 30 cm thick and extend no less than 300 m away from the shore (Morton et al., 2007). Furthermore, tsunami deposits consist of either a single structureless bed or a bed with only a few thin layers, with the presence of thin mud or heavy mineral laminae. A top layer of mud may also be present. The mud layers are usually indicative of the successive waves of a tsunami, allowing the sediment to settle in the time between the two waves (Morton et al., 2007). In sandy storm deposits, mud is very rare due to high and persistent energy flow during a storm. In low inland areas, such as marshes, where the water can be still for longer periods, there can be the occurrence of thin mud drapes or agal mats at the top, however these are often prone to wind and erosion and might not be well preserved (Morton et al., 2007). Other elements of a storm deposit are several lamiae sets, with interchanging coarse and fine textures, as well as laminations of shell fragments (Morton et al., 2007).

The most typical kind of deposits from a storm surge in an enclosed space such as a salt marsh, are washover deposits from a barrier between the marsh and the ocean, if one is present (Donnelly, 2009). The sediments consists of materials from the beach or other environments close to the shore, mostly sands that decrease in grain size the further from the barrier they are

deposited, and these sand grains are commonly more coarse than the fine-grained silts that usually dominate the back-barrier environments (Donnelly, 2009). Such washover deposits can be preserved and used to track intense hurricanes and storms, a field of study called paleotempestology (Donnelly, 2009).

2.4 Study area

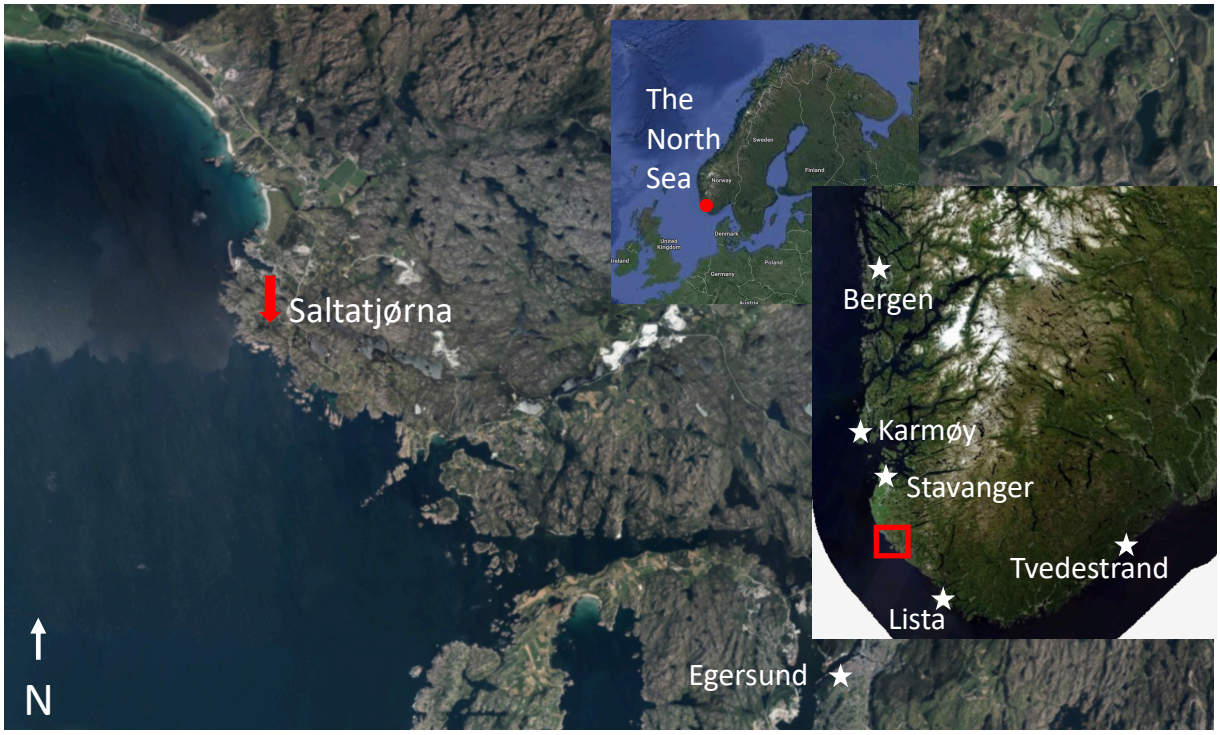

Figure 5: Location of the study area, Saltatjørna, on the southwest side of Norway (Kartverket, 2023a).

Saltatjørna is a brackish pond with fringing salt marshes, located in Hå municipality, Jæren region, Rogaland county. It is located on the western side of southern Norway, on the coast of the North Sea (figure 5). Saltatjørna is connected to the North Sea through a narrow and rocky inlet on its western side (figure 6). A couple of small, freshwater streams also enter the coastal pond.

Figure 6: Aerial photos of Saltatjørna and the study area, taken in 2019, the red dot indicates the location with coordinates of the sample cores (Kartverket, 2023a).

2.4.1 Geology

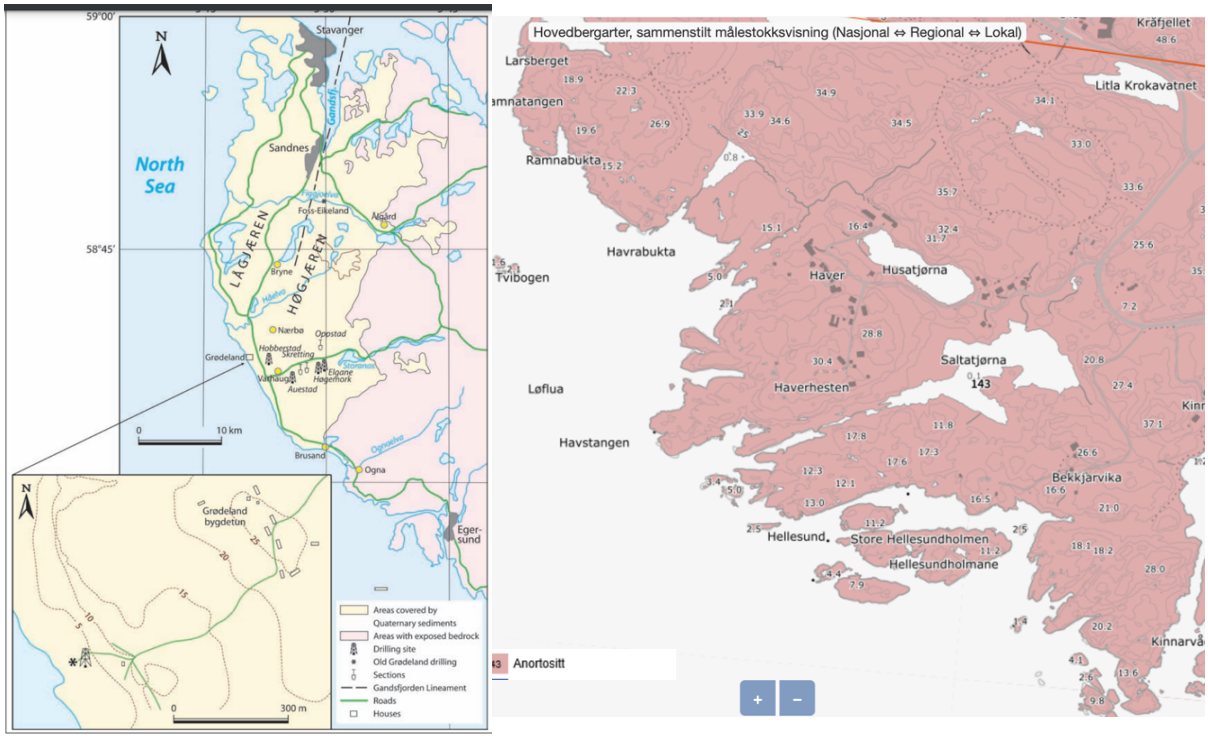

Figure 7: a) The areas that are covered by Quaternary sediments shown in yellow and exposed bedrock in pink and b) showing the type of bedrock found in the area (Norges Geologiske Undersøkelse, 2023a).

The area where Saltatjørna is located is part of the geological area called “Egersundfeltet”. “Egersundfeltet” is an area consisting of anorthositic bedrock, which is an intrusive, igneous

rock (Aasly et al., 2015; Erichsen & Marker, 2000). According to the surficial geology map from Norges geologiske undersøkelse (figure 7) there are no sediments in the area of Saltatjørna, only exposed bedrock, although the remaining part of the Jæren region is thick with deposits from the Quaternary, mostly till, with some sediments from intercalated marine or glaciomarine (Olsen et al., 2013). As small parts of Saltatjørna host saltmarshes, the deposits under the water are likely muds, sands and silts. A gravity core taken from here shows very organic-rich, mud down about 1 m in several locations.

2.4.2 Local climate and hydrology

Rogaland County has a varied landscape, consisting of coasts, fjords, mountains and valleys, which creates contrasts in the climate. The coastal parts are naturally dominated by a maritime climate profile, which is mild and humid with a moderate amount of precipitation of approximately 1500 mm per year. In Rogaland in the next 100 years, a 10% increase is expected in the annual average precipitation, as well as up to 20% increase in the amount of precipitation in periods of high rainfall (Dannevig, 2022; Klimaservicesenter, 2022).

The average annual temperature in southern Rogaland County is between 7-7.4° C. The average annual temperature here is expected to increase by 3.5° C, with up to 4° C higher in the winter months (Dannevig, 2022; Klimaservicesenter, 2022). Such changes will reduce snowfall and increase periods of melting. The area is also quite exposed to winds, as the coastal parts is a fairly open landscape facing the North Sea, although the directionality of the wind depends on the season. (Dannevig, 2022; Klimaservicesenter, 2022). In Jæren Region, the biggest waterways include the river Håelva, which is a low-lying, coastal river, approximately 20 km north of Saltatjørna, and the river Bjerkreimselva, approximately 12 km to the east. Håelva is a small meandering river by Norwegian standards, but is known to overflow under floods, as many of the riverbends are protected by raised blocks (Thomsen, 2004). Bjerkreimselva is the county's biggest waterway, and recently experienced flooding (2015), recording the highest water levels since record keeping started. This flooding event caused damages to roads and railways, and evacuation of Egersund (Figure 5). As both precipitation and snowmelt are projected to increase with climate change, so will the risk of flooding of these rivers (Klimaservicesenter, 2022).

Jæren was forested up until 2-3000 years ago, when a colder climate, combined with the appearance efficient iron axes, turned it into a heather landscape and agriculture. Which was

kept at bay by grazing animals (Thomsen, 2004). Up until the second half of the 1900s, when most of today's forests was planted, for reasons such as to stop sand drift, to create lee around fields and meadows, as well as forestry as its own purpose. The more intense green of today's grass and trees is enhanced by artificial fertilizers and animal manure (Thomsen, 2004).

2.4.3 Sea level

Future *projections*

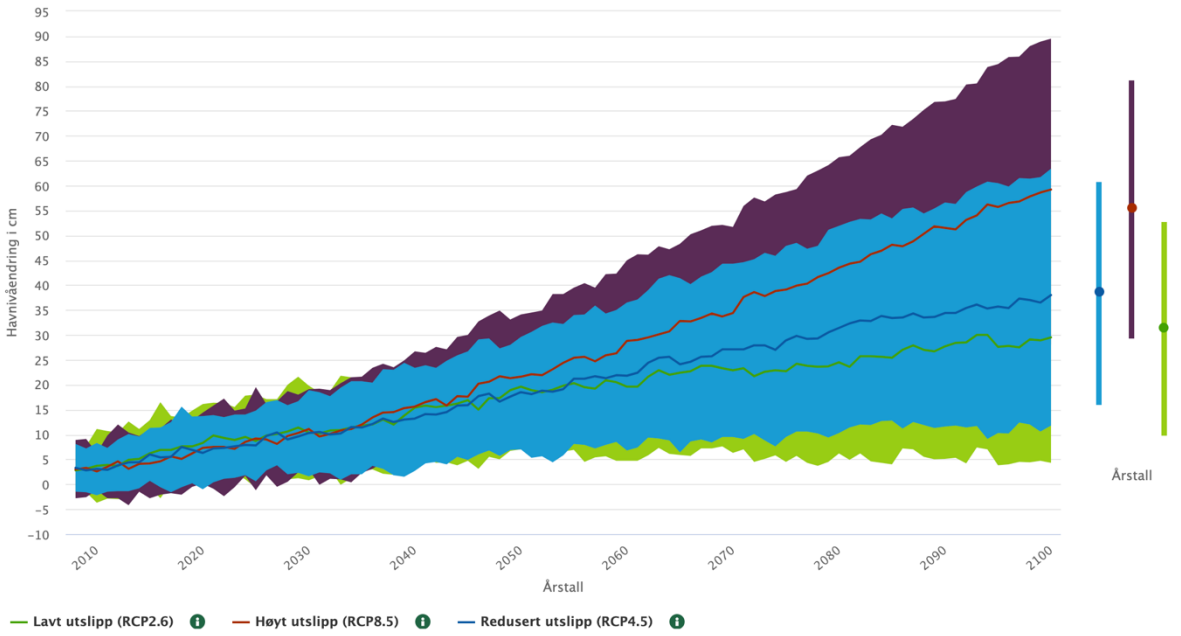

Figure 8: Projections for future sea level for Stavanger area, up to year 2100, based on three different emission rates in lines and the probable interval for the sea level change in the shaded areas (Simpson et al., 2015).

As mentioned in section 2.1.1, future GMSL will rise between 0.26 m to 0.82 m. The vertical land motion in Norway, mainly influenced by the glacial isostatic adjustment, is estimated to be between 1 and 5 mm/year, however it is likely to be in the lower range for the south/southwestern part of Norway (Simpson et al., 2015). Thus an increase in RSL be more noticed here than in the Oslo region, where the vertical motion will likely cause the RSL change to be more or less unnoticeable, especially as the coastal part of Rogaland, particularly Jæren, is fairly flat. The difference could be as much as 30 cm difference in the RSL change within 100 years. In Stavanger (figure 5), where the closest tide gauge is, the mean RSL will likely increase between 28-59 cm (figure 8 & 9) (Simpson et al., 2015). The numbers will likely be even higher if for instance, ice caps melt faster than expected and trigger a collapse in Antarctica (Kartverket, 2023).

Figure 9: A projection of how a 200 year flood will affect the study area in 90 years (Norges Geologiske Undersøkelse, 2023b).

Reconstructed sea levels

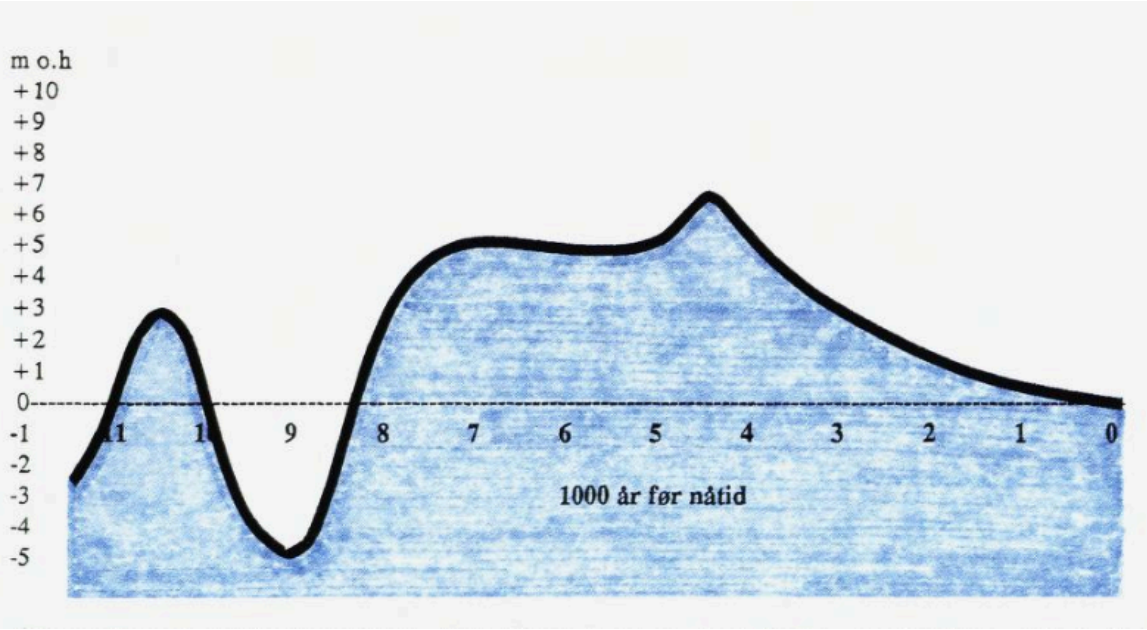

Figure 10: Reconstructed sea level curve for Hå/Jæren (Thomsen, 2004).

Figure 10 shows a simplified drawing of reconstructed sea levels in the Jæren area, that is slightly north of the study area, and that is covered in Quaternary sediments from the deglaciation (market yellow in figure 7a). RSL change here was generally due to glaciation, deglaciation and glacioisostasy (Thomsen, 2004).

Several other studies have been conducted in southern and western Norway to determine how RSL has changed since deglaciation. The one closest to this study area was conducted in Karmøy, approximately 90 km north of Saltatjørna (figure 5). Here, radiocarbon dating from two isolation basins were compared with microscopic phytoplankton, macrofossils, lithostratigraphic evidence and XRF, to determine deglaciation and date sediments (Vasskog et al., 2019). The study showed a deglaciation at approximately 18 000 cal. BP (Vasskog et al., 2019). The sea level curve (figure 11) shows several fluctuations, two above and two below present mean sea level. The first low is concurrent with the Bølling-Allerød lowstand at around 13-10 000 cal. BP, and the following rise with the colder Younger Dryas period (Vasskog et al., 2019). The second low is timed to the Holocene transition and and the second rise to the Holocene regression, known as the Tapes regression. The Tapes regression is a period in which eustatic sea level rose faster than the ongoing glacioisostatic uplift along the Norwegian coast (Romundset et al., 2009). This RSL rise was most noticed in the outermost coast where the glacioisostatic uplift was slower, up to a 20 m rise. The further inland, the less noticeable the transgression was (Svendsen & Mangerud, 1987 in Romundset et al., 2009). From around 7000 cal. BP the sea levels are falling again, and there is indication of an acceleration at 4000 cal. BP. In general, it shows that at deglaciation, the RSL was approximately between 16 and 19 m above present (Vasskog et al., 2019).

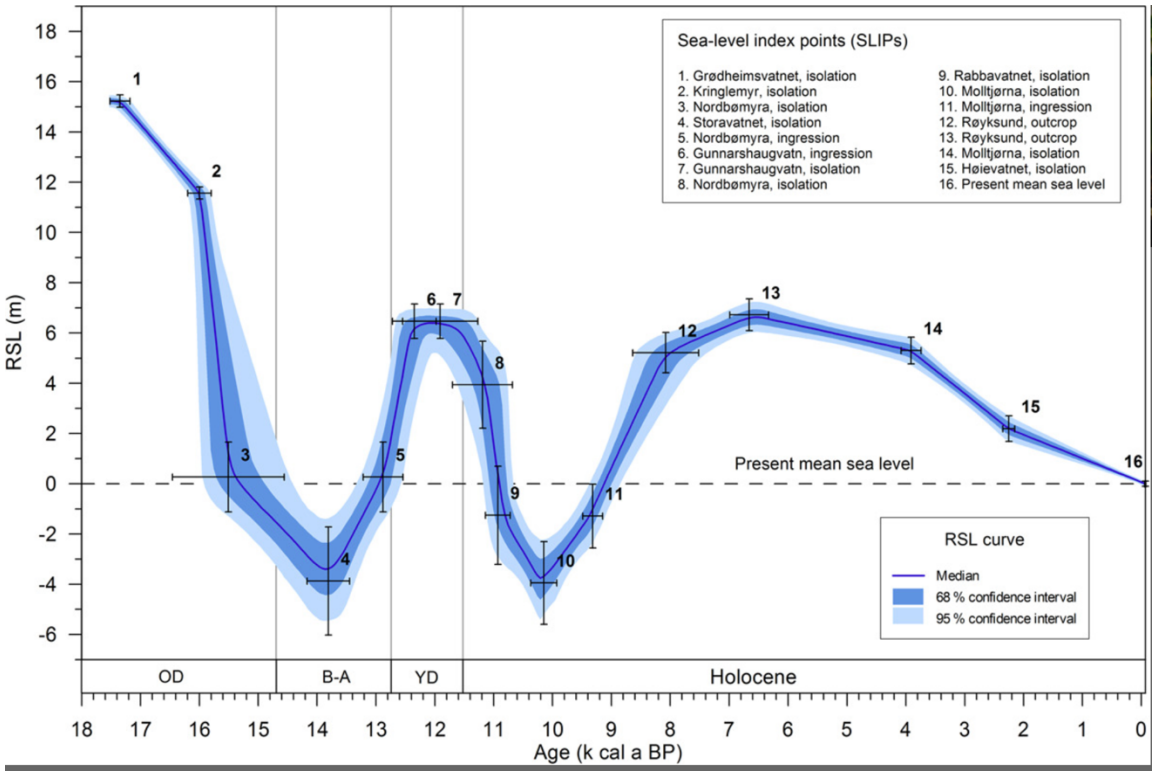

Figure 11: Reconstructed sea level curve of Karmøy (Vasskog et al., 2019).

Another study conducted in Hardangerfjorden close to Bergen, about 200 km north of the study area (figure 5), is based on macrofossils from five different raised lakes/mires, providing sea level records throughout the Holocene (figure 12) (Romundset et al., 2009). In this areas, deglaciation happened much later, around 11 500 cal BP, and as such the sea level didn't experience as many fluctuations (Romundset et al., 2009). The study also hypothesizes that the isostatic rebound was slightly delayed compared to the deglaciation, as the curve seems to indicate a lower rate of sea level emergence before 10 800, however this could also be a dating uncertainty and is not confirmed (Romundset et al., 2009). The rise in sea level was fast the first few years after deglaciation, the slowed considerably. Between 8000-6500 the emergence almost stopped, in concurrence with the Taped regression (Romundset et al., 2009). After this period the emergence again increased, until the past 1500 years where the rate has been gradually decreasing (Romundset et al., 2009).

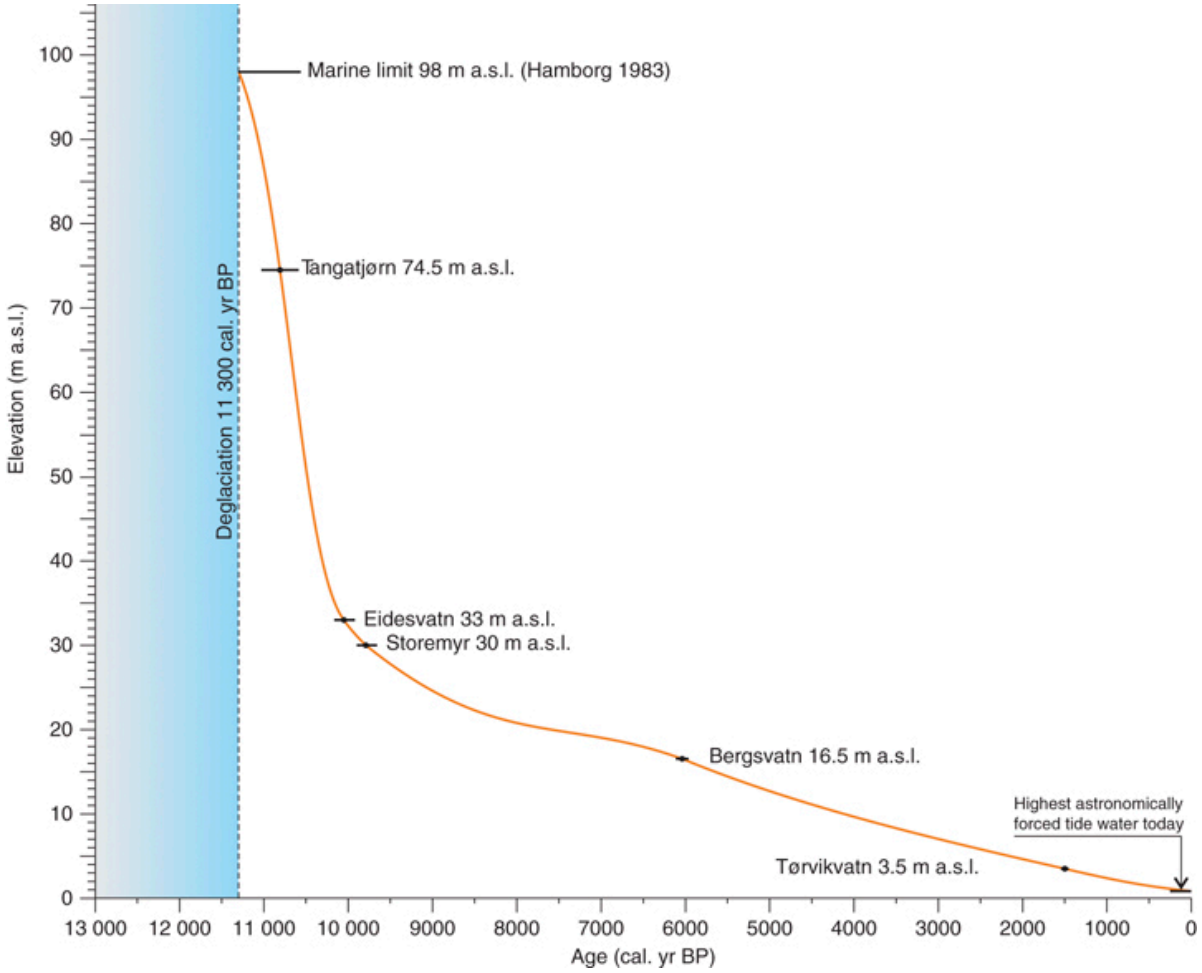

Figure 12: Reconstructed sea level curve from Hardangerfjord outside of Bergen (Romundset et al., 2009).

Finally, a study was conducted along the Skagerrak coastline, close to Tvedestrand town in southern Norway, approximately 180 km east from the study area (figure 5). This study collected sediment samples from 24 isolation basins and used radiocarbon dated macrofossils and biostratigraphy (Romundset et al., 2018). Results from this study (figure 13) shows deglaciation from 11 800 cal. BP, with a slow regression of the sea level the first 600 years, followed by a period of fast regression in the following 600 years (Romundset et al., 2018). Also here it can be interpreted as a delayed response to the unloading of the ice sheet. Also this sea level curve shows a period with close to no sea level regression from 8800-7300 cal. BP, also concurrent with the Tapes Transgression (Romundset et al., 2018). However between 7300-7100 there was a big drop in elevation, which is around the height of the Tapes transgression standstill at Lista (Romundset et al., 2018). No adequate explanation has been found for this anomaly, however the data is pretty well-documented (Romundset et al., 2018). The remaining period until today shows a steady decrease, except one short period of a few hundred years where the regression spiked. Also for this anomaly does there only exist speculations (Romundset et al., 2018).

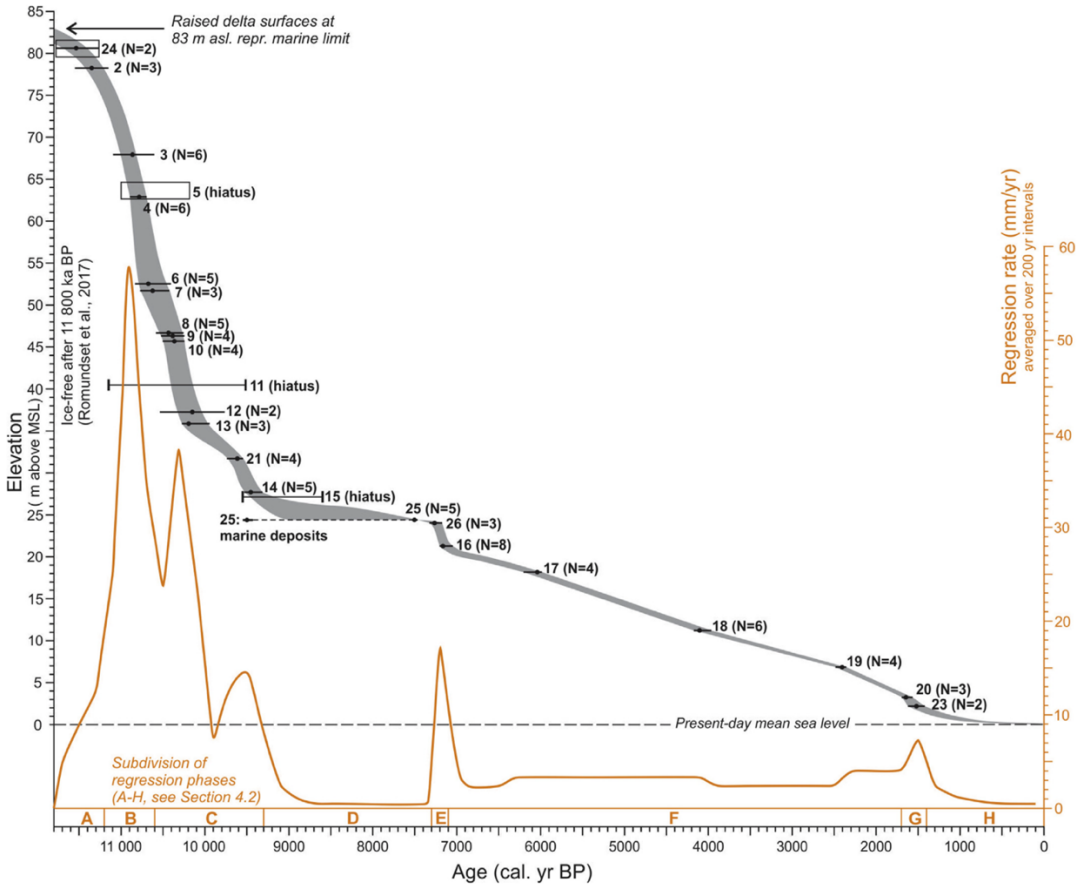

Figure 13: Reconstructed sea level curve from Skagerrak coastline, close to Tvedestrand (Romundset et al., 2018).

2.4.4 Tides

Section 2.1.2 mentions that an amphidrome point exists just outside the coast if Egersund, meaning there are practically no astrological tides there. As Saltatjørna is located approximately 12 km north of Egersund, it is safe to assume that there are fairly low astronomical tides there as well. However, the closest tide gauge, at Stavanger (approximately 55 km away), has measured as much as 90 cm difference between highest and lowest observed astronomical tide, with average differences at spring tide of approximately 45 cm reference). If the astronomical tides are close to zero, then storm surges should be easy to recognize in coastal sedimentary records. Even with the influence of astronomical tides, Saltatjørna is very protected from the North Sea via a narrow, bedrock inlet and might not experience much influence from astronomical tides either way. Current return heights for the Stavanger tide gauge are 1.01 m for 20 year return heights, 1.15 m for 200 year return height, and 1.23 m for 1000 year return height. These are among the lowest in the country, with the most extreme being in the northern half of the country. Although sea level projections for the future are uncertain, early indications show a weak increase (only 2-6%) in the storm surges of the future (Kartverket, 2023c; Simpson et al., 2015).

2.4.5 Past storms and tsunamis

There are very few records of historical storms hitting the eastern North Atlantic basin, Norwegian Sea and North Sea, although there are many paleotempestology studies from the western side of the North Atlantic basin, which is also more prone to heavier hurricanes than the Norwegian cost. Previous studies have looked into tsunami deposits on the Norwegian coast, though none of these studies were conducted very close to Saltatjørna. The biggest tsunami was cause by the Storegga landslide approximately 8100-8200 years before present (Bondevik et al., 1997; Karstens et al., 2023). This landslide happened underwater, over 450km to the north of the study area, out in the Norwegian Sea. Sediments have been discovered at Austrheim (close to Bergen, figure 5), around 260 km to the north of Jæren, that estimated a tsunami wave of 3-5 meters. (Bondevik et al., 1997; Bondevik et al., 1998). Other studies have found signs of a tsunami like events approximately 2000-2200 years ago, likely caused by an earthquake on land, or close to the coast, in western Norway (Møre region) (Bøe et al., 2002). Another study at Lista (figure 5) in southern Norway has documented a sedimentary layer that may have originated from a tsunami, although it is still missing a few classic markers, such as an erosional lower boundary, grading of the deposit and redeposited debris above the gravel

layer (Romundset et al., 2015). The grading for intendance, is a expected as the wave has different settling velocities, with decreasing energy, cause a fining of deposits upwards (Romundset et al., 2015). However, this event would have occurred in southernmost Norway approximately 5500 years before present, which would coincide with the Garth tsunami that has been documented in Shetland (Romundset et al., 2015).

2.5 Analytical concepts

2.5.1 Loss on Ignition

Loss-on-ignition (LOI) in sea-level research is a widely applied method for analyzing the organic and carbonate elements of sediment samples (Plater et al., 2015). LOI measures the remaining inorganic material after dried sediment is ignited for a specific period of time at a specific temperature (Heiri et al., 2001). Soil and sediments from most environments comprise minerogenic sediments like sand, silt or clay, as well as organic matter, carbonates (biogenic sediments), and water (Veres, 2002). Since most organic matter oxidizes at approximately 500-550 °C, the amount of organic material in a sample can be calculated from the weight of a dried sample before and after the samples are ignited (Heiri et al., 2001).

$$\mathrm{LOI}_{500°C} = \frac{mass_{105°C} - mass_{500°C}}{mass_{105°C}} x100$$

The standard LOI method includes placing a few grams of sediment or soil in heat-resistant ceramic crucibles, drying them in an oven at 105 °C to remove any moisture, placing them in a muffle furnace, and igniting them at 475-550 °C for 2-3 hours (Heiri et al., 2001; Plater et al., 2015; Veres, 2002). The samples are weighed before drying, after drying and after ignition, and using the formula above, the percentage of organic material is calculated. $LOI_{500°C}$ represents loss of sample after ignition as a percent of the total sample, where $Mass_{105°C}$ is the weight after drying, and $mass_{500°C}$ is the weight after ignition, in grams.

The specifics of the LOI method varies somewhat in the literature, usually in terms of how long samples are dried and/or ignited for, at what temperature, and for how long (Heiri et al., 2001; Plater et al., 2015).Some studies, for example, have shown that larger samples with a high percent content of organic matter require more than 2-3 hours for full combustion of organic material, while smaller samples need less (Heiri et al., 2001; Plater et al., 2015).

However, as LOI is strongest in the first 2-2.5 hours, many use this as an initial limit (Heiri et al., 2001; Plater et al., 2015).

The temperature of the muffle furnace can also be adjusted for the type of sediments being analyzed, as clay may lose structural water at 500 °C, metal oxides might lose structural water at 280-400 °C, inorganic carbon can be lost between 425 and 520 °C, and volatile salts at 550 °C (Heiri et al., 2001; Plater et al., 2015; Veres, 2002). The position of the samples in the furnace may also affect LOI results as samples placed in the center can experience warmer temperatures than those located along on the edges, and too many samples per batch can cause cross-contamination (i.e. floating ash settling in different crucibles) (Heiri et al., 2001).

If loss on ignition is applied to sedimentary strata, that for instance is retrieved using a coring device, it can provide information about climate and environmental change in the past. The best places to find continuous sedimentary records that can be cored include lakes, mires and coastal basins (Plater et al., 2015). From LOI data, information on accumulations rates, ecosystem production, decomposition, shrinkage, compaction, water-level changes, and carbon cycling can be deduced (Plater et al., 2015). LOI can also give indications of "terrestrialization", or subtle or temporary changes that might not be obvious using other methods (Plater et al., 2015). The percentage of the organic matter after LOI gives us information about how organic rich the local environment was and, by examining core samples through stratigraphic sequences, if this changed through time. If the organic content increases through time for example, this can indicate an environment that experienced favorable conditions for plant growth, possibly a warmer and wetter climate; if organic content decreases, this may indicate a switch to a less favorable climate for plant growth (Heiri et al., 2001; Plater et al., 2015).

Loss on ignition has been used in many sea level studies to support other proxy data that indicate a transition from freshwater to marine conditions. Field-based assessments from transitional stratigraphic evidence of the boundary between fresh water and marine deposits is more commonly used where available, and LOI is often reserved as a follow-up laboratory analysis (Heiri et al., 2001; Plater et al., 2015). In a saltmarsh, for example, which grow in low-energy, intertidal zones up to the highest level of tidal inundation, organic-rich, peat sediments accumulate. At the highest water-levels, which is at and above the upper limits of tidal influence, organic sediments accumulate, and becomes gradually more inorganic further down the intertidal zone. In the lowest part of the tidal zone, where the tidal flooding is longer and

more frequent, the sediment tend to be mostly inorganic, as the constant flooding will prevent the survival of terrestrial plant growth (Heiri et al., 2001).

The position in the intertidal zone called transgressive overlap, where organic sediments such as Phragmites or monocotyledonous peat transition to minerogenic deposits, can be used as an approximations of water level of mean high water spring tide - 20 cm, +/- 20 cm (Plater et al., 2015).

In salt marshes, regressive overlap occurs where marine influence is decreased and minerogenic sediments are replaced by organic deposits. If the organic deposits are Phragmites or monocotyledonous peat, this gives an indication that sea level is M^1-20 cm (where M^1 is the average of highest astronomical tide and mean high water of spring tide) (Plater et al., 2015). Minerogenic sediments are a common deposit in saltmarshes, Loss on ignition has been used to identify lithological changes related to sea-level rise in salt marsh environments (e.g. Woodroffe, 1991; Parkinson, 1989; Larcombe and Carter, 1998).

Shennan et al. (1996, in Plater et al., 2015), showed that in the transition from marine organic clay sediments to overlaying freshwater sediments, LOI will increase from 4-8% to 33-52%. Another study by Zong et al. (in Plater et al., 2015) showed that following earthquakes in Alaska and the concomitant submergence of saltmarshes (due to vertical downward motion of coastal areas affected by the earthquake), LOI decreases from 40% to 10-20%.

Shaw et al. (in Plater et al., 2015) showed a correlation between microtidal saltmarshes and elevations and distance across the saltmarsh. The study documented a decreasing trend in LOI towards the seaward edge, showing a clear distinction between the upper and lower environments of the saltmarsh (with LOI values of 60% for the upper levels and 25-40% for the lower levels). As for depth, the values of LOI are low (less than 10%) in the area further down-core than 20 cm. Between 20 and 11 cm there are values around 25% and the upper 8 cm have values between 70 and 80% (Shaw et al. 2012 in Plater et al., 2015).

2.5.2 XRF

X-ray Fluorescence (XRF) is a method of scanning a core with X-ray radiation . During XRF scanning, an electron is ejected from the inner shell of an atom after being excited by a primary X-ray source which is followed by an outer electron filling this now-vacant spot (Richter et al., 2006). The energy difference between these two shells is emitted as electromagnetic

radiation of different wavelengths (fluorescence). This wavelength holds specific characteristics for each element, and thus XRF results will reflect the concentration of elements present in a sediment or soil sample. XRF is a rapid method for identifying the elements present in a sediment or soil sample (in many cases, a sediment core, but hand-held XRF scanners can be used on rocks and individual soil or sediment samples) (Richter et al., 2006). Of the 60+ elements that can be scanned using XRF identified in Rothwell and Croudace (2015), the properties of the nine which are used in this analysis (Ca, Si, Cl, K, Ti, Fe, Br, Sr, Zr) are described below.

Calcium

Calcium (Ca) is an element of the second group of the periodic table, meaning an alkali earth element (Salminen et al., 2006). Ca is very abundant in the continental crust and forms several minerals (Salminen et al., 2006). Anorthosite, for example, which is abundant in the study area (Figure 7), consists mainly of calcium-rich plagioclase feldspar, and thus is abundant of calcium (Salminen et al., 2006). Calcium carbonate is also a proxy for oceanic productivity and a common indicator for marine influence. Amounts of calcium is typically less during glacial periods and higher during interglacial periods, and thus it forms a good basis for constructing stratigraphic frameworks for the Quaternary on timescales of thousands to hundreds of thousands of years (Richter et al., 2006).

Iron

Iron (Fe) is part of the eight group in the periodic table of elements, and is abundant on Earth, both as an element, and as a metal (Salminen et al., 2006). It forms much of the inner and outer core, and is as such, abundant in mafic rocks (Salminen et al., 2006). Iron is useful in XRF studies to decipher changes in terrigenous sediments supply (Rothwell & Croudace, 2015).

Ca/Fe

Ca can especially in combination with Fe show the ratio between biogenic carbonate and terrigenous material (Richter et al., 2006; Rothwell & Croudace, 2015). Ca may form from detrital or biogenic origins, where the detrital origins may be determined by anti-correlations with Fe, to see if the terrigenous supply indicated by Fe correlates with the marine origins of Ca (Richter et al., 2006; Rothwell & Croudace, 2015). In areas with carbonate bedrock, detrital origins are indicative of estuarine environments (Rothwell & Croudace, 2015). A possible

limitation of interpreting Ca in XRF readings is that the levels might reflect dilutions of terrigenous material rather than changes in productivity (Rothwell & Croudace, 2015). However, as this thesis does not go back to interglacial/glacial timescales, the most useful application of Ca in XRF data is to measure changes in the amount of marine plankton (with calcium carbonate tests) that have been deposited in coastal basins. Since brackish environments (e.g. coastal ponds) are inhabited mainly by zooplankton with non-calcareous tests, an increase in Ca can indicate an influx of zooplankton from open marine environments during, for example, a storm or tsunami, or, over the longer term, due to relative sea-level rise (Edwards & Wright, 2015).

Strontium

Strontium (Sr) is another element of the second group of the periodic table and is chemically similar to Ca (Salminen et al., 2006). The biogenic and detrital origin of Ca can be distinguished together with Sr (Ca:Sr) (Rothwell & Croudace, 2015). Since Sr levels are fixed by calcifying organisms at the same time as Ca, it can be used as another marker for biogenic material. Sr can be used to distinguish foraminiferal calcite and coralline aragonite, for example in cold-water carbonate banks (Richter et al., 2006; Rothwell & Croudace, 2015).

Bromine (Br)

Bromine (Br) is a halogen element that does not occur naturally on its own, but rather occurs as compounds in different crustal rocks (Rothwell & Croudace, 2015; Salminen et al., 2006). Bromine is a very good indicator of marine organic matter, as terrestrial organic matter is not very strong in Br, whereas sediments formed in saline environments have much higher levels of Br (Rothwell & Croudace, 2015; Salminen et al., 2006). Bromine is thus, a good proxy for delineating marine vs freshwater sediments. One study indicated that Br contents of more than 200 cps/s (counts per second) signify that the organic matter was marine rather than from freshwater (McHugh et al., 2008 in Rothwell & Croudace, 2015). Together with other proxy data, Br is a very good indicator for tracking sea-level changes (Rothwell & Croudace, 2015).

Zirconium

Zirconium (Zr) is another metallic element, that also forms a number of resistant minerals (Salminen et al., 2006). It is abundant in the crust and appears in igneous rocks. Zr can be used to distinguish tephra and is often high in ash layers (Rothwell & Croudace, 2015).

Chlorine (Cl)

Chlorine (Cl) is another halogen element and occurs mostly in oceanic rocks (Salminen et al., 2006). Together with Br, the ratio of Cl:Br can be used as an indicator of salinity contribution in lakes (Salminen et al., 2006).

2.5.3 Radiocarbon dating

Radiocarbon dating is a very common method for absolute dating of organic material. The radioactive isotope ^{14}C, which is the result of a reaction, are rapidly oxidized to carbon dioxide and is thus stored in various global reservoirs, mixed in the atmosphere, biosphere and hydrosphere, and absorbed by both the oceans and by all living organisms (Hajdas, 2008; Lowe & Walker, 2015). As ^{14}C is continually produced, and all living matter absorbs CO_2, then the living organisms will continuously use ^{14}C to build new tissue, which will be in isotopic equilibrium until the organism dies (Hajdas, 2008; Lowe & Walker, 2015). When it does die, the ^{14}C amount will decompose without a substitution. Thus the date of death can be determined from the amount of ^{14}C (Hajdas, 2008; Lowe & Walker, 2015). ^{14}C has a half-life of 5570 +/- 30 years, as the internationally agreed on constant, expressed in years before presents, in which the present refers to 1950 AD (Hajdas, 2008; Lowe & Walker, 2015). The age of the organism can only be dates as long back as the half-life allows, and after approximately 55 000 years, the ^{14}C is no longer present, thus limiting the dating to after that time (Hajdas, 2008).

As the amount of ^{14}C is very small (1: 1 000 000 compared to ^{12}C) and also emits very low-energy b particles, and therefore very sensitive equipment is required (Lowe & Walker, 2015). Two methods are often use to measure the remaining ^{14}C in order to date it: Radiometric dating or accelerator mass spectrometry (Lowe & Walker, 2015). Radiometric dating detects and counts the b emissions from ^{14}C, either in gas or liquid variation, and uses the emission time to calculate the activity of the sample (Lowe & Walker, 2015). Accelerator mass spectrometry (AMS) uses mass spectrometers to count the isotope ratio of ^{14}C compared to ^{12}C and ^{13}C, which are more stable (Lowe & Walker, 2015). The age is calculated by comparing this ratio to a stand of know content. AMS is often considered more favorable, as it can count smaller samples and usually take a lot less time, however it is a more costly method (Lowe & Walker, 2015).

3 Methods

3.1 Fieldwork

The fieldwork for this study was conducted by Chantel Nixon, Max Holthuis, Jake Martin, and Maria Peter (Institutt for geografi, NTNU) in June 2020 and August 2021. Saltatjørna was selected as a study site because it is a low-elevation (intertidal) basin, connected to the North Sea by a narrow, bedrock channel, and contains several fringing salt marshes inside the basin (Figure 6). Collectively, these characteristics increase the likelihood of finding clear signals in salt marsh sediment cores for recent and past RSL change, whether rapid and temporary (e.g. storms and tsunamis), or longer-term, semi-permanent changes due to climate-related sea-level change.

Fieldwork at the Saltatjørna coastal pond included extracting sediment cores from a fringing saltmarsh along its inland edge (Figure 6) using a Russian-style coring device. Two, cores were extracted from the same borehole (from the surface to 1.72 m below the surface): SALTA2.1 and SALTA2.2. Following the extraction, photographing, and wrapping of the first 1 m of core, the Russian corer was sent down the same borehole and another 1 m core was extracted. However, the corer itself did not reach 2 m depth, but rather 1.72 m where it could not be pushed down any further due to some impenetrable layer such as wood, sand, gravel, or bedrock. As the core barrel of SALTA2.2 was filled with a full, 1 m of sediment, the upper 30 cm of SALTA2.2 was determined to either overlap with the lower 30 cm of SALTA2.1 or loose sediment that had fallen down inside the borehole was captured inside the corer during closing of the chamber. As such, the upper 30 cm of sediment inside core SALTA2.2 is not included in the analysis.

The elevation of the sill (i.e. the tidal inlet) between Saltatjørna and the open ocean (the North Sea) was surveyed using an Altus APS3 GNSS rover connected to CPOS (a Real-Time Kinetic (RTK) positioning service in Norway that gives positioning data with centimeter accuracy and avoids the need for setting up a local base station). The upper (inland) edge of the wrack zone (defined in this study as the zone above mean high tide where marine organic and plastic debris (for example, seaweed and fishing industry debris such as ropes and net floats) become stranded and accumulate) was also surveyed with the Altus GNSS rover. Elevations are reported according to the vertical datum NN2000.

Once the sediment cores were collected, they were labelled, wrapped in plastic film, placed in thicker plastic core bags, and transported to Norges geologiske undersøkelse refrigeration facilities in Trondheim where they were kept at 4° C until follow-up lab work could take place.

3.2 Lab Analyses

3.2.1 XRF imaging and processing

To obtain XRF data on the cores from Saltatjørna, an ITRAX core scanner (CS-XRF) was used. The core scanning occurred in November 2020 at the Earth Surface Sediment Laboratory at the University of Bergen. Before scanning, the core surface was cleaned (i.e. the upper 1 cm of sediment was carefully scraped off and evened out to create a flat surface) and then covered with thin microfilm foil to avoid contamination during scanning, cross-contamination of the core surface, and drying of the core surface during the scan. The scanner was outfitted with a Molybdenum (Mo) X-ray tube and scanned at 29 mA and 29 kV. Each scan had an exposure time of approximately 10 seconds per 1 mm.

After the scan, a selection of elements (Ca, Sr, Fe, Br, Zr and Cl) were selected from the results, and processed using the centered log-ration (clr) transformation, as done by Weltje et al. (2015). This step is taken to normalize the elemental composition data, minimizing the effect from moisture content, organic matter content and sensor drift in the data. The elements were selected based on their average counts per second (cps), only including those with an average of more than 300 cps. This to ensure data quality of each elemental measurement. After that the elements with the most relevant properties to this thesis were selected from those with a high enough cps.

3.2.2 LOI

The lab work for this thesis started on the 31st of January, in the Physical Geography Lab at Dragvoll campus, NTNU. Four visually distinct layers comprised mainly of shell fragments and one with gravel and sand were observed in the field in SALTA2.1 and SALTA2.2 and are the main focus of this thesis. These layers are henceforth referred to as shell layers (or sandy-gravelly layer in the case of the latter).

SALTA2.1 was sampled for LOI every 1 cm for the upper 10 cm, every 1 cm through each shell/sandy-gravel layer, plus 5 cm above and 5 cm below each of the shell/sandy-gravel layers.

This was done to capture any variability in organic content of the sediments before, during, and after the events that resulted in the deposition of the shell and sandy-gravel layers. The sampling intervals were measured using a wooden measuring tape placed beside the cores, and an empty syringe with the tip cut off and a small spatula were used to extract sediment samples from the cores at the desired depths. The syringe was used to minimize variability in volume of samples. Each sample was then placed in a numbered, pre-weighed crucible, and weighed.

Once the samples were weighed, they were placed in a drying oven at 60° C. This varies from the recommended temperature of 105°C for 24 hours as the available oven was unable to reach a higher temperature. Samples stayed in the oven for 3-4 days at this temperature. After drying the samples were weighed again and then placed in a Nabertherm Muffle Furnace. The temperature of the furnace was set to 475 deg C, and the samples were in it for 8 hours. Up to 12 samples were placed in the muffle furnace at a same time. Once cooled in the oven, samples were then re-weighed. The following formula for calculating LOI was used, as per (Plater et al., 2015):

$$\mathrm{LOI}_{500°\mathrm{C}} = \frac{mass_{105°\mathrm{C}} - mass_{500°\mathrm{C}}}{mass_{105°\mathrm{C}}} x100$$

3.2.3 Computed Tomography (CT) Scanning

A ProCon Alpha Core CT scanner performed helical scans of SALTA2.1 and SALTA2.2 cores at the Earth Surface Sediment Laboratory at the University of Bergen. Fraunhofer Volex and FEI Avizo 3D software were used by a technician (J. Magne, University of Bergen) to process the CT scan images such that shells, shell fragments, and sediment grains larger than medium sand were shown in color.

4 Results

4.1 Saltatjørna

Saltatjørna is a brackish coastal pond that has a narrow tidal inlet. The low-gradient edges of the pond are occupied by fringing saltmarshes, while the rest of the shoreline consists of steep rocky cliffs. Based on an inspection of all available aerial photos on norgeibilder.no from 1967-2019, it is clear that the fringing salt marsh in Saltatjørna did not exist 50-60 years ago and seems to have started growing since the late 1990s or early 2000s (figure 14). The area has also clearly become much more forested since 1967. In summary, trees and other vegetation, including small salt marshes, have grown in around the edges of Saltatjørna in the past 56 years.

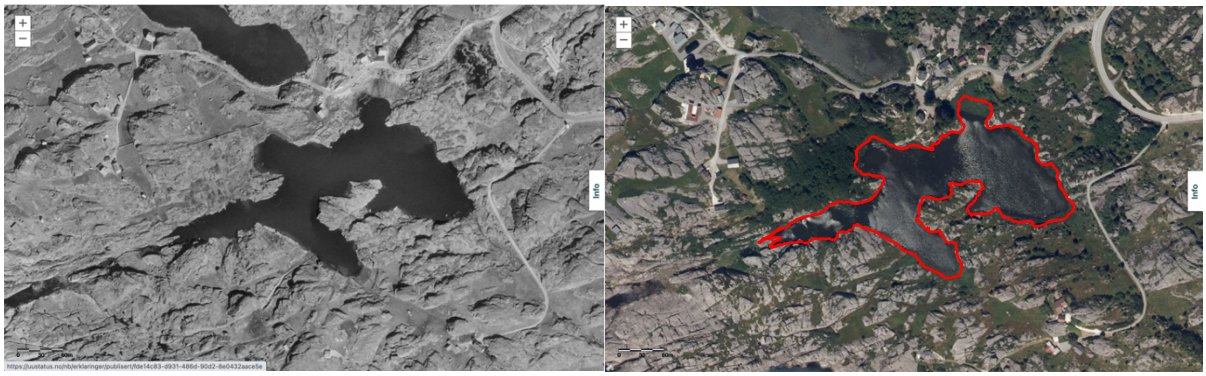

Figure 14: Aerial photos from 1967 and 2019, comparing amount of vegetation and fringing marsh in the area. The red line marks the outline out the old pond (Kartverket, 2023a).

Because of a micro tidal range in this area and the elevation of the sill below the narrow tidal inlet connecting Saltatjørna to the North Sea, it was considered likely that Saltatjørna received little input of seawater on a daily basis, and storms large enough to fully breach the sill and flood the pond would only occur during bigger storm-surges. As mentioned in section 3.1, the elevation of the sill in the tidal inlet was measured, the location of which can be seen in figure 15a and figure 16. The wrack line at the inland end of Saltatjørna, which is the upper limit of marine debris that is deposited during storms, etc., was also surveyed (Figures 15b and 18).

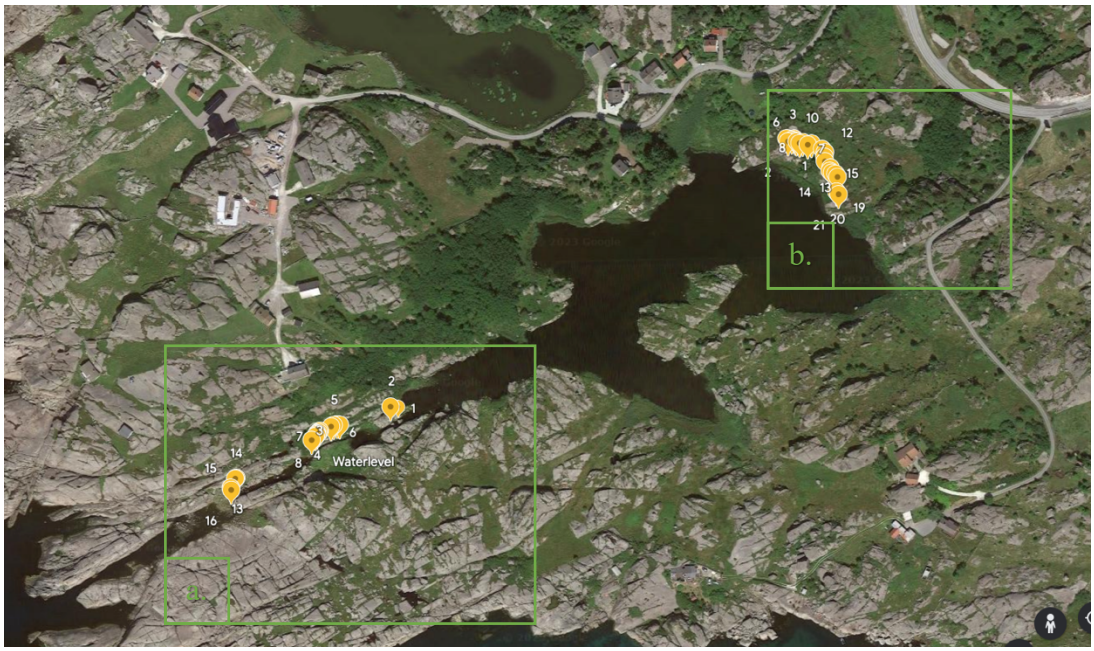

Figure 15: Overview photo of the sill elevation and wrack line surveys in the study area (Google, n.d.).

4.1.1 Sill profile

The elevation of the sill profile includes 16 measurements along a transect (measurements taken in the center of the channel). Locations of the elevation measurements are shown in figure 16 and results shown in figure 17.

Figure 16: Close up of the spread of sill profile locations (Google, n.d.).

In figure 17 it can be seen that the elevation farthest inland is very close to zero, with a maximum elevation of 10 cm and minimum -17 cm, except the last five points which were taken much closer to the open sea (figure 14).

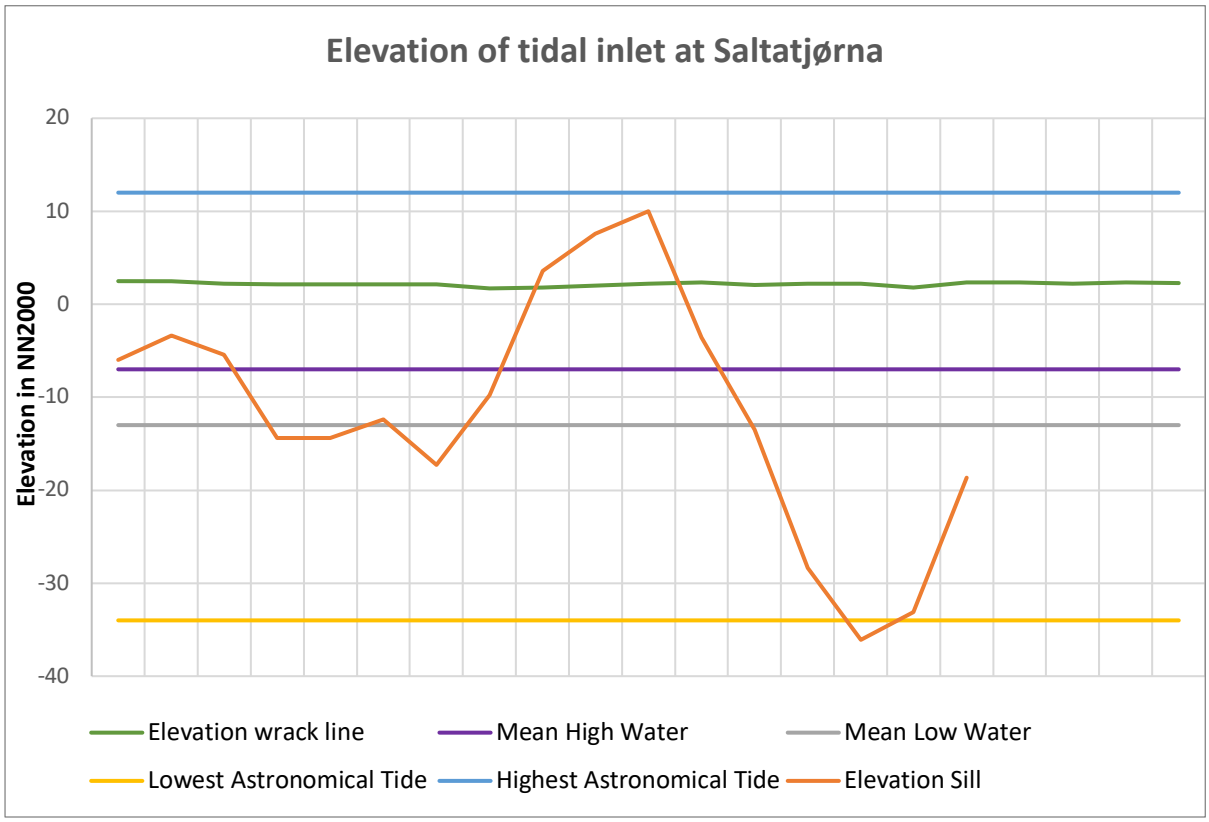

Figure 17: Graph of sill profile elevation, with tidal water levels and wrack line.

4.1.2 Wrack line

A wrack line was clearly visible at the back of Saltatjørna near where the cores were taken and which can be seen in figure 18. Here marine debris, such as plastic floats, ropes, and other fishing equipment, as well as seaweed (which does not grow inside Saltatjørna) has been deposited during a recent storm, much above the normal water levels. The wrack deposit overlies and sits above terrestrial vegetation, which would not exist if the area was continually flooded. Figure 19 shows the GPS points in the survey of the wrack line and figure 20 displays the elevations of the points.

Figure 18: Photos from the study area, showing the deposited debris.

Figure 19: Close up of the spread of wrack line locations (Google, n.d.).

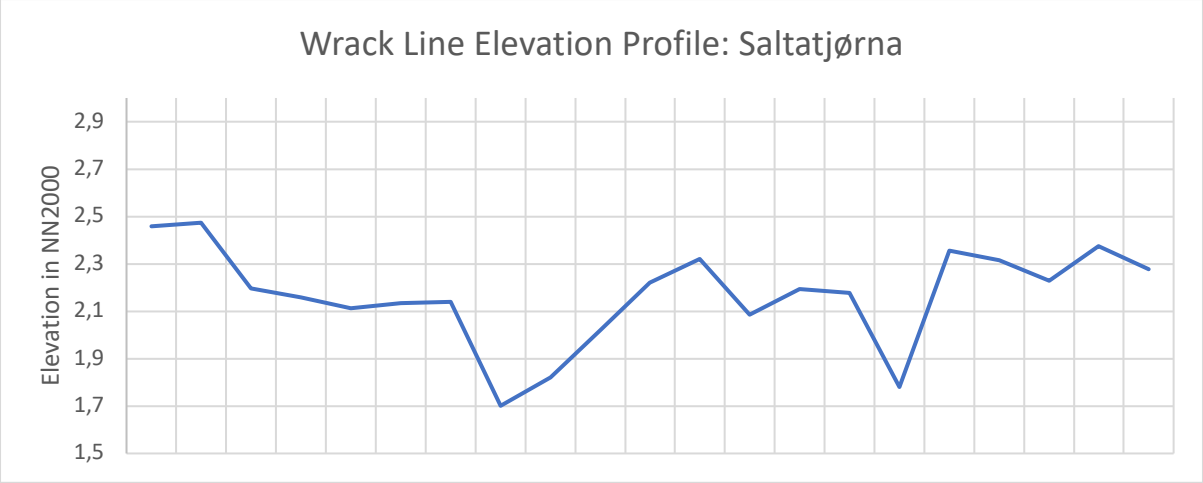

Figure 20: Graph of wrack line elevation

4.2 Imaging

Figure 21: Sketch of the stratigraphy with descriptions

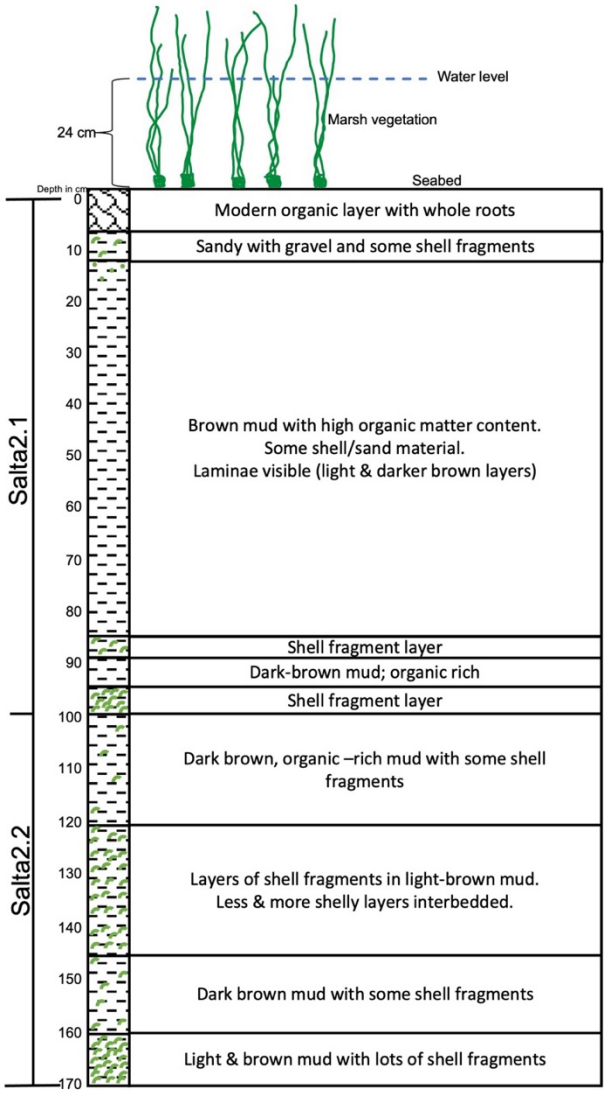

Different images was taken of the whole 2 m of sediment cores, however, as the SALTA2.2 core only actually went to a depth of 70 cm, the top 30 cm of that core are not included in the results. An adjusted image has been created below in figure 21, where the full 170 cm of stratigraphy below the fringing salt marsh at the inland end of Saltatjørna with description is shown.

Figure 22 consists of three images of each of the cores, one photograph, one CT scan and one ortho scan. The pictures represent 2 m of sediment core. In the photograph, some layers with abundant white specs are clearly visible, which are the broken shell layers, presumably deposited during a storm, and are the main focus of this thesis. The images have been separated into sub-sections based on the broken shell layers and other strata.

The CT scans show the shells and gravel mostly as red or white, standing out clearly from the organic-rich mud that makes up most of the core stratigraphy.

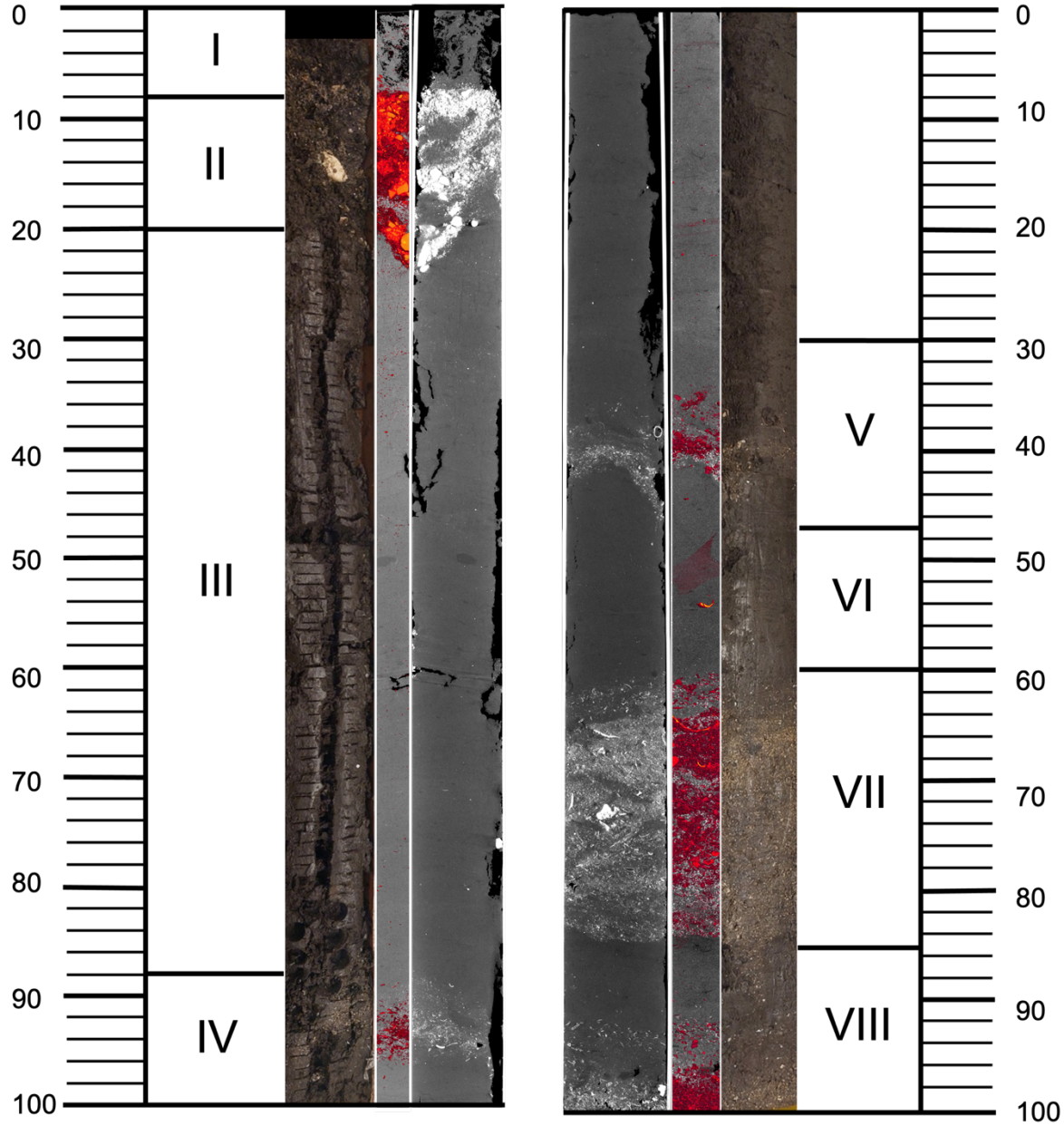

Figure 22: Photographs, CT scans and ortho scans, together with a scale and the separate sections. The CT scans shows air as white, grey low-density, fine-grained, organic-rich sediments, and red as shells, shell fragments, and sediment particles larger than medium sand. The more orange and orangey-red particles that occur towards the top of SALTA2.1 are gravel and coarse sand.

4.3 Salta2.1

4.3.1 Core stratigraphy

The top core was divided into 4 segments. The first segment (I) extends from approximately 0 (surface of the salt marsh, which was under 24 cm of brackish water at the time of coring) to 9 cm down core. Segment I consists mostly of newer organic matter and whole roots.

The second segment (II), which occurs from 10 - 20/25 cm, contains abundant sand and gravel, as well as a few whole shell fragments embedded, most notably a very large subangular fragment. This fragment was approximately 3 cm long and 1,5 cm wide and occurred between 14-17 cm core depth. The transition between segment I and II two segments is abrupt in the scanned images. The transition between segment II and III is more gradual. The sediments seems to change at 20 cm, however some of the larger pieces of gravel continue all the way to 35 cm.

Segment III is a 68 cm long section of brown, organic-rich mud. Some scattered shell fragments were observed in Segment III. This section also shows visible laminae with lighter and darker brown layers. Segment III ends right above a broken-shell layer (Segment IV). The contact is somewhat gradational.

Segment IV is 12 cm, extending from 88 cm to the base of the core (100 cm). This shell layer consists of many small (< 10 mm) fragmented shells in a matrix of brown, organic-rich mud. A close up of the CT scan of this shell layer is shown in figure 23 . Here the forms of different shells can be seen clearly, with some indication of fining upwards (i.e. shell fragments become less dense as you move up in the core). Some of the shell fragments appear to come from gastropods (single, spiraling shell), while others appear to come from bivalves (two, somewhat flat, rounded shells joined together by a hinge).

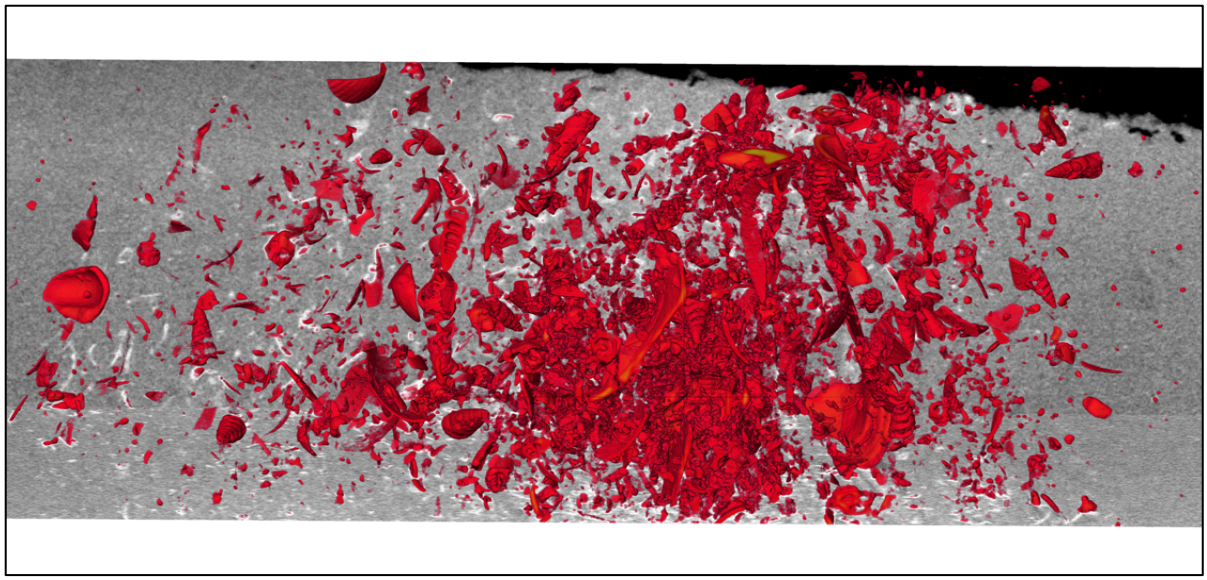

Figure 23:: Close up CT scan from Salta2.1, at around 87-97 cm depth.

4.3.2 Core diagram and XRF measurements

Figure 24 shows Salta2.1 and changes in relative abundances of Sr, Ca, Br, Fe, and loss on ignition (LOI; percent organic matter); the latter only for some parts of the core. This diagram clearly shows that certain changes in the XRF measurements coincide with the broken shell and gravelly sandy layers. Segment II shows two spikes in Ca and Sr. simultaneously, as Br dips almost identically to the Ca spike, as well as a smaller dip in Fe. This segment has less than 15% percent organic matter, with the rest of the samples being minerogenic. Segment III ,which is mostly brown mud, shows very stable readings in all elemental proxies, except for a small spike in Ca at around 80-85cm depth. Segment IV and second shell layer again shows a big spike in Ca, a simultaneous, but smaller spike in Sr, as well as small dips in Br and Fe, with a more significant dip in Fe in this segment.

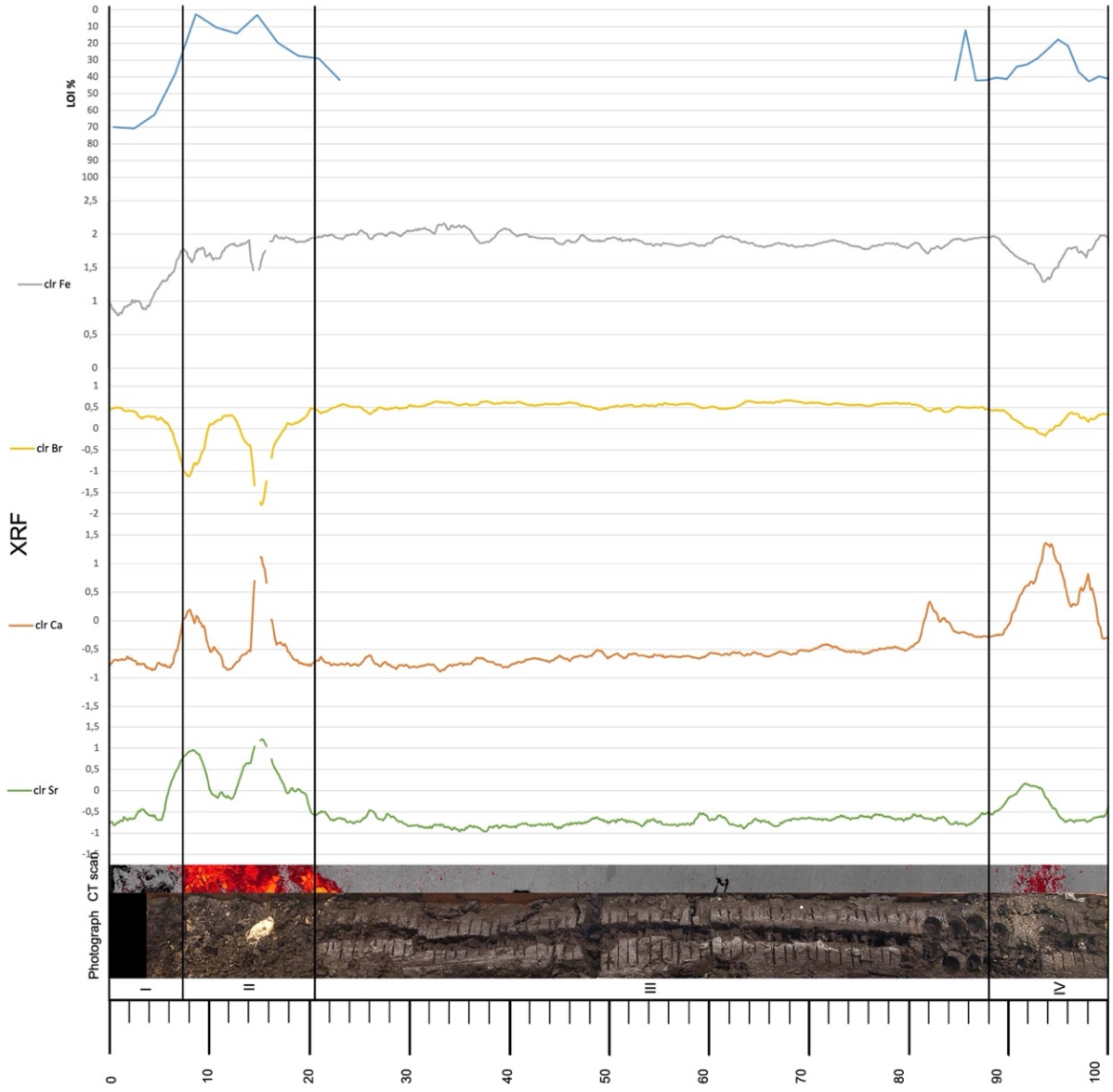

Figure 24: Core diagram from Salta2.1, consisting of scale-bar, photograph, CT scan, XRF results of Sr, Ca, Br and Fe, and LOI % .

Figure 25 is an extract of the elemental proxies that dips during the shell layers, and also includes the values for Cl and Zr, in addition to Fe and Br. Here the difference in the variation of the first shell layer in Segment II is much more apparent, where Br shows a decrease of 2.5, whereas Fe is approximately 0.5. Cl and Zr behave in a similar matter, with simultaneous dips of around 1 at 15 cm down core. The second shell layer in Segment IV is much more clearly defined, with all the elements making a simultaneous dip of around 0.5. In figure 26, which shows the elements that spike, the trend seems to be opposite, with the spikes are more coincident in Segment II, and differ more in Segment IV. The two spikes in Segment II are around 1.5-2 for both Ca and Sr, whereas in Segment IV, Ca spikes by 2 and Sr by 0.5-1.

Furthermore, Sr makes a tiny dip concurrently with the spike in Ca that occurs just above Segment IV, at around 85cm depth.

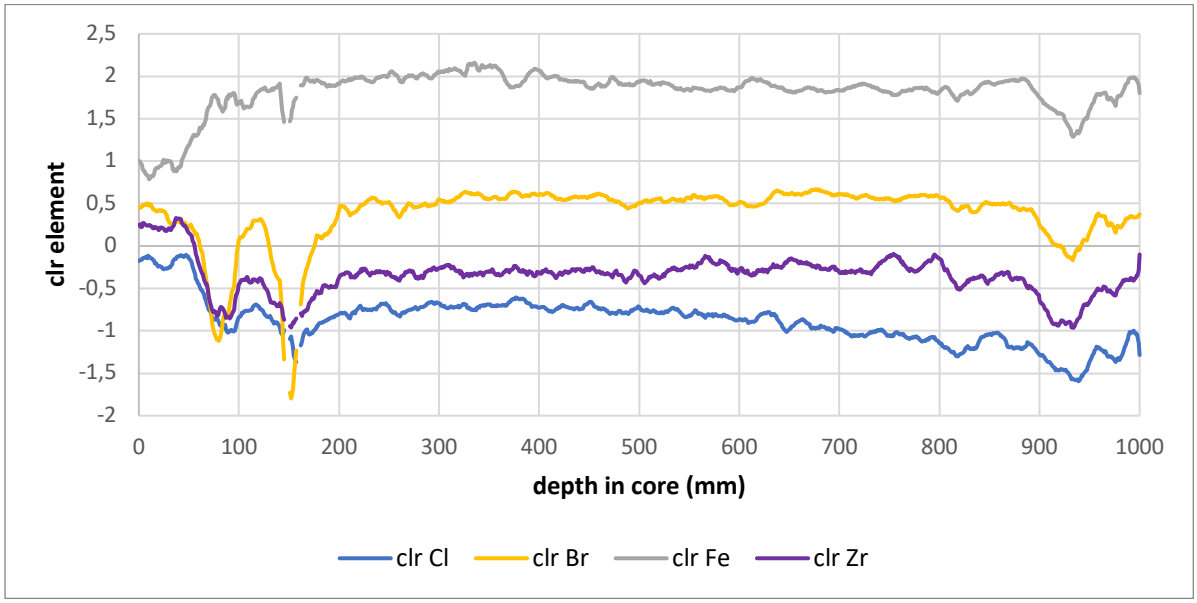

Figure 25: XRF results of Cl, Br, Fe and Zr.

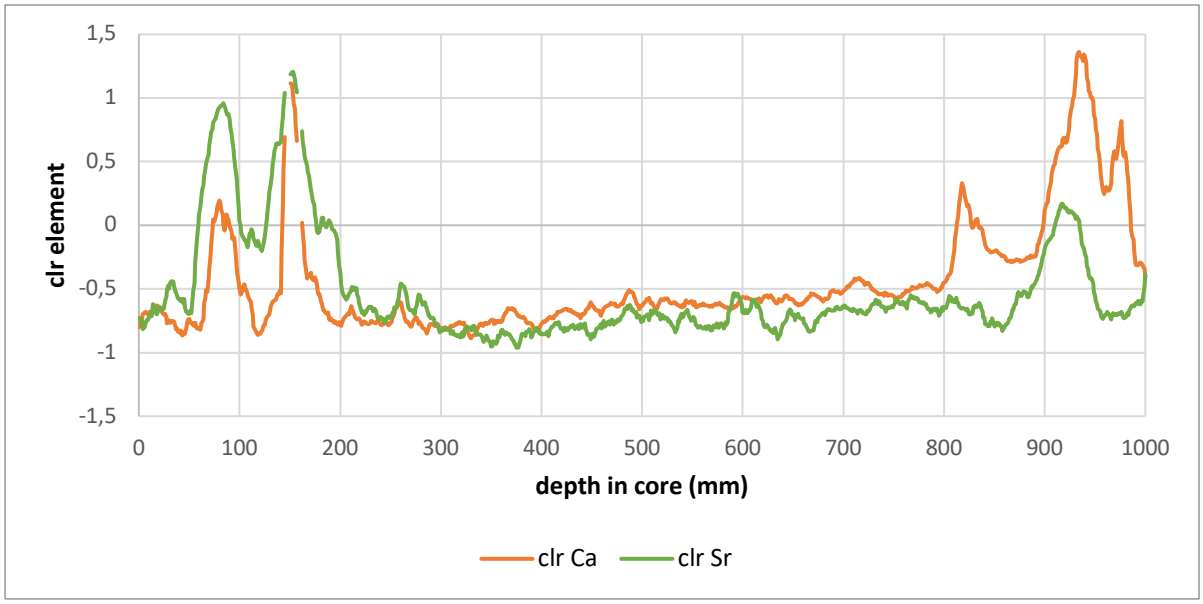

Figure 26: XRF results of Ca and Sr.

4.3.3 LOI

The percent of organic content is greatest in the upper 5 cm of SALTA2.1, at between 60-70% (figure 27 and table 1). Below 5 cm LOI decreases rapidly to less than 5% organic matter. It then remains low, under 15% until 16 cm depth. After that it steadily increases again and then the last measurement is at 42%. After this the measurements stop until the lowest 15 cm of the same core, where the organic content starts off again at 42%. The LOI percentage makes a quick drop to 12% after 1 cm, before it goes back up again to the forties, where it remains fairly

stable for 5 cm. For the remaining 10 cm of the core, the LOI takes a slow, and steady dip down to 18%, before it goes back to the forties (figure 28 and table 2).

Table 1: LOI % of the upper 23 cm, per 2 cm

LOI %	Sample depth
69.95	0.50
70.77	2.50
62.57	4.50
38.34	6.50
2.49	8.50
10.51	10.50
14.15	12.50
3.06	14.50
19.65	16.50
27.52	18.50
29.03	20.50
41.80	22.50

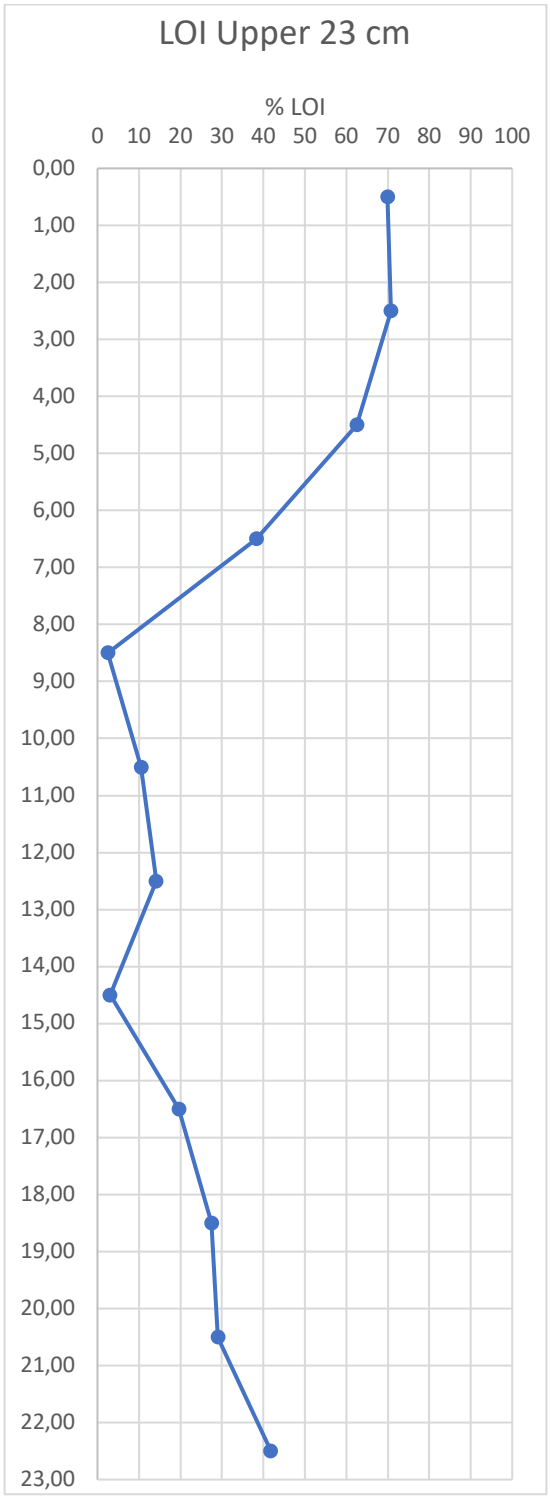

Figure 27: LOI % of the upper 23 cm, per 2 cm

Table 2: LOI % of the lower 15 cm per 1 cm

LOI %	Sample depth
42,09	82,50
12,21	83,50
42,27	84,50
41,94	85,50
40,47	86,50
41,33	87,50
33,81	88,50
32,57	89,50
28,93	90,50
23,43	91,50
17,59	92,50
21,59	93,50
36,94	94,50
42,75	95,50
39,65	96,50
41,23	97,50

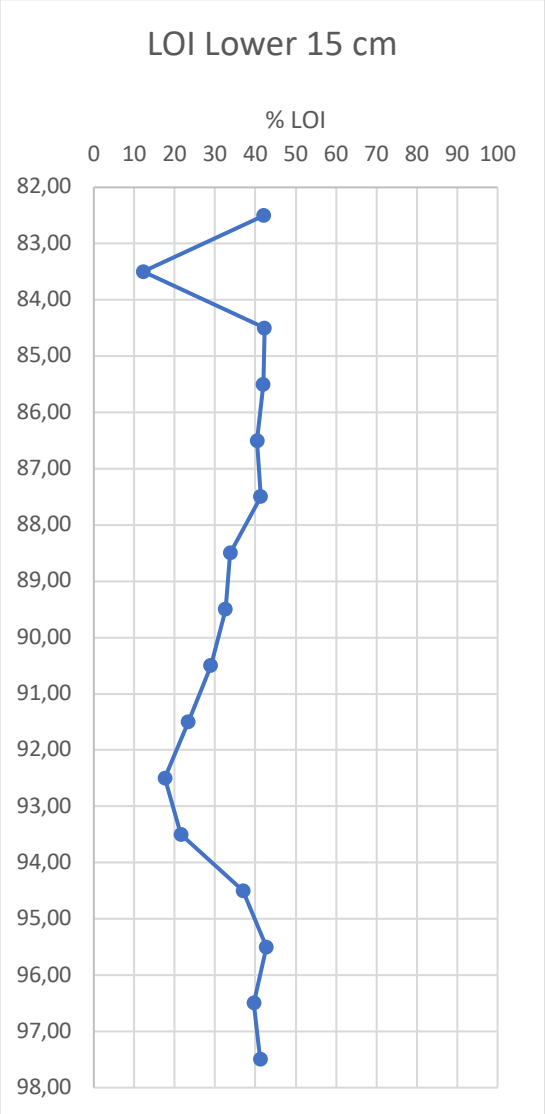

Figure 28: LOI % of the lower 15 cm, per 1 cm

4.4 Salta2.2

4.4.1 Core stratigraphy

SALTA2.2 was taken as a 1 m core, but as mentioned above, the uppermost 30 cm may overlap with the lowermost 30 cm of SALTA2.1, or material fell down into the borehole from above. The upper 30 cm of SALTA2.2 has thus been separated as a segment without number and will not be analyzed further. The second core was divided into four additional segments.

Segment V begins at 30 cm down core and ends at 47 cm and consists of some whole and broken shell fragments in a brown, organic-rich mud matrix and extends from of brown, organic-rich mud with fine laminae. The contact between Segment V and Segment VI at 45 cm is gradational.

The next segment (VI) is mostly brown, organic rich mud again, with just a few shell fragments imbedded approximately halfway. It extends from 45- 60 cm down core.

The largest shell layers makes up Segment VII. It's around 25 cm long, extending from 60 cm to 85 cm ,with layers of more and less amounts of shells embedded. The surrounding mud is lighter brown. The embedded shells appear different in size, and the contact with the next segments is distinct and abrupt. The segments shows signs of erosion at the top.

The final segments (VIII) is partially dark brown mud with some shell fragments, and partially a final shell layer, that also show signs of erosion at the top. The shell layer stretches all the way to the bottom of the core, and appears to have a great amount of shells embedded.

4.4.2 Core diagram and XRF measurements

Figure 29 shows a core diagram of the Salta2.2 core, where the top 30 cm is discarded, and how the elemental proxies relate to the broken shell layers. The first shell layer, in Segment V, follows the trend of the previous core; spikes in Sr and Ca together with dips in Fe and Br over the area with most shells. Segment VI, with mostly brown, organic mud and a few scattered shells shows stable elemental abundances, except for Ca, which varies somewhat. Segment VII, which is the biggest broken shell layer observed in SALTA2.1 and 2.2, shows the same trend as the other broken shell layers, with an increase in Ca and Sr, and decrease in Fe and Br, which all then remain relatively stable throughout the layer. Segment VIII varies through its

upper sections where the concentration of broken shell is less than lower down, but has spikes in Ca and Sr, and dips in Fe and Br from 165 to 172 cm.

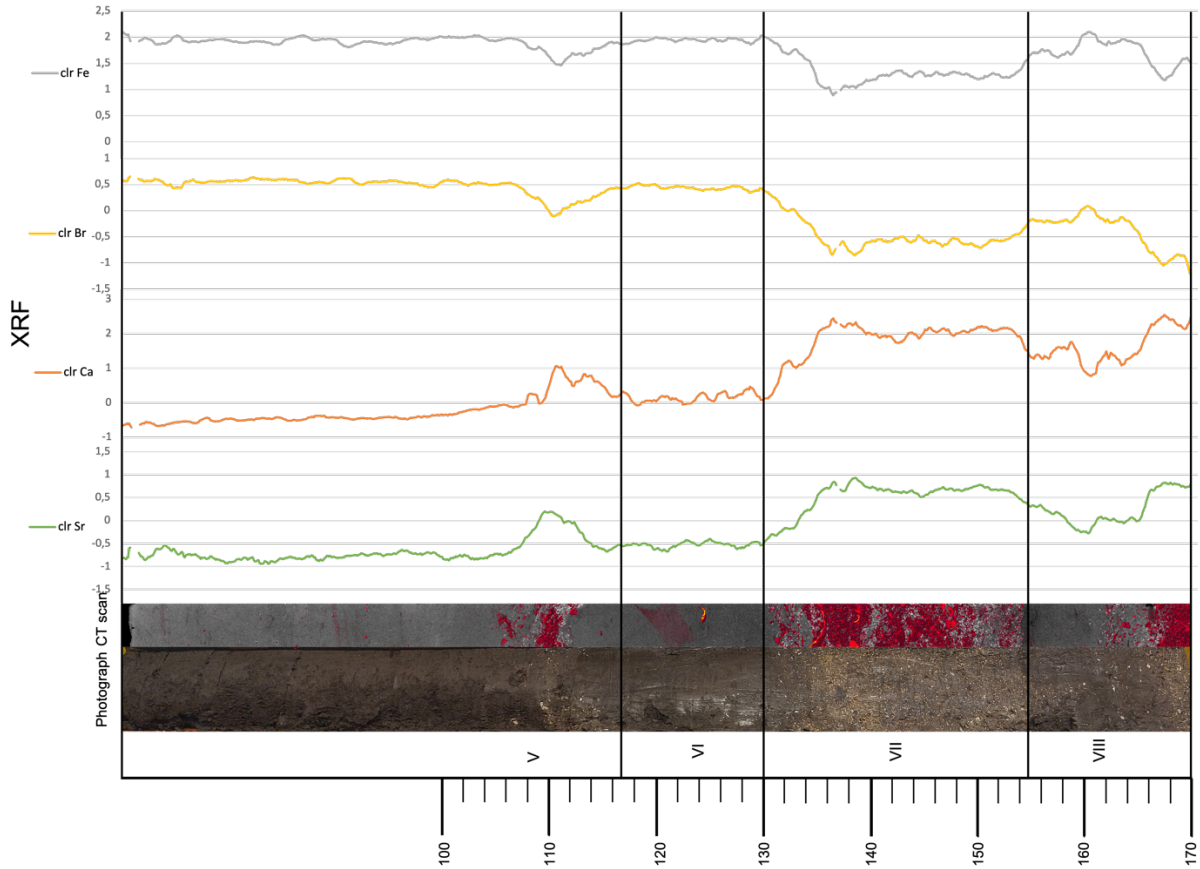

Figure 29: Core diagram from Salta2.2, consisting of scale, photograph, CT scan, XRF results of Sr, Ca, Br and Fe.

Figure 30 shows the XRF results from the elements that dips during the shell-layers, including Cl, Fe, Br and Zr. The figure shown that these elements follow each other throughout the core, although with slightly larger variations in Br and Fe (which is why they were included in the core diagram). The variations are small at Segment V, with only 0.5, but closer to 1-1,5 over Segment VII. At Segment VIII layer Br drops below -1 at the very end, where Fe and Cl actually shows a small increase.

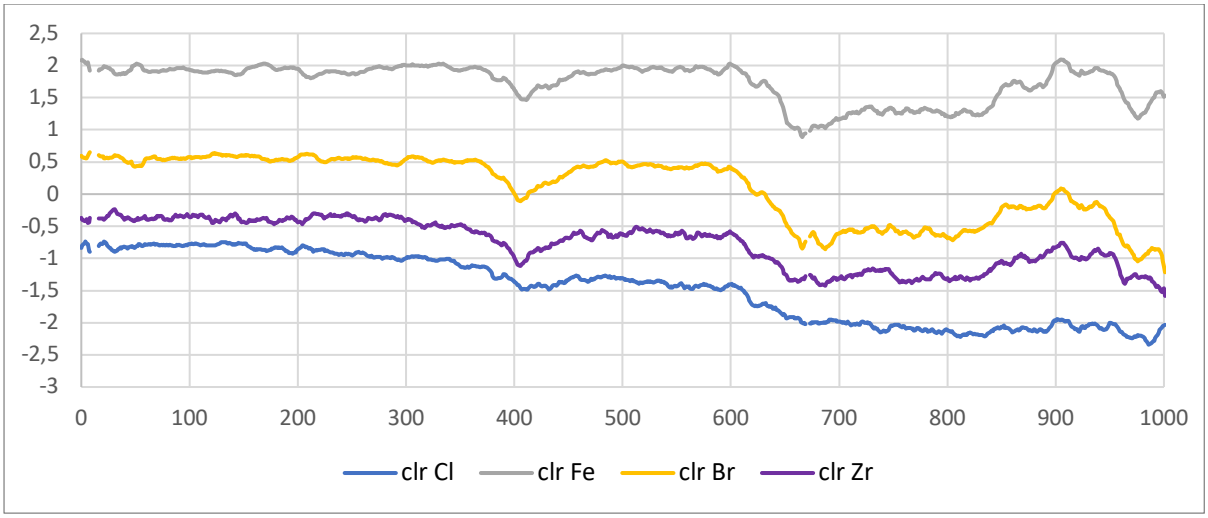

Figure 30: XRF results of Cl, Fe, Br and Zr.

Figure 31 shows how the last two elements work together. Both Ca and Sr spikes about 1 over the shell layers in Segment V. The rest of the core these two elements run pretty parallel, with spikes over the shell layers, although the figure also shows how much more variations Ca throughout the muddy parts.

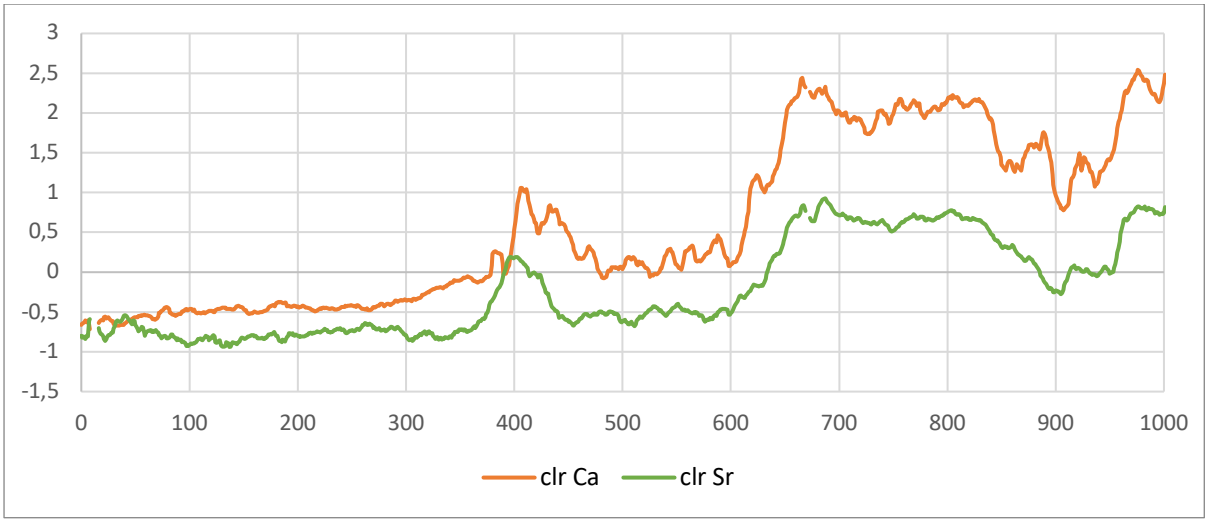

Figure 31: XRF results of Ca and Sr.

5 Discussion

One hundred and seventy-two cm of sediment core was extracted from a fringing salt marsh on the east end of a shallow, intertidal basin, called Saltatjørna, located approximately 1 km south of the community of Sirevåg, SW Norway (Figure 5). The core was collected as part of a bigger sea level project (QUANTSEA) with aims to reconstruct recent RSL change in Norway.

Four prominent layers in the cores, comprised mainly of broken shell, and one comprised of gravelly-sand, stand out from otherwise organic-rich, fine-grained sediments. Given the position of Saltatjørna at almost exactly mean sea level, but separated from the North Sea by an approximately 150 m long, narrow bedrock channel, it is suspected that these broken shell layers represent large storm events, since shells have not been observed in the pond sediments, but are common in the North Sea. If the broken layers of shell are related to large storms or tsunami events (both tsunamis and storms, if large enough, are capable of delivering North Sea seawater, sediment, and organic matter, including shells, into Saltatjørna), the geochemistry of these storm layers should differ from that of sediments reflecting normal conditions at Saltatjørna. The aim of this study has been to characterize the geochemical signature for each of the proposed storm layers, compare these signatures to look for similarities, and also use the geochemistry to confirm or refute that it represents a major marine incursion event. The elevation of the modern wrack line, knowledge of past RSL change in this area, the elevation of the shell layers, and of the sill will also help determine the origin of the shell layers and the approximate size of the storms that deposited them, although radiocarbon samples (which have been sent for dating, but as of the time of writing, have not come back from the commercial lab) will be needed for correlation with past RSL change and an estimation of the size of the events that transported the broken shells into Saltatjørna. Nonetheless, core data will be discussed in terms of stratigraphy, XRF analysis, LOI (for SALTA2.1), and environmental setting, followed by a synthesis of all of the data collected so far and the potential in the sedimentary records of Saltatjørna for revealing past storminess in SW Norway.

5.1 Environmental change

Core stratigraphy may not relate to storms or relative sea-level change, but rather to other changes in the catchment, such as vegetation. Based on the arial photos of Saltatjørna in 1967 (the oldest available, figure 14), it appears rocky and barren of trees and other vegetation and basically no fringing salt marsh can be seen. Both trees and other vegetation, including salt marshes have since grown in around the edges of Saltatjørna , already by the 1990s. The tree growth is likely due to people planting them for environmental reasons, rather than a natural change due to climate, for example (Thomsen, 2004).

The absence of the salt marsh ≥50 years ago may explain the gravelly-sandy layer at the top of the core (Segment II). A potential explanation is that it could have been some sort of thin beach, if sea level was lower at the time (approximately 30 cm lower given the depth of the gravel-sand layer in the core and the water depth at the coring site). A more detailed RSL curve than is currently available for this area is needed to determine the likelihood of this hypothesis. Other explanations for the gravelly-sandy layer towards the top of SALTA2.1 include a heavy rainfall event or season, bringing coarse, terrestrial sediments to Saltatjørna with water run-off from flooding in nearby rivers, or it could be a remnants from a small rockfall from the adjacent bedrock cliff or even dumping of gravel and sand during road or other construction (there is a road approximately 65 m NNW). New cores from this area are needed to determine the origin of Segment II. Interpretation of XRF data in Segment II is discussed below in section 5.2.

5.2 Core Stratigraphy

Four discrete layers of broken shell, ranging from 5cm to 25 cm thick, were observed at 90 cm, 110 cm, 130 cm and 165 cm (Segment IV, V, VII and VIII), in addition to one sandy-gravelly layer between approximately 10-20 cm (Segment II) (figure 21*)*. The rest of the core was comprised of thinly laminated, lighter and darker brown, organic-rich mud (Segment II and VI) (mostly fine silt; *Figure 22*). The uppermost ca. 10 cm of the core consists mainly of roots of *Bolboschoenus maritimus* and *Phragmites australis* (common Norwegian names havsivaks and takrør, respectively), and which had a very high LOI of 70%.

Below the modern root layer, Segment II is starting at approximately 8 cm down-core, is a 12 cm thick layer of gravel and sand with some minor organic-rich brown mud (fine silt). This layer can be seen by eye and in the CT scans (Figure 22). Results from XRF analysis over this

interval show a spike in Ca and Sr, and low (2-14%) LOI values. Higher relative abundances of Ca and Sr may indicate a more marine environment, however the increase in Ca and Sr appears to be two, short-lived events or outliers (Figure 24 and 26) rather than sustained higher average values in throughout this segment. The spikes in Ca and Sr at 14-16 cm down core may reflect a single, large shell, calcareous foraminifera, or a large piece of white gravel, such as white anorthosite, which is the local bedrock. Anorthosite has calcium in it, so the Ca spike may be produced from that. The first of these spikes does not seem to have any significant correlative change in Fe, and the second spike, only by a small amount, which is inconsistent with the other layers of broken shells (Segments IV, V , VII and VIII). The XRF data is discussed further below.

The color of the gravel and sand on the CT scan Segment II is bright red-orange compared to the color of the shell fragments lower down. The red indicates that it is denser than sediments, and the brighter color indicates it has a higher density than the shells in the other sections that are darker in color.

Of the four broken shell layers Segment IV, V and VIII are all relatively thin layers (≤10 cm), whereas the last layer (Segment VII) is 25 cm thick. The different thicknesses of the broken shell layers could indicate a difference in magnitude and/or duration of a storm event. Overall Segments IV, V , VII and VIII show similar characteristics in the XRF data, with elevated abundances of Ca and Sr, and simultaneous dips in Fe and Br (as well as Zr and Cl). This will be discussed more below. The CT scan shows approximately the same density (same color of red) of the shell layers, surrounded by small amounts of air (white), except for a few larger shell fragments in Segment VII, which appears to have a higher density.

There is no LOI data for the last three layers, but the LOI value over the second also seems to indicate a drop from 40% down to16% and back up to 40% around the shells. An additional drop from 42% to 17% and back up to 42% also happens around 80 cm down, around the same place as where the Ca levels spikes without the Sr, Fe and Br levels follow. Any immediate cause cannot be seen for this in photos or in the CT scan. Between the shell layers is mostly dark brown mud, which is organic rich. This seems to be concurrent with the available LOI data, which shows LOI to be around 40-50% outside of the broken shell layers, however as LOI was not completed throughout the core, limited interpretations can be made. The bases of the shell layers in Segment VII and VIII are erosional, indicating a high-energy event. As the storms passed, the thin, flat, and light shell fragments slowly settled onto the bed of the pond,

where they have been buried by organic-rich sediments reflecting more average conditions in Saltatjørna (which are likely relatively low energy as it is probably too small and of limited fetch for generating waves any larger than a few tens of cm).

5.3 Complementary observations of past sea-level change and storms at Saltatjørna

The peak elevation of the tidal channel between Saltatjørna and the North Sea is 10 cm NN2000 (figure 15). As the tidal range has been estimated to be around 20 cm (Kartverket, 2023b), with mean high tide at -7 cm and highest astronomical tide at 12 cm (Kartverket, 2023b), Saltatjørna is likely disconnected from the North Sea more often than it is connected. Indeed, it would seem that it is only connected when the tide approaches highest astronomical tide (12 cm) and during storm surges. However, wave height along this open coast is likely greater than 20 cm much of the time, which would raise water levels and enter the bedrock inlet into Saltatjørna.

Figure 32: Photo of lichen migration in the study area.

Relative sea-level trends from Stavanger, which is 50 km north of Saltatjørna, show an increasing trend the last century (Simpson et al., 2015). Relative sea-level that is rising 1.7 mm per year along this stretch of coastline indicates that Saltatjørna likely received less marine input in the past when RSL was lower, but can expect more marine input in the future. The vertically-upwards migration of lichen on the bedrock near the water line in the tidal outlet may confirm this trend (Figure 32)

The wrack line also shows that Saltatjørna's water level is most often affected by storms rather than tides. The modern wrack line (figure 17) mostly stays between 1.5 and 2 m NN2000 and shows that the debris from the open sea drifts into Saltatjørna and becomes stranded above normal water levels (above high tide). The plastic debris, driftwood, and seaweed that forms the wrack line here lies over well-established terrestrial vegetation, suggesting storms with associated water levels 1.5-2 m above the shoreline do not occur very often.

5.3 XRF

An XRF analysis reflects the concentration of elements in the core. The XRF results show an overall trend of Ca and Sr increasing in the broken shell layers, and a simultaneous decrease in Fe and Br. One important thing to keep in mind when studying the results of an XRF analysis is that the data is in some degree relative to one another. The data is normalized in a closed sum, which means that when one element decreases, (at least) one other element must simultaneously increase, to keep the total stable. Thus, some of the trends may be caused by this and not by any environmental factor. The thing to remember is that a lot of elements were originally included in the analysis but were excluded from interpretation. Of all the elements scanned, it was the ones included in the results (Ca, Sr, Fe, Br, Cl and Zr), that most notably reacted to each other, rather than other elements that were not relevant for this research anyway. The fact that the relevant elements were the ones that actually reacted to each probably validates the results some more.

5.3.1 Ca & Sr

Ca and Sr clearly seem to be enriched in the shell layers. Generally speaking, Ca and Sr are often used to indicate marine productivity. Ca is commonly a good indicator for carbonate stratigraphy, aragonite preservation, core correlation, marine transgression and marine influence, which indicate that the shell layers enriched in Ca come from a marine source. High levels of Ca are a strong indicator for high marine productivity (Davies et al., 2015; Rothwell & Croudace, 2015).

High Sr levels mostly following high Ca levels through the broken shell layers is a good indication that these layers reflect a strong marine influence at the time of deposition. In climates where the levels of lakes and ponds tend to decline, evaporative minerals, such as calcium carbonate ($CaCO_3$) may be deposited. The deposition of this mineral can be seen the XRF profiles of lakes sediments. Generally Sr levels can indicate an abundance of pteropods (planktonic marine snails) and biogenic origins. Biogenic $CaCO_3$ from coccoliths and foraminifera has a greater Sr content than inorganic $CaCO_3$ or dolomite (Hodell et al., 2008, in Davies et al., 2015). Co-variation of Ca and Sr indicates that the Ca is mainly coming from biogenic $CaCO_3$ (Davies et al., 2015; Richter et al., 2006). Since Sr mainly originates from marine shells that calcify simultaneously as Ca (such as aragonite), it can also be very useful as a complementary proxy, to distinguish whether the Ca levels originate from marine

influence or rocks. High levels of Sr can also be an indicator of high salinity, especially together with laminated or partially laminated sediments (Davies et al., 2015; Rothwell & Croudace, 2015).

Ca can also be found in rocks such as anorthosite, which is what the study area mostly consists of (figure 7) (Rothwell & Croudace, 2015). It's a possibility that the anomaly around 80-85 cm is related to that, where Ca increases while Sr does not. This also occurs together with a sharp drop in LOI. Decreases in LOI could happen due to the LOI signal being drowned by a huge influx of sediment, such as from storms. A marsh with vegetation can get covered by a relatively thick layer of sediment or shells after a storm, which will cause the percentage of organic material to decrease, despite that the amount of vegetation stayed the same, only the amount of sediment input changed (Heiri et al., 2001).

5.3.2 Sr/Ca ratio

Both Ca and Sr can also be covariate in volcanic and/or glacial processes as well. Therefore the Sr/Ca ratio can be useful in indicating aragonite in shallow waters and authigenic carbonate precipitation and identifying the layers. Higher Sr/ Ca values can be interpreted as reflecting greater pteropod content, and thus you'd expect the ratio to go up over the shell layers (e.g. Krinsley and Bieri, 1959 in Rothwell & Croudace, 2015). The Sr/Ca ratios are not so clear however (figure 33). It increases a great deal over Segment II, except around the random piece at 14-16 cm where the ratio approaches zero. Then it seems to drop over the Segment IV, and increase over Segment V. Then it drops again over Segment VII, and increase over Segment VIII, making it hard to draw any conclusions from this ratio alone. This could be partially due to their relative to each other, since both Sr and Ca increase individually when looking at the CLR- transformed data of the elements, simply indicating a slightly different composition of the biogenic carbonates.

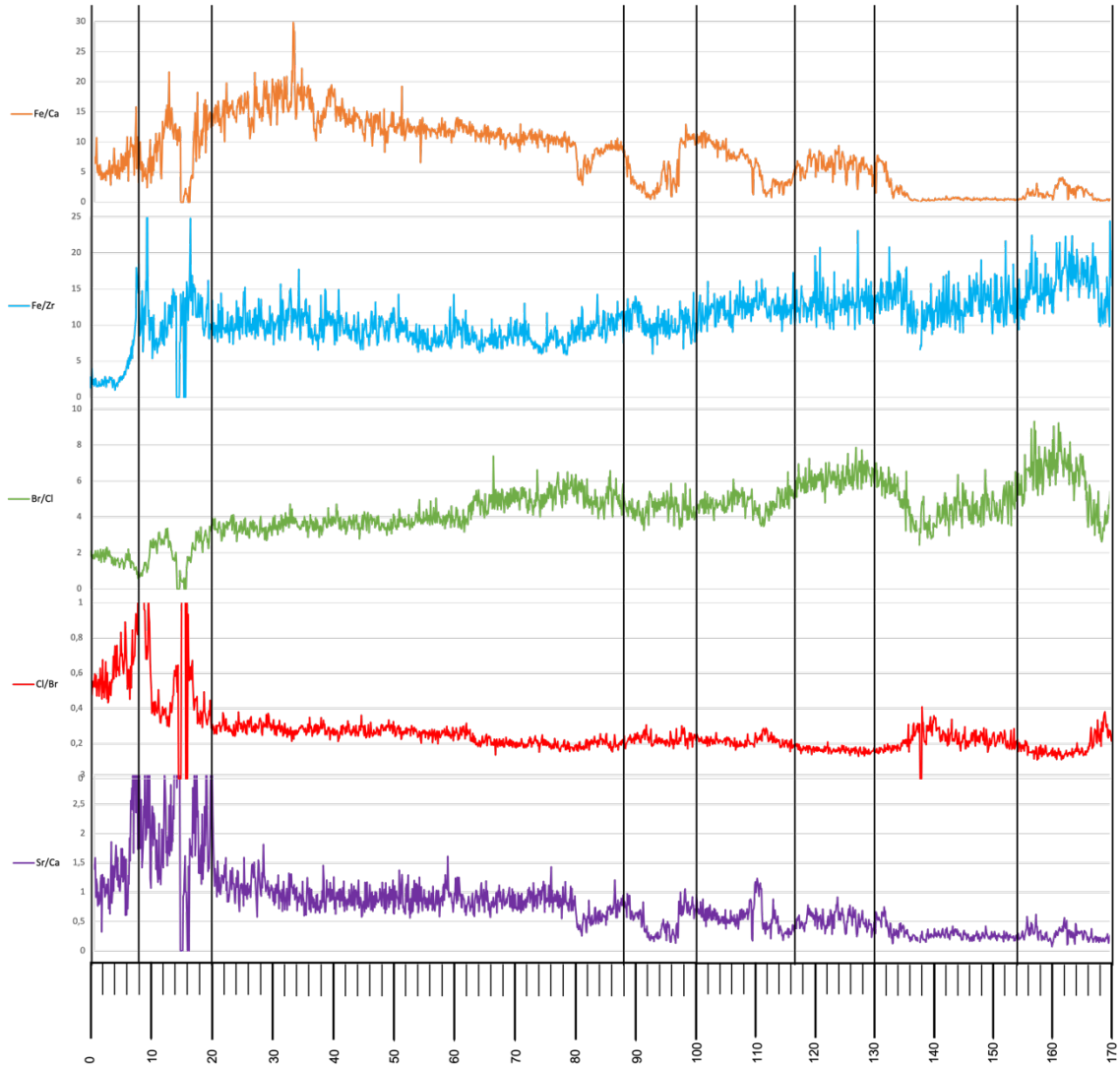

Figure 33: XRF results converted into element ratios for the whole 170 cm core.

5.3.3 Fe & Zr

Fe & Zr are two other elements that seem to follow the shell layers, though inversely to Ca and Sr, and they seem to be detrital. Fe is a very common element that can be interpreted and used in many ways in core stratigraphy; for example, terrigenous sediment delivery, aeolian dust input/hinterland aridity/variation in wind strength, changes in carbonate productivity, increased input from terrestrial sources, rainfall and run-off proxy (Davies et al., 2015; Rothwell & Croudace, 2015).

Zr tends to be more abundant in silts containing heavy minerals such as zircon and is usually linked to the coarse grains of the sediment (it is a heavier and more weathering resistant element). It can also signify tephra and detrital inputs, much like Fe (Davies et al., 2015;

Rothwell & Croudace, 2015). Even though Zr is detrital, it also correlates very well with Cl and Br, in addition to Fe in the cores from Saltatjørna.

5.3.4 Fe/Zr ratio

Fe/Zr has been used as a precipitation/surface runoff proxy in the Sahara (Hanebuth and Lantschz, 2008 in Rothwell & Croudace, 2015), as well as an indicator of aridity in low Fe/Zr and humidity in higher Fe/Zr. However this core is from such a different environment, and the biggest changes in the ratio (figure 33) is at the very top and very bottom of the core (Segment II and VIII), it might not be that relevant. Wilhelm et al. (2013 in Davies et al., 2015), suggests the ratio might be used to determine flood layers related to grain-size sediments, which could that mean the grain size is bigger there. The higher ratio in Segment II correlates to the fact that it consists of mostly gravel.

5.3.5 Fe/Ca ratio

The correlation and ratio of Fe and Ca can also be useful to identify storm layers. Ca and Fe show a trend of anti-correlation over the shell layers (figure 33), which indicates shifts between marine and terrestrial. Davies et al. (2015) states that Fe and Ca commonly anti-correlate and that Fe/Ca can gives relative proportions of terrigenous fluxes versus marine carbonates.

The exception in the correlation is the small spike in Ca that happens around 80-85 cm depth at the bottom of Segment III, where there is no prominent shell layer and a spike in Sr does not occur. It seems to be close to no visible dip in neither Fe and Br either, although the Fe/Ca ratio does show a visible dip, indicating that something does potentially happen here. Maybe the terrigenous flux stayed the same, but there is a larger influx of marine carbonates for some reason. It could also be that some elements do react, but just not clearly enough to make any conclusions.

Generally, the Fe/Ca ratio does shows tendencies to dip over the biggest shell layers (figure 33), including the very topmost gravel piece, and most notably over the longer shell layer located approximately 135-155 cm deep in Segment VII. The low Fe/Ca values in the shell layers indicate a relative increased presence of Ca. On the other hand, where Fe/Ca values are relatively high, this indicates an influx of terrigenous material.

Some care should be taken though, since storms can also bring in big amounts of Fe, where minerogenic sediments from the marine shelf are being dropped on the marsh, drowning out the Ca-signal from the marine carbonates. In addition to shells, storms can also transport marine clays (containing Fe) (Davies et al 2015). That could maybe explain the not so strong reaction of Fe in Segment II. Another explanation could be that the Fe comes from the sand and gravel in this segment.

5.3.6 Br & Cl

Br & Cl are two elements that are both present in saltwater, and at the same time can be bound to organic matter, making them a bit complicated. Br is a single of organic matter decay, and can indicate both marine and terrestrial environments. It has potential use in identifying organic content in lake sediments, determining presence of organic carbon content and increased productivity (Gilfedder et al. 2011, Kalugin et al. 2007 in Davies et al. 2015), as well as maritime influence such as sea spray and increased storminess (Unkel et al, 2009 in Davies et al., 2015). Since Br in this XRF data seems to be working together with both Fe and Zr (figure 2 and 30), which are detrital, it is most likely to be terrestrial indicator (Davies et al., 2015; Rothwell & Croudace, 2015).

As for Cl it's so much around in saltwater, it is most likely marine. As Br also correlates with Cl, which is a component of saltwater, this correlation can determine that the water component is saltwater and not freshwater. As per McHugh's study in 2008 , the magic number for determining salt water vs freshwater was 200 cps/s, and in this study the Br levels hardly dipped below 200, with the exception of the areas between 14 and 16 cm deep, which is where the big angular piece was found, in between all the gravel (McHugh et al., 2008 in Rothwell & Croudace, 2015).

5.3.7 Br/Cl ratio

Br/Cl has been used to detect the presence of organic rich layers and increased porosity. This ratio (figure 33) does show a decrease over the most shelly parts in Segment VII, as well as small decreases in Segment V and at the end in Segment VIII. There is however not any strong change in the ratio at the shell layer in Segment IV. On the other hand, a study by Yao et al. (2020) used instead the Cl/Br ratio to identify storm deposits, where higher levels, meaning an increase in Cl and decrease in Br, was consistent with marine incursion events, such as a storm surge, as a storm surge can cause a saltwater intrusion. As such it seems Cl/Br serves as a good

indicator for storm events. This does seem consistent with some of the shell layers, as the ratio increases in Segment VII and VIII, in addition to the very top parts of the core (figure 33).

Bunzel et al. (2021)use the ln(Br/Cl) ratio to look at storm events, where they state that abrupt drops in the ln(Br/Cl) is likely due to the signal of marine organic matter supply (which they say the ln(Br/Cl) ratio stands for) being diluted by the influx of siliciclastics from the storm event. Even though the ln has not been calculated here, this might indicate that the changes in the Cl/Br ration is not just an of influx of Cl. It might just be a relative increase in other elements that suppresses the Br signal, making it look like a decrease in Br. It still means that the Cl/Br ratio seems to serve as a good indicator for storm events.

5.4 LOI

LOI seems to follow the XRF proxies for the section for which there is data. Decaying organic matter is eventually a loss in organic matter content, meaning that LOI values tend to decrease over time (and therefore, with depth in sediment cores). If there is a big influx of minerogenic sediment, this will also lead to lower LOI values, meaning the LOI value is diluted by the sediment influx. As such, the dip in LOI associated with Segment IV likely reflects increased sand and silt also transported into Saltatjørna during a large storm event (figure 24).

5.4 Summary

The results shows that generally Ca and Sr increase in the broken shell layers, and that at the same time, Fe and Br decrease. The anti-correlation between Ca and Fe indicates a shift between marine and terrestrial as Fe is a very good indicator for terrigenous supply, especially since it correlates with Br and Zr, which co-vary similarly. The XRF data also line up with the LOI data (where available), which overall seems to indicate that the broken shell layers were deposited during a large storm and storm surge event. The core stratigraphy and other environmental data supports the hypothesis that the main marine influence at Saltatjørna is not regular tidal flooding.

6 Conclusions

The trend of the relative sea-level change in SW Norway is increasing at a rate of 1.7 mm per year, and accelerating (Simpson et al., 2015). It is predicted to increase by up to 0.26 and 0.82 m globally over the next century(Simpson et al., 2015). Relative Sea Level change is mostly caused by climate change factors, such as human contribution to CO_2 levels, causing global warming, which in turn causes thermal expansion and melting glaciers and ice sheets. Other factor that influence the more short term rise and fall in RSL is the cyclical astronomical tides, and extreme weather factors such as storm surges, the latter of which can normally bring in 1-3 m of extra water. The global changes in climate do not only affect the global sea levels, but they are also creating more frequent and more intense extreme weather.

The two cores taken from the fringing saltmarsh of Saltatjørna in Rogaland, Norway hold a record of the effects of past changes in RSL. Data from the cores have been analyzed together with other environmental data from Saltatjørna to evaluate the effects of storm surges in almost entirely closed off ponds such as Saltatjørna, and whether such weather events can be reconstructed from visible broken shell layers in the cores, which stand out from the otherwise organic rich sediments of the cores. Overall, the shelly layers appear similar both in photos and CT, where the gravelly layer stands out in density. Inspection of vegetation change suggests that Saltatjørna was likely a pond at the time these sediments were deposited.

The XRF result mostly correlate with the initial hypothesis that the shell layers are storm layers. Ca and Sr are clearly enriched in the shelly layers, which is a clear proxy for a marine influence, pteropods and biogenic calcium carbonate, however the Sr/Ca ratio only supports a marine environment for the third and fifth layer. There is also the anomaly around 80 cm where Ca and LOI support marine influence, but Sr does not follow. Fe, Zr, Cl and Br all inversely follow the Ca and Sr levels, except for the two previously mentioned anomalies in the gravelly layer, and the one at 80 cm . Fe and Zr are typical detrital elements that normally indicate terrigenous sediment delivery, or rainfall and water run-off. The anti-correlation between these two groups of elements does support the idea of marine influence, especially Ca and Fe. The Fe/Ca ratio also clearly depicts the shell layers with noticeable drops in the

same depth as the shells. This ratio also shows a dip in both the anomalies as well. Higher levels of Fe/Ca does indicate an increase in terrigenous material, and this ratio also remains consistently low over the longest shell layer.

Br and Cl does not show any big significant trends, other than determining that the water influence is indeed likely saltwater rather than freshwater. The Br/Cl ratio does support marine influence by a decrease over the last three layers. The Cl/Br ratio also supports the indication of saltwater intrusion from storm surges. In addition the LOI does seem to mirror Ca levels, and works as an addition confirmation of these results. A dip in LOI is a dilution of the LOI signal due to the influx of material from a storm. These analytic data all supports evidence for marine influence, for most of the layers. All the elemental proxies are consistent for the third and fifth layers, although most of them also supports the indication for all the shell layers. If this analytical data suggesting that the shelly layers are representative of marine influence, is compared with the other environmental and observational data, such as erosional effect of the last two layers, wrack line debris and tidal ranges, that suggest that the biggest marine influence of Saltatjørna is from the rare storm surge rather than regular tides or even small storms, such as the ones that produced the wrack line observed in 2020.

References

Aasly, K. A., Heldal, T., & Meyer, G. B. (2015, 03/02/2020). *Anortositt*. NGU. Retrieved 16/02/2023 from https://www.ngu.no/emne/anortositt

Arthur, M., & Marone, C. (n.d.). *Tides in two easy pieces*. EARTH 540: Essentials of Oceanography. Retrieved 13/02/23 from https://www.e-education.psu.edu/earth540/content/c6_p1.html

Benn, D. I., & Evans, D. J. A. (2010). *Glaciers & Glaciation* (2. ed.). Hodder Education.

Bøe, R., Lepland, A., Blikra, L. H., Longva, O., & Sønstegaard, E. (2002). *Postglacial mass movements in western Norway with special emphasis onm the 2000-2200 BP and 2800-3200 BP periods - final report* (2002.020). NGU. https://www.ngu.no/upload/Publikasjoner/Rapporter/2002/2002_020.pdf

Bondevik, S., Svendsen, J. I., Johnsen, G., Mangerud, J., & Kaland, P. E. (1997). The Storegga tsunami alonong the Norwgian coast, its age and runup. *Boreas*, *26*(1), 29-53. https://doi.org/10.1111/j.1502-3885.1997.tb00649.x

Bondevik, S., Svendsen, J. I., & Mangerud, J. (1998). Distinction between the Storegga tsunami and the holocene marine transgression in coastal basin deposits of western Norway. *Journal of Quaternary Science*, *13*(6), 499-575. https://doi.org/10.1002/(SICI)1099-1417(1998110)13:6<529::AID-JQS388>3.0.CO;2-1

Bunzel, D., Milker, Y., Müller-Navarra, K., W., A. H., & G., S. (2021). North Sea salt-marsh archives trace past storminess and climate variability. *Global and Planetary Change*, *198*. https://doi.org/10.1016/j.gloplacha.2020.103403

Chappell, J. (2004). Sea Level. In A. S. Goudie (Ed.), *Encyclopedia of Geomorphology* (Vol. 2, pp. 917-925). London: Routledge.

Dannevig, P. (2022). *Rogaland (klima)*. SNL. https://snl.no/Rogaland_-_klima

Davies, S. J., Lamb, H. F., & Roberts, S. J. (2015). Micro-XRF Core Scanning in Palaeolimnology: Recent Developments. In I. W. Croudace & R. G. Rothwell (Eds.), *Micro-XRF Studies of Sediment Cores. Developments in Paleoenvironmental Research*. Springer.

Donnelly, J. P. (2009). Paleotempestology, The Sedimentary Record of Intense Hurricanes. In V. Gornitz (Ed.), *Encyclopedia of Paleoclimatology and Ancient Environments. Encyclopedia of Earth Sciences Series.* (pp. 763-766). Dordrecht: Springer.

Edwards, R., & Wright, A. (2015). Foraminifera In I. Shennan, A. J. Long, & B. P. Horton (Eds.), *Handbook of Sea-Level Research* (pp. 3-25). John Wiley & Sons, Ltd.

Erichsen, E., & Marker, M. (2000). *Anortositt i "Egersundfeltet" - Pukkpotensialet* (2000.016). NGU. https://www.ngu.no/upload/Publikasjoner/Rapporter/2000/2000_016.pdf

French, J. R. (2004). Saltmarsh. In A. S. Goudie (Ed.), *Encyclopedia of Geomorphology* (Vol. 2, pp. 898-900). London: Routledge.

Google. (n.d.). *Map of Saltatjørna* https://earth.google.com/web/search/58.494123+5.802557/@58.72230966,5.8552527 3,152.04800479a,106604.23751075d,30.00001303y,0h,0t,0r/data=CigiJgokCamjZn1 wP01AEeNJ7IcPP01AGSp_N8e7ORdAIYg80YvYMRdAMikKJwolCiExMnBMRU xTN1lEdHZ4VUlsemwwLTdiVk04Vks0UXctdmIgAQ

Gornitz, V. (2019). Storm Surge. In C. W. Finkl & C. Makowski (Eds.), *Encyclopedia of Coastal Science* (pp. 1627-1631). Cham: Springer.

Hajdas, I. (2008). Radiocarbon dating and its application in Quaternary studies. *E&G Quaternary Science Journal*(1/2), 2-24. https://doi.org/10.3285/eg.57.1-2.1

Healy, T. R. (2019a). Estuaries. In C. W. Finkl & C. Makowski (Eds.), *Encyclopedia of Coastal Science* (pp. 798-803). Cham: Springer.

Healy, T. R. (2019b). Salt Marsh. In C. W. Finkl & C. Makowski (Eds.), *Encyclopedia of Coastal Science* (pp. 1459-1460). Cham: Springer.

Heiri, O., Lotter, A. F., & Lemcke, G. (2001). Loss on ignition as a method for estimating organic and carbonate content in sediments: reproducibility and comparability of results. *Journal of Paleolimnology*, *25*, 101-110. https://doi.org/10.1023/A:1008119611481

Holden, J. (2012). *An Introduction to Physical Geography and the Environment* (3 ed.). Pearson Education Limited.

IPCC. (2023). *Climate Change 2023: Synthesis Report. A Report of the Intergovernmental Panel on Climate Change. Contribution of Working Groups I, II and III to the Sixth Assessment Report of the Intergovernmental Panel on Climate Change* (AR6).

Jakobsen, A. (2018, 11/09/20). *Hvorfor er det ikke flo og fjære utenfor Egersund*. Havforskningsinstituttet. https://www.hi.no/hi/nyheter/2018/mai/hvorfor-ikke-flo-og-fjare-utenfor-egersund

Jones, J. A. A. (1997). *Global Hydrology*. Pearsons Education Limited.

Karstens, J., Haflidason, H., Berndt, C., & Crutchley, G. J. (2023). Revised Storegga Slide reconstruction reveals two major submarine landslides 12,000 years apart. *Communications Earth & Environmet*, *4*, Article 55. https://doi.org/10.1038/s43247-023-00710-y

Kartverket. (2023a). *Norge i bilder*. Retrieved 12.04.23 from https://www.norgeibilder.no/

Kartverket. (2023b). *Result for Sirevåg vasstandsmålar (Hå)*. https://www.kartverket.no/en/at-sea/se-havniva/result?id=1086343&location=Sirev%C3%A5g+vasstandsm%C3%A5lar

Kartverket. (2023c). *Resultat for Stavanger vannstandsmåler (Stavanger)*. https://www.kartverket.no/til-sjos/se-havniva/resultat?id=1082307&location=Stavanger%20vannstandsm%C3%A5ler

Klimaservicesenter, N. (2022). *Klimaprofil Rogalan*. https://klimaservicesenter.no/kss/klimaprofiler/rogaland

Lowe, J., & Walker, M. (2015). *Recontructing Quaternary Environments* (3. ed.). Routledge.

Morton, R. A., Gelfenbaum, G., & Jaffe, B. E. (2007). Physical criteria for distinguishing sandy tsunami and storm deposits using modern examples. *Sedimentary Geology*, *200*(3-4), 184-207. https://doi.org/10.1016/j.sedgeo.2007.01.003

NOAA. (2023, 20/01/23). *Where is the highest tide?* Retrieved 13/02/2023 from https://oceanservice.noaa.gov/facts/highesttide.html#:~:text=The%20highest%20tide%20in%20the%20world%20is%20in%20Canada.&text=Kent.-,The%20highest%20tides%20in%20the%20world%20can%20be%20found%20in,that%20average%20around%2030%20feet%20.

Norges Geologiske Undersøkelse. (2023a). *Hovedbergarter, sammenstilt målestokksvisning*. NGU. Retrieved 05.03.23 from https://geo.ngu.no/kart/berggrunn_mobil/?map=detaljert&extent=-35944,6520111,-34677,6520760

Norges Geologiske Undersøkelse. (2023b). *Marin grense og tidligere havdekte områder*. NGU. Retrieved 02.03.23 from https://geo.ngu.no/kart/minkommune/?kommunenr=1119

Olsen, L., Sveian, H., Ottesen, D., & Rise, L. (2013). Quaternary glacial, interglacial and interstadial deposits of Norway and adjacents onshore and offshore areas. *Geological Survey of Norway Special Publication*(13). https://www.ngu.no/upload/Publikasjoner/Special%20publication/Spec_Publ13.pdf

Parnell, K. (2004). Storm Surge. In A. S. Goudie (Ed.), *Encyclopedia of Geomorphology* (Vol. 2, pp. 999-1000). London: Routledge.

Plater, A. J., Kirby, J. R., Boyle, J. F., Shaw, T., & Mills, H. (2015). Loss in ingition and organic content. In I. Shennan, A. J. Long, & B. P. Horton (Eds.), *Handbook of Sea-Level Research* (pp. 312-330). John Wiley & Sons, Ltd.

Richter, T. O., van der Gaast, S., Koster B, V., A , Gieles, R., de Stigter, H. C., de Haas, H., & van Weering, T. C. E. (2006). The Avaatech XRF Core Scanner: technical description and applications to NE Atlantic sediments. In R. G. Rothwell (Ed.), *New techniques in sediment core analysis* (pp. 39-50). Geological Society

Romundset, A., Fredin, O., & Høgaas, F. (2015). A Holocene sea-level curve and revised isobase map based on isolation basins from near the southern tip of Norway. *Boreas*, *44*(2), 255-444. https://doi.org/10.1111/bor.12105

Romundset, A., Lakeman, T. R., & Høgaas, F. (2018). Quantifying variable rates of postglacial relative sea level fall from a cluster of 24 isolation basins in southern Norway. *Quaternary Science Reviews*, *197*, 175-192. https://doi.org/10.1016/j.quascirev.2018.07.041

Romundset, A., Lohne, Ø. S., Mangerud, J., & Svendsen, J. I. (2009). The first Holocene relative sea-level curve from the middle part of Hardangerfjorden, western Norway. *Boreas*, *39*(1), 87-104. https://doi.org/10.1111/j.1502-3885.2009.00108.x

Rothwell, R. G., & Croudace, I. W. (2015). Twenty Years of XRF Core Scanning Marine Sediments: What do Geochemical Proxies Tell Us? In R. G. Rothwell & I. W. Croudace (Eds.), *Micro-XRF Studies of Sediment Cores. Developments in Paleoenvironmental Research*. Springer.

Salminen, R., De Vos, W., & Tarvainen, T. (2006). *Geochemical atlas of Europe*. Geological Survey of Finland.

Simpson, M. J. R., Nilsen, J. E. Ø., Ravndal, O. R., Breili, K., Sande, H., Kierulf, H. P., . . . Vestøl, O. (2015). *Seal Level Change for Norway. Past and Present Observations and Projections to 2100.* (1/2015). NCCS.

Smithson, P., Addison, K., & Atkinseon, K. (2002). *Fundamentals of the Physical Environment* (3. ed.). Routledge.

Thomsen, H. (2004). Håevla og jærlandskapet. *Sjå Jæren* 12-21. https://www.jaermuseet.no/samlingar/wp-content/uploads/sites/16/2011/06/2004.02-H%C3%A5elva-og-j%C3%A6rlandskapet.pdf

Vasskog, K., Svendsen, J. I., Mangerud, J., Haaga, K. A., Svean, A., & Lunnan, E. M. (2019). Evidence of early deglaciation (18 000 cal a bp) and a postglacial relative sea-level curve from southern Karmøy, south-west Norway. *Journal of Quaternary Science*, *34*(6), 410-423. https://doi.org/10.1002/jqs.3109

Veres, D. S. (2002). A Comparative Study Between Loss on Ignition and Total Carbon Analysis on Mineralogenic Sediments. *Studia Universitatis Babes-Bolyai Geologia*, *47*(1), 171-182. https://doi.org/10.5038/1937-8602.47.1.13

Weltje, G., Bloemsma, M., Tjallingii, R., Heslop, D., Röhl, U., & Croudace, I. W. (2015). rediction of Geochemical Composition from XRF Core Scanner Data: A New Multivariate Approach Including Automatic Selection of Calibration Samples and Quantification of Uncertainties. In I. W. Croudace & R. G. Rothwell (Eds.), *Micro-XRF Studies of Sediment Cores. Developments in Paleoenvironmental Research* (pp. 507-534). Springer.

Yao, Q., Liu, K., Rodrigues, E., Bianchette, T., Aragón-Moreno, A. A., & Zhang, Z. (2020). A Geochemical Record of Late-Holocene Hurricane Events From the Florida Everglades. *Water Resources Research*, *56*. https://doi.org/10.1029/2019WR026857

Appendix

CLR transformed XRF data from the shell layers.

Position in core (mm)	CLR_Ca_smooth	CLR_Fe_smooth	CLR_Br_smooth	CLR_Sr_smooth
59	-0,804005069	1,311793014	0,098012804	-0,00088126
60	-0,812246579	1,341439132	0,065978202	0,083816921
61	-0,819261012	1,391431686	0,014766619	0,138003039
62	-0,765830602	1,37875854	-0,047260096	0,234314259
63	-0,758239932	1,396938531	-0,067906155	0,278300047
64	-0,733118632	1,420253175	-0,124047126	0,316640709
65	-0,616998444	1,427349286	-0,225101608	0,385603286
66	-0,567181365	1,453018521	-0,298729705	0,444100349
67	-0,511043759	1,496762831	-0,376058428	0,48419798
68	-0,523720131	1,564301003	-0,431970906	0,521805874
69	-0,430467744	1,621058662	-0,507990926	0,556373374
70	-0,341479649	1,63848746	-0,585856964	0,62660536
71	-0,241151681	1,65276453	-0,691296065	0,695084727
72	-0,153976343	1,692810124	-0,76440057	0,731552992
73	-0,043357532	1,749418818	-0,885282651	0,755389166
74	0,043792501	1,759426607	-0,966223128	0,801195833
75	0,03065381	1,777676341	-1,006257591	0,823347835
76	0,061783888	1,778430214	-1,040225238	0,840084657
77	0,085797987	1,763634228	-1,065354876	0,860354287
78	0,155939009	1,736992494	-1,105995569	0,892884424
79	0,164888916	1,724864137	-1,10578918	0,912499669
80	0,194197935	1,674585597	-1,118581515	0,924446637
81	0,18415093	1,642503815	-1,084571019	0,933413092
82	0,112467235	1,64498965	-1,040488257	0,939234647
83	0,091210161	1,598737443	-0,971304385	0,948437291
84	0,009947235	1,582043275	-0,888917091	0,95988147
85	-0,04370544	1,614282609	-0,816585761	0,934044912
86	0,00016748	1,625913378	-0,814643156	0,917037358
87	0,08559706	1,708864677	-0,847788332	0,886418506
88	0,063233562	1,754431763	-0,834949456	0,868823163
89	0,043254819	1,733805678	-0,801066997	0,872619298
90	-0,01808046	1,787996088	-0,746478001	0,830872949
91	-0,023680352	1,779419367	-0,677999721	0,769972833
92	-0,051160911	1,771741609	-0,612154042	0,715204563
93	-0,106846182	1,782842357	-0,544991282	0,667683481
94	-0,092086701	1,801491902	-0,514863529	0,593419437
95	-0,103950453	1,79914535	-0,466594085	0,526821815
96	-0,202153515	1,77620033	-0,347814501	0,440390786
97	-0,335556611	1,703514678	-0,204381268	0,363715339
98	-0,383454466	1,667101938	-0,091499369	0,280226205
99	-0,44707112	1,681711616	0,002572544	0,14205835
100	-0,487476777	1,680513267	0,067469754	0,035491667
101	-0,543623654	1,703257775	0,104343536	-0,00156636
102	-0,539467005	1,713289303	0,106819558	-0,062342788
103	-0,505193293	1,683380984	0,103003627	-0,086322483
104	-0,467704936	1,64473618	0,112575584	-0,101730444
105	-0,463127269	1,616351578	0,135094128	-0,116571962
106	-0,50999794	1,63786491	0,159811813	-0,123477957
107	-0,508859819	1,643623581	0,174873312	-0,139657199
108	-0,542288314	1,640573528	0,198345491	-0,170991311
109	-0,565772028	1,640213116	0,203408317	-0,138491088
110	-0,582491606	1,636768468	0,200047954	-0,067768564

111	-0,599601943	1,639440891	0,20609205	-0,055488577
112	-0,645322903	1,642778311	0,219865312	-0,029003688
113	-0,702291403	1,677822691	0,253755546	-0,058529477
114	-0,796814489	1,725864492	0,288307053	-0,103005628
115	-0,81563556	1,748450104	0,297300584	-0,128746684
116	-0,818402597	1,750993346	0,299027572	-0,137923171
117	-0,844932637	1,796267144	0,297808388	-0,159769147
118	-0,863312635	1,806982299	0,301012196	-0,122156985
119	-0,854229432	1,81499395	0,301953186	-0,13633931
120	-0,84796896	1,823914716	0,310092908	-0,173186606
121	-0,85009351	1,833207719	0,314651899	-0,178131938
122	-0,833112228	1,847952859	0,317040671	-0,200358684
123	-0,823603511	1,849389872	0,302000129	-0,180810529
124	-0,784024036	1,854898932	0,280232734	-0,141160904
125	-0,778242792	1,84431454	0,263374834	-0,082030474
126	-0,747785153	1,865519939	0,225852069	-0,037079433
127	-0,725230116	1,835273246	0,180010194	0,048708915
128	-0,716440589	1,828088451	0,127821272	0,110985379
129	-0,702692848	1,826522099	0,074152048	0,200052399
130	-0,694317882	1,825160258	0,01915926	0,266576399
131	-0,639034009	1,829754587	-0,045986003	0,320088368
132	-0,614912271	1,832269201	-0,112975838	0,403444763
133	-0,59741804	1,852032781	-0,186119902	0,472855062
134	-0,59620348	1,840772518	-0,23002112	0,546948255
135	-0,590131223	1,86405666	-0,279775625	0,585630649
136	-0,582534541	1,85846557	-0,316016665	0,621860128
137	-0,56978815	1,859667189	-0,338018169	0,641713679
138	-0,53934601	1,87324558	-0,36114945	0,643049995
139	-0,53710137	1,885846391	-0,378857737	0,637431381
140	-0,511811993	1,901515083	-0,394884591	0,649151986
141	-0,536165448	1,910932578	-0,403511823	0,652337015
142	-0,197373038	1,757392382	-0,580780053	0,749701551
143	0,133513215	1,59273159	-0,789654985	0,849554201
144	0,443106352	1,555271523	-1,070688753	0,935698869
145	0,69520169	1,462665009	-1,338162446	1,037945371
151	1,114386084	1,469646479	-1,733207633	1,184630256
152	1,109268355	1,510971083	-1,797878434	1,201055013
153	1,019423045	1,594003124	-1,765501424	1,20678195
154	0,953906336	1,645627709	-1,684845568	1,185894618
155	0,912795198	1,702430899	-1,564752886	1,146115013
156	0,781679841	1,723526035	-1,393582849	1,097183376
157	0,66187933	1,750394837	-1,232613193	1,04360668
160	0,22734314	1,872823419	-0,905203738	0,858218679
162	0,021140627	1,894921178	-0,686665541	0,736054951
163	-0,048539254	1,895273218	-0,553898881	0,659757453
164	-0,162269367	1,892627318	-0,452982635	0,59556438
165	-0,278877176	1,917450571	-0,380538896	0,542241421
166	-0,344681849	1,955562755	-0,333638259	0,501117173
167	-0,418000617	1,98199697	-0,284970784	0,467902003
168	-0,395874529	1,985438723	-0,25995328	0,41607961
169	-0,38631092	1,969546663	-0,221221839	0,388050066
170	-0,391805267	1,95036919	-0,186308114	0,340447936
171	-0,373630511	1,9418427	-0,14031916	0,277413244
172	-0,412374963	1,937288273	-0,097970591	0,249152927
173	-0,428792178	1,954518846	-0,072818757	0,187463988
174	-0,433426907	1,949567297	-0,045103859	0,163000259
175	-0,408368578	1,930536245	-0,007558167	0,095948476
176	-0,435776514	1,941627748	0,024135682	0,026816677
177	-0,460618571	1,953152333	0,08043538	-0,04292599

178	-0,541030789	1,957247269	0,126575974	-0,061702806
179	-0,539652486	1,948229149	0,116887959	-0,049858705
180	-0,561170284	1,947186357	0,112338733	-0,023267956
181	-0,605922108	1,937147825	0,108143273	0,021470943
182	-0,616468597	1,926906857	0,091148221	0,056896379
183	-0,663275432	1,917096352	0,091597735	0,059658065
184	-0,666435096	1,922047061	0,11045058	0,002143572
185	-0,686522359	1,92365362	0,123279092	-0,003526321
186	-0,691276245	1,910006123	0,141734823	-0,014986266
187	-0,697461949	1,897013979	0,134153822	0,003472167
188	-0,683719392	1,879414755	0,13437511	0,026669797
189	-0,73606916	1,884755464	0,157650324	0,039536614
190	-0,747463084	1,895445471	0,17261673	0,025676974
191	-0,730386177	1,889024219	0,171256091	0,010299777
192	-0,749263336	1,885439728	0,208964424	-0,029077822

Position in core (mm)	CLR_Ca_smooth	CLR_Fe_smooth	CLR_Br_smooth	CLR_Sr_smooth
898	-0,032621284	1,781566653	0,313597953	-0,246105457
899	0,036642658	1,757872919	0,272969456	-0,220243207
900	0,114160378	1,746736022	0,241135009	-0,184930848
901	0,156146789	1,731827908	0,225560002	-0,151251405
902	0,167821538	1,72344214	0,218445789	-0,146721142
903	0,181166072	1,713499759	0,211612312	-0,129135596
904	0,250482615	1,683805039	0,187461119	-0,122925323
905	0,29401205	1,681551806	0,185952394	-0,111741477
906	0,343086763	1,672823673	0,163851723	-0,098748304
907	0,399212156	1,659772156	0,138989014	-0,08640551
908	0,445044489	1,652294289	0,130255492	-0,07849345
909	0,465607388	1,641954949	0,121473894	-0,043643946
910	0,482806195	1,630157119	0,103005156	-0,007557157
911	0,523992258	1,626552173	0,074015028	0,017368988
912	0,561093685	1,621374619	0,055826467	0,05275525
913	0,596165832	1,609203044	0,033451994	0,078438314
914	0,603149179	1,604806741	0,028858313	0,111840266
915	0,618676974	1,600820679	0,013790728	0,13150103
916	0,61935254	1,588909978	0,012514578	0,156496998
917	0,62467095	1,578251316	0,011258218	0,168401712
918	0,674336738	1,556894168	-0,001111706	0,171337547
919	0,689511363	1,563085216	0,004055021	0,145424491
920	0,681044608	1,569241869	0,002851136	0,134512997
921	0,649048703	1,561061912	0,003168781	0,138849175
922	0,659063679	1,555715602	-0,014037823	0,122785367
923	0,695556671	1,548476368	-0,014453171	0,110007138
924	0,74488398	1,539630722	-0,035122705	0,098077636
925	0,831299742	1,489334299	-0,077108644	0,116777329
926	0,89672055	1,467613342	-0,093747862	0,108351106
927	0,937383256	1,453054843	-0,111118621	0,106293371
928	0,982536541	1,433367054	-0,120688619	0,094981609
929	1,015925913	1,413659396	-0,127466867	0,090119493
930	1,072943458	1,394592785	-0,128181466	0,075109707
931	1,184678151	1,361661804	-0,140177337	0,050362055
932	1,304152183	1,309984984	-0,150876767	0,069500716
933	1,351509862	1,29084462	-0,169965331	0,05422576
934	1,361986257	1,289761188	-0,146602208	0,033687338
935	1,334126729	1,308104163	-0,098781424	-0,0251057
936	1,327984692	1,316814137	-0,07411669	-0,078132932
937	1,323800011	1,335540629	-0,047383709	-0,140892871
938	1,290366973	1,356314329	-0,03126987	-0,171024059

939	1,343686589	1,327931146	-0,047001738	-0,177254336
940	1,326177523	1,345100084	-0,036179785	-0,221248363
941	1,276771572	1,369977006	-0,011484619	-0,252395511
942	1,16274031	1,424702312	0,022402953	-0,32516973
943	1,11879857	1,44681351	0,052350156	-0,344299077
944	1,054133861	1,474604597	0,071037394	-0,395032384
945	1,039931153	1,490371526	0,069408151	-0,419532962
946	1,005769866	1,506253083	0,072577435	-0,41183629
947	1,007176028	1,495502875	0,068307833	-0,424509122
948	0,973856299	1,51952991	0,08963087	-0,457778852
949	0,866883956	1,584128492	0,134018125	-0,521733811
950	0,834520243	1,597622123	0,15834994	-0,557603139
951	0,760517429	1,626082187	0,186002753	-0,596308095
952	0,705517996	1,649509234	0,210831992	-0,624196728
953	0,601452356	1,683567535	0,248164104	-0,656615076
954	0,556444229	1,694905549	0,262637863	-0,66303528
955	0,449123317	1,730237261	0,29528685	-0,675927092
956	0,3827074	1,760663366	0,328160545	-0,715207816
957	0,310132521	1,783682952	0,356583587	-0,730818094
958	0,280819761	1,788773026	0,365295075	-0,734939227
959	0,245797115	1,794520934	0,381091994	-0,70785717
960	0,269234622	1,789408064	0,369000557	-0,711766406
961	0,298270794	1,780633183	0,349796355	-0,699731958
962	0,287095492	1,790555065	0,348961152	-0,680005025
963	0,272446568	1,800378517	0,348694403	-0,69405581
964	0,276766477	1,804289711	0,34887499	-0,702651415
965	0,28859327	1,805484273	0,353105082	-0,710107748
966	0,325895519	1,809089053	0,333277316	-0,741109309
967	0,443387283	1,772495768	0,287500143	-0,712942961
968	0,538329367	1,733989552	0,253551083	-0,689324719
969	0,581859497	1,723034076	0,239594172	-0,703016264
970	0,534911823	1,73414172	0,250693846	-0,698790641
971	0,522921331	1,745111945	0,269032557	-0,693123619
972	0,559598353	1,732623108	0,25992398	-0,704128132
973	0,62184652	1,711604741	0,243015348	-0,694884252
974	0,674159587	1,699683177	0,22225569	-0,690731368
975	0,75352715	1,682371912	0,187447407	-0,694781104
976	0,817831432	1,652286585	0,159521409	-0,67849083
977	0,699485071	1,706948591	0,196411661	-0,69366403
978	0,552719643	1,764199257	0,236677587	-0,726651475
979	0,540227804	1,766939375	0,232920978	-0,728698436
980	0,570113128	1,760776016	0,222379738	-0,725135234
981	0,498664522	1,766934983	0,219282847	-0,712708983
982	0,424696093	1,784144045	0,229222453	-0,691292198
983	0,330427161	1,812861472	0,249644753	-0,703259629
984	0,223335257	1,834400986	0,261688066	-0,67052399
985	0,1044053	1,866009894	0,285825489	-0,65545821
986	-0,035452532	1,908690461	0,320830607	-0,642178149

Position in core (mm)	CLR_Ca_smooth	CLR_Fe_smooth	CLR_Br_smooth	CLR_Sr_smooth
376	-0,11367863	1,950483442	0,487127037	-0,59756203
377	-0,110022463	1,94351076	0,480919458	-0,581247178
378	-0,086777259	1,935754652	0,465446955	-0,586243868
379	-0,073049805	1,930635287	0,45092413	-0,563775249
380	-0,058040591	1,92427472	0,441238899	-0,527994981
381	-0,057381174	1,913037991	0,42736504	-0,505832039
382	-0,060615403	1,89967445	0,414117451	-0,465363955
383	-0,052035007	1,887661176	0,397588157	-0,412731677

384	-0,036883548	1,87374109	0,377302248	-0,373970911
385	0,083622005	1,83977864	0,345547918	-0,3646758
386	0,231473263	1,800810254	0,317724458	-0,349697362
387	0,256708296	1,793845917	0,308822667	-0,327730361
388	0,259631404	1,783900384	0,302254965	-0,295861116
389	0,262042605	1,777838843	0,283094668	-0,267598228
390	0,243589729	1,771317775	0,266897438	-0,23154604
391	0,239362122	1,7700697	0,25453188	-0,20392489
392	0,241395351	1,767432392	0,253435446	-0,189318179
393	0,229477369	1,767234598	0,245548039	-0,171316099
394	0,22180291	1,770730739	0,235413922	-0,137945614
395	0,110099861	1,789329457	0,243833562	-0,078026389
396	-0,027117354	1,811699611	0,254293897	-0,032368931
397	-0,017147272	1,796842183	0,227675558	0,007444365
398	-0,015296627	1,790659022	0,211522476	0,053892615
399	0,004013936	1,774257395	0,194543998	0,109893479
400	0,052843471	1,754949055	0,176012466	0,151929604
401	0,089590878	1,74228452	0,14988429	0,178412535
402	0,143076825	1,722654553	0,119062198	0,192466685
403	0,241818795	1,699891435	0,091835741	0,19002583
404	0,351686792	1,664564975	0,058756442	0,17950047
405	0,446649752	1,648590304	0,031746111	0,177237552
406	0,534701908	1,626440949	0,007260957	0,184319312
407	0,637468191	1,603743219	-0,022229151	0,188885024
408	0,774514998	1,56581072	-0,064307706	0,189670013
409	0,860251665	1,544722015	-0,086696019	0,188876026
410	0,927159674	1,528245646	-0,104449487	0,176139375
411	1,013037222	1,501733418	-0,103193481	0,154605488
412	1,05989599	1,486577569	-0,105538145	0,145819731
413	1,05881323	1,477171726	-0,095120901	0,132068643
414	1,031644001	1,476628622	-0,075984589	0,11585871
415	1,02179332	1,473995654	-0,065938001	0,104400968
416	1,011005514	1,473176816	-0,063827954	0,090235838
417	1,045309808	1,458868239	-0,060186738	0,073352713
418	0,966662991	1,479146172	-0,025645908	0,056290637
419	0,901912413	1,509717211	0,014210069	-0,012473996
420	0,840796032	1,536468028	0,036547779	-0,051767344
421	0,769616708	1,561726246	0,038276031	-0,034281598
422	0,730979299	1,583091474	0,049858046	-0,029195744
423	0,710736969	1,598184283	0,046200861	-0,013338303
424	0,667769088	1,617468705	0,053976259	-0,004175261
425	0,627147279	1,629962057	0,061527628	-0,011241838
426	0,612623936	1,641241242	0,080134135	-0,024280439
427	0,503065364	1,67883392	0,117049325	-0,044971301
428	0,484388981	1,690275104	0,125399405	-0,064818395
429	0,487995406	1,680019072	0,117942777	-0,03739876
430	0,562559169	1,661087408	0,115671974	-0,032398372
431	0,61487802	1,657560843	0,128296434	-0,089577983
432	0,61961171	1,662254238	0,14135304	-0,133810236
433	0,606081211	1,674206948	0,167332474	-0,172411571
434	0,631053558	1,680447461	0,174546156	-0,21280118
435	0,640974267	1,687268892	0,180219223	-0,254808168
436	0,68640627	1,683413886	0,172254988	-0,268039023
437	0,755051743	1,652412308	0,156030104	-0,268666966
438	0,82480162	1,64396049	0,154725032	-0,305428659
439	0,837753527	1,655804562	0,169777957	-0,365183054
440	0,783167672	1,678412823	0,182889219	-0,418530825
441	0,762121384	1,683643249	0,192890616	-0,439208141
442	0,75950442	1,689759429	0,193908798	-0,453506742

443	0,773482593	1,693516042	0,192059717	-0,470780733
444	0,785155343	1,693389045	0,192535256	-0,483423711
445	0,784329001	1,694591889	0,200454107	-0,486264362
446	0,729227951	1,713519982	0,220010693	-0,503581164
447	0,673025582	1,756675119	0,249692863	-0,570730111
448	0,604359965	1,778789248	0,271955223	-0,56784955
449	0,613558922	1,773676826	0,26464161	-0,558785277
450	0,613600056	1,771687335	0,262014001	-0,551032264
451	0,611687864	1,779637358	0,270951309	-0,559487245
452	0,600515056	1,77851295	0,284569519	-0,580654609
453	0,570844042	1,78031731	0,292970257	-0,597843521
454	0,527106784	1,791472224	0,30727678	-0,597886048

Position in core (mm)	CLR_Ca_smooth	CLR_Fe_smooth	CLR_Br_smooth	CLR_Sr_smooth
628	1,162181226	1,68408197	0,0132872	-0,162720675
629	1,188661687	1,67456139	-0,000722944	-0,161929781
630	1,221094026	1,671635645	-0,007962664	-0,171960799
631	1,207332161	1,678055686	-0,004358077	-0,175773901
632	1,188245183	1,693628787	0,000230917	-0,177322498
633	1,135468201	1,71211882	0,016582694	-0,172410543
634	1,074300327	1,743831622	0,025706964	-0,161340236
635	1,044653204	1,754233321	0,025823475	-0,169287306
636	1,032633155	1,765980748	0,023661194	-0,153723626
637	1,006031136	1,766426259	0,013435877	-0,122611235
638	1,032530233	1,751905016	-0,019161144	-0,083516099
639	1,073686081	1,716892531	-0,049549741	-0,030472847
640	1,102712571	1,686109018	-0,079393899	0,023484081
641	1,09220524	1,677176954	-0,105649795	0,071729663
642	1,107044862	1,661551891	-0,12464012	0,10591343
643	1,126630986	1,646242032	-0,151511977	0,131414141
644	1,138811165	1,626390867	-0,169629748	0,157615426
645	1,207327651	1,599233932	-0,190543932	0,184517716
646	1,235546561	1,582917649	-0,203199459	0,207041348
647	1,283099348	1,569985457	-0,229492538	0,206096147
648	1,300613397	1,558203665	-0,226216552	0,232700085
649	1,332404136	1,551452039	-0,243039791	0,227709432
650	1,372658269	1,535161714	-0,248349279	0,229553793
651	1,453049035	1,492739089	-0,254971607	0,240904147
652	1,532521253	1,443200368	-0,28263926	0,264306003
653	1,607659976	1,400534907	-0,311372297	0,300734071
654	1,687714915	1,357506015	-0,33754046	0,347168146
655	1,761479231	1,311037435	-0,370919105	0,393635832
656	1,880890627	1,231179505	-0,432020199	0,449565493
657	1,968817668	1,156555242	-0,459216049	0,518586791
658	2,036344685	1,108056482	-0,50329105	0,559219456
659	2,080086937	1,090143845	-0,512440276	0,594300726
660	2,106932383	1,070439841	-0,535710815	0,621180254
661	2,115749454	1,059320368	-0,567224255	0,642760595
662	2,144499455	1,043111203	-0,595171842	0,657936477
663	2,153326236	1,039087319	-0,613814103	0,678992905
664	2,165006942	1,022670558	-0,634151406	0,693210867
665	2,18155314	1,016088944	-0,652047254	0,706017539
666	2,19684321	1,022169717	-0,657148109	0,710879522
667	2,197952872	1,033812284	-0,664314242	0,705111868
668	2,217635445	1,037472289	-0,673702261	0,699865919
669	2,254742078	1,016092697	-0,698291764	0,711976673
670	2,377078482	0,952745021	-0,780644887	0,745779775
671	2,424542475	0,910506151	-0,818678494	0,80103459

672	2,444175961	0,887335764	-0,846434315	0,833248625
673	2,367377179	0,924283516	-0,814957526	0,843789781
674	2,347198506	0,932610304	-0,776873429	0,825591751
675	2,318228075	0,94334841	-0,736943984	0,772993296
679	2,263389558	0,985065591	-0,658771988	0,678407051
680	2,232088428	1,015964559	-0,626052165	0,651369522
681	2,212421143	1,042146344	-0,603403932	0,641129591
682	2,196916056	1,067071996	-0,591326464	0,638655238
683	2,190660755	1,065840048	-0,609671555	0,6424964
684	2,225243469	1,065710873	-0,659739438	0,668137374
685	2,263403432	1,052765702	-0,692458709	0,725106037
686	2,289867626	1,044589526	-0,73068322	0,774548301
687	2,299957179	1,032465971	-0,765564011	0,821574526
688	2,302097726	1,051924825	-0,776329647	0,846917909
689	2,272623952	1,060761826	-0,787673629	0,877270628
690	2,2444859	1,061464394	-0,802886453	0,906427126
691	2,263005315	1,057495437	-0,825911272	0,913525909
692	2,278935976	1,050819165	-0,839265098	0,922627645
693	2,332485797	1,022654371	-0,856173569	0,928113279
694	2,264149051	1,043081378	-0,828356815	0,9174761
695	2,214244318	1,068048414	-0,815838048	0,882849135
696	2,190413226	1,084279413	-0,806223266	0,863877136
697	2,172873198	1,093191417	-0,798502334	0,854254304
698	2,152520945	1,094140485	-0,780165673	0,838992693
699	2,132902115	1,102108317	-0,770969497	0,811917066
700	2,108146082	1,122837404	-0,736267736	0,797265212
701	2,049529602	1,139530296	-0,693444347	0,766512005
702	2,020500051	1,158308369	-0,654843107	0,746018284
703	1,981968779	1,183135542	-0,624036781	0,732283995
704	2,031666644	1,166151192	-0,614941321	0,731980897
705	2,034390159	1,158340827	-0,613426791	0,721982458
706	2,017701354	1,163548469	-0,608053749	0,713716531
707	2,00084474	1,174366911	-0,59912019	0,709450689
708	1,969365323	1,176434546	-0,600992301	0,724052199
709	1,980763669	1,183227923	-0,576770494	0,73648903
710	1,971199822	1,191789223	-0,572747974	0,720440501
711	1,998411173	1,188843845	-0,584099959	0,712047683
712	2,007107543	1,18515071	-0,588384526	0,704977324
713	1,964900789	1,213263113	-0,564246142	0,684531422
714	1,912243459	1,249882931	-0,564670395	0,663839379
715	1,882959489	1,259590236	-0,5516815	0,686244506
716	1,876792815	1,266444791	-0,545572667	0,692282254
717	1,914570505	1,258554732	-0,558994907	0,686899113
718	1,925240015	1,273685398	-0,547572631	0,669594274
719	1,918297686	1,275192047	-0,561031846	0,651101276
720	1,94951169	1,261905682	-0,588804785	0,647973246
721	1,943309863	1,266648093	-0,58940202	0,666935154
722	1,899595499	1,281082424	-0,581743149	0,664491437
723	1,929157373	1,264063781	-0,598847054	0,680507333
724	1,936282683	1,255012947	-0,595394168	0,682790143
725	1,918049196	1,270403101	-0,596478207	0,672036209
726	1,92045012	1,281308201	-0,594355397	0,656853767
727	1,878941873	1,310563822	-0,583618695	0,630194363
728	1,84648789	1,318188182	-0,584176895	0,620315157
729	1,811105619	1,318130712	-0,570089147	0,627683041
730	1,754423486	1,342587897	-0,534292496	0,633124369
731	1,743709727	1,351249695	-0,526353167	0,625108204
732	1,734591255	1,357800211	-0,534701471	0,624812075
733	1,739344746	1,353761191	-0,533172964	0,615970602

734	1,731926738	1,361609343	-0,521447137	0,619787105
735	1,759483849	1,354937203	-0,506695256	0,603517982
736	1,754987298	1,362931655	-0,499796748	0,596741909
737	1,785815815	1,328585454	-0,508796271	0,624384966
738	1,813137407	1,311052131	-0,501130695	0,632232676
739	1,847575236	1,303876647	-0,509229946	0,623768538
740	1,904200389	1,292204961	-0,52429269	0,611747493
741	1,936003772	1,291262065	-0,54569774	0,599617908
742	2,013358516	1,257785632	-0,578931234	0,610106873
743	2,021735283	1,260052653	-0,583471276	0,628356548
744	2,028275623	1,244521523	-0,588828847	0,639045532
745	2,034040902	1,251381946	-0,609304834	0,652133487
746	2,035643816	1,238730848	-0,614687596	0,658868019
747	1,994845029	1,268444372	-0,588029283	0,633791415
748	1,979443861	1,293201119	-0,580705926	0,606311249
749	1,992584893	1,301533972	-0,577133983	0,597689117
750	1,951032526	1,311765674	-0,560970483	0,593126229
751	1,911336195	1,317570389	-0,531687501	0,587508109
752	1,864435273	1,338054547	-0,485053863	0,560404518
753	1,870566967	1,346078944	-0,481128923	0,530770639
754	1,927142408	1,343622826	-0,503461089	0,511381851
755	1,963190049	1,32368412	-0,511626438	0,512146979
756	1,985900761	1,319368223	-0,518463402	0,520567024
757	2,0424209	1,291754225	-0,540244553	0,525046585
758	2,111321589	1,252318178	-0,57569476	0,548081718
759	2,102457189	1,253892627	-0,574541354	0,563541929
760	2,104317721	1,265079482	-0,566768558	0,567306394
761	2,158245193	1,264493268	-0,600364089	0,573805661
762	2,175787209	1,267983965	-0,617322521	0,602137293
763	2,175539029	1,255821573	-0,622223848	0,617181749
764	2,142187297	1,257176803	-0,608595028	0,629614269
765	2,098175487	1,281876492	-0,584656733	0,62172639
766	2,072234976	1,290415699	-0,585442588	0,631962894
767	2,069695784	1,307642486	-0,590069122	0,659233621
768	2,050649235	1,32880794	-0,578273417	0,662108695
769	2,041547798	1,328594307	-0,597789176	0,667556518
770	2,054533955	1,319152243	-0,622440411	0,675688421
771	2,073029582	1,29239705	-0,622934123	0,685102498
772	2,097592972	1,286019962	-0,630595712	0,685867171
773	2,116760776	1,294834169	-0,6336905	0,700098792
774	2,138163015	1,284221557	-0,663966711	0,704181356
775	2,160740731	1,266206614	-0,682499495	0,730304425
776	2,147806638	1,264412872	-0,667095755	0,710275731
777	2,11467141	1,277247176	-0,647305526	0,685948436
778	2,087560311	1,282611009	-0,646070558	0,673181136
779	2,116684274	1,283648365	-0,643939483	0,673299482
780	2,117013693	1,278433552	-0,639005707	0,679299713
781	2,039800587	1,312348339	-0,605188206	0,697076386
782	1,995067689	1,320409217	-0,581748143	0,700706866
783	1,971833794	1,313008506	-0,570498559	0,696968663
784	1,943540988	1,333763162	-0,540275503	0,686609971
785	1,939193054	1,33889602	-0,517978398	0,658071464
786	1,970194847	1,335894246	-0,522567492	0,648248002
787	2,002338619	1,321119876	-0,53738912	0,660544514
788	2,012297187	1,317542953	-0,539821712	0,675655278
789	2,012627996	1,316500357	-0,532721127	0,666742377
790	2,019635934	1,315046965	-0,545010585	0,667906633
791	2,032205335	1,303570814	-0,577844434	0,654689226
792	2,059157295	1,286784162	-0,608329723	0,645491206

793	2,073988189	1,286999128	-0,622020453	0,645699536
794	2,077828012	1,278712721	-0,621840569	0,660058782
795	2,082403095	1,280776254	-0,643774045	0,666032722
796	2,057588347	1,298626606	-0,641367368	0,686292145
797	2,035996708	1,297991124	-0,642728488	0,686363944
798	2,049075801	1,280582077	-0,640208988	0,681906759
799	2,036295055	1,285591717	-0,643251152	0,695748138
800	2,082903311	1,261600909	-0,643477454	0,704643362
801	2,113822941	1,241270121	-0,634212198	0,71436562
802	2,100602445	1,250779754	-0,622922993	0,712814338
803	2,107182927	1,23884644	-0,636741679	0,735666187
804	2,127154569	1,217604579	-0,653675851	0,739017116
805	2,128608754	1,220892649	-0,661513135	0,743767749
806	2,16635554	1,202162898	-0,682976092	0,749510228
807	2,191296751	1,200113462	-0,68284922	0,757330911
808	2,193839409	1,205451026	-0,68194345	0,765945449
809	2,205845533	1,198419407	-0,701817598	0,776601157
810	2,180860894	1,212861675	-0,709328902	0,773639667
811	2,222920218	1,206635977	-0,714707237	0,762794393
812	2,201336043	1,210638569	-0,701009729	0,768680913
813	2,194290132	1,226812855	-0,679270268	0,73504309
814	2,189902218	1,259888632	-0,661198377	0,727419219
815	2,201890098	1,249325315	-0,658595818	0,721799368
816	2,183166453	1,244520993	-0,64468149	0,731769117
817	2,152541883	1,250899384	-0,628936641	0,728737284
818	2,124733521	1,269614596	-0,612852811	0,716856135
819	2,117445066	1,282251727	-0,58449422	0,676724097
820	2,121550059	1,288251732	-0,578209086	0,667120882
821	2,071098788	1,310062923	-0,554632089	0,670365341
822	2,092103221	1,310387327	-0,56381573	0,671108388
823	2,096571252	1,299287319	-0,558669771	0,678667387
824	2,095074145	1,28115912	-0,566359307	0,674819552
825	2,088808135	1,284543121	-0,575997482	0,676879614
826	2,107625169	1,280464971	-0,569383629	0,660428719
827	2,124308983	1,280151051	-0,565241419	0,659155338
828	2,128549273	1,271783011	-0,57740391	0,659986763
829	2,15241659	1,237325978	-0,583166884	0,677700482
830	2,14936553	1,235099931	-0,569744985	0,682868516
831	2,167731459	1,232113557	-0,583544668	0,661654803
832	2,172663252	1,228355728	-0,575686792	0,661821727
833	2,153269028	1,233426913	-0,570372424	0,655406794
834	2,153450847	1,240191154	-0,563525547	0,658158043
835	2,174818016	1,227411721	-0,544781169	0,651396817
836	2,150210214	1,228813917	-0,549244215	0,65478947
837	2,137985363	1,229674444	-0,538197357	0,645508775
838	2,139882705	1,237747324	-0,528721694	0,621863642
839	2,110325644	1,264892012	-0,516323097	0,616049564
840	2,095416654	1,262156963	-0,503742139	0,606254791
841	2,062642726	1,277487513	-0,487022751	0,600132939
842	2,03409858	1,288388434	-0,474149274	0,577615964
843	1,993223088	1,314732015	-0,46945377	0,56096673
844	1,953388824	1,329181001	-0,460002043	0,532228416
845	1,916304038	1,344781581	-0,449764337	0,514334447
846	1,937507252	1,35619348	-0,449944464	0,490494324
847	1,910109474	1,367735765	-0,456242989	0,468628225
848	1,859052443	1,387713723	-0,430125989	0,464093325
849	1,779510787	1,430549698	-0,405239051	0,432733434
850	1,703231963	1,469514065	-0,380138468	0,410441284
851	1,603165814	1,509086719	-0,351854959	0,402899679

852	1,542749742	1,53965953	-0,330950578	0,396829131
853	1,515994566	1,55455183	-0,306467329	0,38283031
854	1,497593244	1,568759166	-0,287413128	0,369954754
855	1,441914708	1,617147253	-0,250898317	0,335774816
856	1,347040542	1,653731399	-0,207996341	0,315009792
857	1,332806494	1,670419598	-0,190501362	0,305840884
858	1,304933706	1,689730825	-0,180497053	0,32139507
859	1,302298671	1,692257391	-0,165490163	0,327559333
860	1,276189015	1,707137502	-0,162546964	0,320272338
861	1,337255889	1,69284842	-0,17035658	0,316670598
862	1,371378533	1,696668416	-0,190706533	0,298972074
863	1,396650415	1,68790204	-0,206310199	0,299304984
864	1,394439227	1,705867582	-0,191005196	0,309480131
865	1,369928759	1,709161901	-0,198965468	0,330007777
866	1,334001746	1,737625402	-0,192477662	0,339301066
867	1,285689868	1,763463103	-0,189466904	0,328005125
868	1,261229938	1,761322085	-0,195579162	0,288549181
869	1,295948454	1,741841151	-0,205090969	0,272661112
870	1,356860894	1,730582002	-0,220870944	0,245020275
871	1,331220618	1,74006274	-0,223263396	0,223798371
872	1,318204595	1,738980617	-0,204983579	0,222089211
873	1,298536365	1,750068398	-0,183660835	0,210050772
874	1,274773348	1,7353101	-0,195993854	0,195300468
875	1,314285461	1,716373362	-0,192839234	0,182214035
876	1,420714886	1,674385526	-0,21502014	0,164738545
877	1,447295072	1,655724087	-0,211075337	0,144577176
878	1,500079894	1,648332593	-0,216692928	0,144726534
879	1,516560333	1,639729507	-0,236295273	0,147771215
880	1,532864854	1,628108738	-0,23468558	0,176733225
881	1,595293926	1,616669329	-0,231819684	0,188129056
882	1,597006394	1,615338021	-0,225139207	0,183721124
883	1,60694362	1,616115523	-0,227546338	0,164395434
884	1,607391849	1,633151125	-0,219895621	0,156739603
885	1,601660847	1,642940782	-0,218589004	0,137987577
886	1,565306993	1,664787009	-0,201474631	0,108760416
887	1,602306916	1,664165555	-0,20701245	0,101698066
888	1,617869983	1,659920947	-0,207285209	0,08722375
889	1,595741682	1,682638404	-0,18637516	0,064501241
890	1,567024075	1,698668569	-0,184788225	0,037460594
891	1,54048017	1,712247496	-0,177383719	0,001520697
892	1,562474395	1,714394181	-0,178419629	-0,04383093
893	1,666482185	1,691810132	-0,202304315	-0,057701134
894	1,74811609	1,662519211	-0,223274184	-0,08208253
895	1,75808983	1,671610878	-0,221934789	-0,104294871
896	1,732003472	1,688820904	-0,217618382	-0,133014092
897	1,675153701	1,714867812	-0,197241943	-0,144387137
898	1,605613493	1,752215686	-0,175589553	-0,162603438
899	1,556276096	1,781201508	-0,15756202	-0,197068024
900	1,497832615	1,810494328	-0,127640442	-0,208833204
901	1,447702548	1,832261899	-0,123153004	-0,199419907
902	1,382930808	1,872735279	-0,104113025	-0,207029394
903	1,230704489	1,927127673	-0,067130961	-0,232028891
904	1,101242799	1,988691241	-0,02361695	-0,252100313
905	1,0173157	2,025202953	0,009137356	-0,249040014
906	0,959314376	2,038037462	0,024982756	-0,231331081
907	0,92297712	2,048081859	0,033370432	-0,239509291
908	0,895295209	2,057215823	0,050395616	-0,24713946
909	0,865159009	2,070065657	0,060382744	-0,241392789
910	0,842686251	2,085191781	0,071665598	-0,268135562

911	0,805347809	2,093978894	0,08701416	-0,277571168
912	0,801074609	2,088183908	0,080662645	-0,259849106
913	0,778605627	2,088368564	0,075070545	-0,221410496
914	0,785657311	2,074205446	0,056929179	-0,161107053
915	0,807211727	2,059340301	0,036572298	-0,124889503
916	0,827939171	2,054854102	0,027809042	-0,108427662
917	0,837356788	2,043762552	0,019059911	-0,079492166
918	0,854469799	2,02848467	-0,005151523	-0,028588833
919	1,012709922	1,965016973	-0,063355075	0,012827359
920	1,157718008	1,911987865	-0,106097531	0,056410231
921	1,181964737	1,912790529	-0,113294341	0,062969611
922	1,1917124	1,910719208	-0,118199628	0,071568394
923	1,23931925	1,894313711	-0,142337685	0,087909226
924	1,297749491	1,877290645	-0,142754532	0,056645427
925	1,335826412	1,868651193	-0,152454823	0,034974126
926	1,365426424	1,865482773	-0,167839854	0,050059937
927	1,417340038	1,858947889	-0,195661429	0,0537743
928	1,490858442	1,843671964	-0,216513352	0,04319741
929	1,366098023	1,889282134	-0,180364838	0,029201278
930	1,274462605	1,920654097	-0,167280758	0,015707912
931	1,342113775	1,89845955	-0,198263158	0,003316198
932	1,446400309	1,868585139	-0,235547841	0,003215335
933	1,425129517	1,873761309	-0,228292013	0,00958648
934	1,385155203	1,884518334	-0,234933691	0,036170245
935	1,371928438	1,883973446	-0,227524502	0,034543774
936	1,353505378	1,886393972	-0,221676386	0,01657882
937	1,312546097	1,894209991	-0,201342514	-8,36886E-05
938	1,263932516	1,910375686	-0,190137871	-0,018457917
939	1,259353361	1,908329568	-0,19533885	-0,021087479
940	1,23877137	1,913027376	-0,193501571	-0,031817695
941	1,171851114	1,926994089	-0,166284378	-0,026304089
942	1,074770577	1,958098959	-0,130554251	-0,02636839
943	1,100475347	1,961497364	-0,129039706	-0,032279294
944	1,108164615	1,963642169	-0,120603331	-0,054588811
945	1,132712341	1,959241932	-0,152181359	-0,042167769
946	1,21546332	1,933572335	-0,173331896	-0,017275914
947	1,259842838	1,928501874	-0,190447017	-0,009008674
948	1,264547502	1,920933423	-0,188225753	0,00872158
949	1,279367786	1,923491377	-0,196445245	0,027858856
950	1,286844562	1,917689225	-0,206406201	0,047333413
951	1,316525212	1,911167238	-0,222500537	0,068217863
952	1,348310592	1,896397232	-0,254053949	0,070182258
953	1,382792496	1,89780642	-0,276146686	0,047730062
954	1,409698182	1,884289352	-0,317233763	0,040201879
955	1,424084651	1,881051048	-0,338824617	0,010613221
956	1,408716677	1,887385259	-0,362970446	-0,015912973
957	1,431076653	1,874777468	-0,376261269	-0,008240867
958	1,474900263	1,868894392	-0,397092324	-0,001652592
959	1,516703704	1,852022959	-0,421775035	0,007209605
960	1,544389872	1,839717783	-0,452382748	0,050442075
961	1,628141319	1,811689287	-0,513705882	0,101565874
962	1,723334395	1,761639305	-0,565339673	0,183186144
963	1,810081253	1,700083235	-0,614520425	0,244746974
964	1,884264696	1,671412514	-0,624490613	0,303409033
965	1,929376898	1,644912508	-0,629943176	0,384366791
966	1,986408434	1,608402679	-0,672651213	0,476122489
967	2,031016853	1,579958383	-0,716552095	0,543068448
968	2,138400573	1,522886839	-0,768294768	0,6052572
969	2,1933957	1,488657853	-0,790561457	0,658513826

970	2,263208562	1,455571957	-0,804173791	0,673584779
971	2,277653677	1,42549104	-0,81305313	0,664791653
972	2,251609122	1,424029333	-0,79286129	0,650736924
973	2,271666317	1,410086712	-0,81108404	0,66770576
974	2,324027571	1,357247779	-0,849838467	0,70580253
975	2,351100056	1,326981213	-0,879026212	0,739004606
976	2,371491772	1,310957192	-0,888681847	0,737050186
977	2,421275321	1,278206758	-0,925244436	0,747550284
978	2,420103387	1,261631426	-0,951267549	0,749597646
979	2,448089288	1,233899325	-0,991944854	0,766655515
980	2,481094548	1,204169368	-1,018659422	0,79781534
981	2,496501325	1,195619278	-1,015538827	0,816288385
982	2,542688336	1,17552085	-1,050388195	0,823765224
983	2,527282668	1,180724156	-1,029341903	0,827342715
984	2,489852955	1,213565686	-1,016579535	0,81228361
985	2,472884664	1,234252026	-1,016068519	0,798005939
986	2,461025996	1,23968963	-0,995531757	0,797573624
987	2,40991325	1,259481955	-0,968838283	0,800364199
988	2,404444203	1,264888364	-0,956794634	0,825142888
989	2,421451322	1,269405269	-0,937085585	0,795975106
990	2,419411539	1,314284687	-0,924112287	0,780540747
991	2,398798851	1,342202327	-0,922311691	0,794746143
992	2,354271688	1,385906298	-0,890222453	0,80595438
993	2,299745173	1,410202209	-0,873527068	0,795140362
994	2,262030662	1,44438188	-0,860268559	0,789496734
995	2,249402568	1,464353552	-0,842035506	0,79147568
996	2,229712081	1,491614948	-0,842357733	0,782497976
997	2,244982501	1,505588211	-0,854180344	0,764439217
998	2,230425279	1,545177595	-0,869035054	0,739169013
999	2,184462988	1,58273937	-0,862147412	0,751743871
1000	2,152946774	1,578803645	-0,861930997	0,750666318
1001	2,137119576	1,588095304	-0,856538055	0,733280455
1002	2,137559296	1,585676344	-0,877632277	0,718989111
1003	2,17227157	1,601439179	-0,911391259	0,731756686
1004	2,23786592	1,585519835	-0,957928872	0,737698689
1005	2,293927684	1,550145571	-1,03356958	0,729797475
1006	2,369019991	1,517466698	-1,126045731	0,746447448
1007	2,481738955	1,531316197	-1,21571126	0,815762564

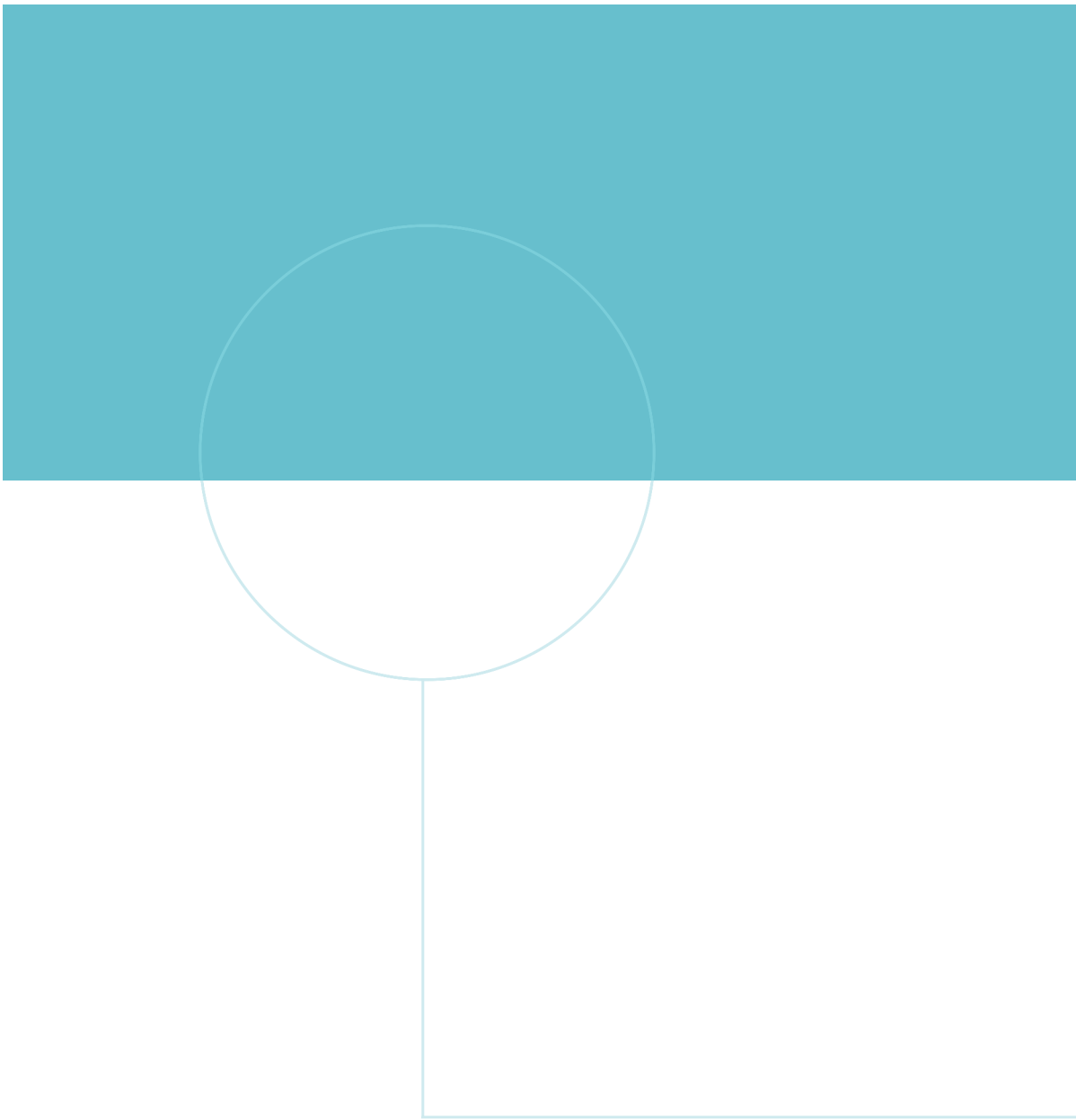

NTNU

Norwegian University of
Science and Technology